ARCHIVES OF MECHANICS **Appears since 1949**

Aims and Scope

ARCHIVES OF MECHANICS provides a forum for original research on mechanics of solids, fluids and discrete systems, including the development of mathematical methods for solving mechanical problems. The journal encompasses all aspects of the field, with the emphasis placed on:

- mechanics of materials: elasticity, plasticity, time-dependent phenomena, phase transformation, damage, fracture; physical and experimental foundations, micromechanics, thermodynamics, instabilities
- methods and problems in continuum mechanics: general theory and novel applications, thermomechanics, structural analysis, porous media, contact problems
- dynamics of material systems
- fluid flows and interactions with solids

Address of the Editorial Office:
Institute of Fundamental Technological Research
Świętokrzyska 21
PL 00-049 Warsaw, Poland

Tel.: (48-22) 826 60 22, Fax: (48-22) 826 98 15, E-mail: publikac@ippt.gov.pl

Abstracted/indexed in:

Applied Mechanics Reviews, Current Mathematical Publications, Mathematical Reviews, MathSci, Zentralblatt für Mathematik, UnCover.

http://am.ippt.gov.pl/

Polish Academy of Sciences
Institute of Fundamental Technological Research

Archives of Mechanics

Archiwum Mechaniki Stosowanej

volume 53 issue 2

Agencja Reklamowo-Wydawnicza A. Grzegorczyk
Warszawa 2001

SUBSCRIPTIONS

Address of the Editorial Office: Archives of Mechanics
Institute of Fundamental Technological Research, Świętokrzyska 21
PL 00-049 Warsaw, Poland
Tel.: (48-22) 826 60 22, Fax: (48-22) 826 98 15, E-mail: publikac@ippt.gov.pl

Subscription orders for all journals edited by IFTR may be sent directly to the Editorial Office of the Institute of Fundamental Technological Research

Subscription rates

Annual subscription rate (2001) including postage is US $ 210.
Please transfer the subscription fee to our bank account: Payee: IPPT PAN,
Bank: PKO SA. IV O/Warszawa,
Account no. 12401053-40054492-3000-401112-001.

All journals edited by IFTR are available also through:

- Foreign Trade Enterprise ARS POLONA Krakowskie Przedmieście 7, 00-068 Warszawa, Poland fax: (48-22) 826 86 73
- RUCH S.A. ul. Towarowa 28, 00-958 Warszawa, Poland fax:(48-22) 620 17 62
- Agencja Reklamowo-Wydawnicza A. Grzegorczyk, Bitwy Warszawskiej 1920r. 3, 00-973 Warszawa, Poland tel./fax: (48-22) 822 49 36

Warunki prenumeraty

Redakcja przyjmuje prenumeratę na wszystkie czasopisma wydawane przez IPPT PAN. Bieżące numery można nabyć a także zaprenumerować roczne wydanie Archiwum Mechaniki Stosowanej bezpośrednio w Dziale Wydawnictw IPPT PAN, Świętokrzyska 21, 00-049 Warszawa, Tel.: (48-22) 826 60 22; Fax: (48-22) 826 98 15.
Cena rocznej prenumeraty z bonifikatą (na rok 2001) dla krajowego odbiorcy wynosi 180 zł

Również można je nabyć, a także zamówić (przesyłka za zaliczeniem pocztowym) we Wzorcowni Ośrodka Rozpowszechniania Wydawnictw Naukowych PAN,
00-818 Warszawa, ul. Twarda 51/55, tel. (48-22) 697 88 35.
Wpłaty na prenumeratę przyjmują także jednostki kolportażowe RUCH S.A. Oddział Krajowej Dystrybucji Prasy, 00-958 Warszawa, ul. Towarowa 28. Konto: PBK.S.A. XIII Oddział Warszawa nr 11101053-16551-2700-1-67. Dostawa odbywa się pocztą zwykłą w ramach opłaconej prenumeraty z wyjątkiem zlecenia dostawy pocztą lotniczą, której koszt w pełni pokrywa zleceniodawca. Tel.: (48-22) 620 10 39, fax: (48-22) 620 17 62

Arkuszy wydawniczych 8. Arkuszy drukarskich 9/A5.
Papier offset. kl III 70 g. B1.
Oddano do składania w lutym 2001 r. Druk ukończono w kwietniu 2001 r.
Skład i łamanie: G. Wasilewska. Druk i oprawa: Drukarnia OMIKRON, Stare Babice ul. Kutrzeby 15.

Arch. Mech., **53**, 2, pp. 91–104, Warszawa 2001

On resonances of nonlinear elastic waves in a cubic crystal

W. DOMAŃSKI and T. JABŁOŃSKI

Institute of Fundamental Technological Research
Polish Academy of Sciences
Świętokrzyska 21, 00–049 Warsaw, Poland
e-mail: wdoman@ippt.gov.pl or tjablon@ippt.gov.pl,

USING THE METHOD of weakly nonlinear geometric optics, we obtain asymptotic transport evolution equations for high-frequency, small amplitude nonlinear elastic waves in a cubic crystal. Both geometrical and physical nonlinearities are included in our model. We expand strain energy up to the third order terms with respect to the strain matrix components. The nonlinear resonant asymptotic equations obtained are of integro-differential type. The coefficients of these equations are called resonant interaction coefficients (*RIC*). They determine whether and between which waves the nonlinear resonant interactions occur. We have calculated all the *RIC* in the explicit analytical form for three different crystalline directions of a one-dimensional wave motion. Comparison of the results shows that the direction of propagation influences the resonant interactions in an essential way. Moreover, our analytical formulas for *RIC* can be used to determine the material constants of a crystal.

1. Introduction

THE NONLINEAR RESONANCE of two waves, contrary to the classical linear superposition, consists in producing a new wave with a fixed wave number and frequency being the combination of the componential wave numbers and frequencies. The generation of the second harmonics is a classical example. Recently, the analysis of nonlinear resonant interactions of waves attracts many mathematicians and physicists. In the last decade, a new asymptotic method called *weakly nonlinear geometric optics*, *WNGO* in short, was mathematically rigorously developed to analyze nonlinear resonances [1 – 3].

In this paper we are interested in resonant interactions of nonlinear elastic waves in anisotropic media. For simplicity, we focus on a cubic crystal being the simplest nonlinear, anisotropic, elastic medium. To analyze the problem of resonant interactions we derive the equations of motion as the first order quasilinear hyperbolic system of partial differential equations (PDE). Both the geometrical and physical nonlinearities are included in our model.

Employing *WNGO* we reduced our complicated system of PDE to a relatively simpler set of transport evolution equations with integro-differential terms

that describe the nonlinear resonances of the interacting waves. These transport equations can be solved, in general, numerically only. The solution gives the information how the shapes of particular waves evolve in time and space. Even before solving the set of our asymptotic equations, the knowledge of the analytical form of all the nonvanishing *RIC* provides useful physical information: which waves interact, how strong the nonlinear resonance is and what new waves are produced.

We start with a general formulation of nonlinear dynamical elasticity equations in three space dimensions. After expanding the strain energy up to the third order terms in an arbitrary anisotropic homogeneous medium, we specify the energy form explicitly for a cubic crystal. Then, for simplicity of our presentation, we restrict ourselves to the one space dimension and show the analytical formulas characterizing our hyperbolic system of PDE for three selected directions of wave propagation. Finally, we calculate analytically all the *RIC*, which we then briefly analyze.

2. Nonlinear elasticity equations

2.1. General form in three-dimensional space

We consider the equations of nonlinear elasticity which, in Lagrangian coordinates, take the following form:

$$\begin{aligned} \rho_0 \frac{\partial \mathbf{v}}{\partial t} &= \nabla(\mathbf{F}\,\mathbf{T}), \\ \frac{\partial \mathbf{F}}{\partial t} &= \nabla \mathbf{v}, \end{aligned} \tag{2.1}$$

where we introduce: $\mathbf{v} = \dfrac{\partial \mathbf{u}}{\partial t}$ – velocity, $\mathbf{u}$ – displacement, $\nabla \mathbf{u}$ is the displacement gradient matrix with respect to the space variable $\mathbf{x} = [x_1, x_2, x_3] \in \mathbb{R}^3$, t – time, ρ_0 – density and $\mathbf{F} = \mathbf{I} + \nabla \mathbf{u}$ is the deformation gradient.

In a nonlinear hyperelastic medium the stress tensor $\mathbf{T}$ is characterized by the relation:

$$\mathbf{T} = \frac{\partial W}{\partial \mathbf{E}}, \tag{2.2}$$

where the strain energy $W = W(\mathbf{E})$ is an analytic matrix-valued function that we later expand up to the third order terms with respect to the strain matrix $\mathbf{E}$ components, and

$$\mathbf{E} = \frac{1}{2}(\mathbf{F}^T\mathbf{F} - \mathbf{I}). \tag{2.3}$$

Using the definition of $\mathbf{F}$ we can express the strain tensor $\mathbf{E}$ as the function of the gradient of displacement:

$$\mathbf{E} = \mathbf{E}(\nabla\mathbf{u}) = \frac{1}{2}\left\{\nabla\mathbf{u} + (\nabla\mathbf{u})^T + (\nabla\mathbf{u})^T\nabla\mathbf{u}\right\}. \tag{2.4}$$

It shows that we include *geometrical nonlinearity* in our formulation, apart from the so-called *physical nonlinearity* expressed in $W(\mathbf{E})$ (cf. (2.5) below).

2.2. Nonlinear anisotropic medium

We assume the expansion of the energy W in the following physically nonlinear form:

$$W(\mathbf{E}) = \frac{1}{2}\sum_{i,j,k,l}^{3} c_{ij,kl}E_{ij}E_{kl} + \frac{1}{6}\sum_{i,j,k,l,m,n}^{3} c_{ij,kl,mn}E_{ij}E_{kl}E_{mn}. \tag{2.5}$$

Given the explicit form of the energy $W = W(\mathbf{E})$ as a function of the strain $\mathbf{E}$, we compute the stress $\mathbf{T} = \{T_{ij}\}_{i,j=1}^{3}$ by formally differentiating W with respect to $\mathbf{E}$:

$$T_{ij} = \sum_{k,l}^{3} c_{ij,kl}E_{kl} + \frac{1}{2}\sum_{k,l,m,n}^{3} c_{ij,kl,mn}E_{kl}E_{mn}. \tag{2.6}$$

Then employing the formula (2.4), we obtain the energy $\widetilde{W}$ as the function of the gradient of displacement: $\widetilde{W}(\nabla\mathbf{u}) := W(\mathbf{E}(\nabla\mathbf{u}))$.

From now on, to shorten the notation, we use the standard abbreviated indices c_{ij}, c_{ijk}, $i,j,k = 1,...,3$ according to the known rule:

$$\begin{array}{llllll} 1,1 & \to & 1 & 2,2 & \to & 2 \qquad 3,3 \to 3 \\ 2,3 & \to & 4 & 3,2 & \to & 4 \qquad 1,3 \to 5 \\ 3,1 & \to & 5 & 1,2 & \to & 6 \qquad 2,1 \to 6 \end{array} \tag{2.7}$$

2.3. Cubic crystal

After BIRCH [4], the explicit form of the strain energy function $W = W(\mathbf{E})$ in the simplest cubic crystal is the following:

$$
\begin{aligned}
(2.8)\qquad W = {} & \frac{1}{2}\hat{c}_{11}(E_{11}^2 + E_{22}^2 + E_{33}^2) + \hat{c}_{12}(E_{11}E_{22} + E_{22}E_{33} + E_{11}E_{33}) \\
& + \hat{c}_{44}(E_{12}^2 + E_{21}^2 + E_{23}^2 + E_{32}^2 + E_{31}^2 + E_{13}^2) + \hat{c}_{111}(E_{11}^3 + E_{22}^3 + E_{33}^3) \\
& + \hat{c}_{112}\{E_{11}^2(E_{22} + E_{33}) + E_{22}^2(E_{11} + E_{33}) + E_{33}^2(E_{11} + E_{22})\} \\
& + \frac{1}{2}\hat{c}_{144}\{E_{11}(E_{23}^2 + E_{32}^2) + E_{22}(E_{13}^2 + E_{31}^2) + E_{33}(E_{12}^2 + E_{21}^2)\} \\
& + \frac{1}{2}\hat{c}_{166}\{(E_{11} + E_{22})(E_{12}^2 + E_{21}^2) + (E_{22} + E_{33})(E_{23}^2 + E_{32}^2) \\
& + (E_{11} + E_{33})(E_{13}^2 + E_{31}^2)\} \\
& + \hat{c}_{123}E_{11}E_{22}E_{33} + \hat{c}_{456}(E_{12}E_{23}E_{31} + E_{21}E_{32}E_{13}),
\end{aligned}
$$

provided that the wave propagation direction is $\mathbf{z}_1 = [1, 0, 0]$. The coefficients $\hat{c}_{ij}$, $\hat{c}_{ijk}$ in (2.8) are related to c_{ij}, c_{ijk} in (2.5), (2.7) as follows: $\hat{c}_{ij} = c_{ij}$,

$$
\begin{aligned}
\hat{c}_{111} &= \frac{1}{6}c_{111}, & \hat{c}_{144} &= 2c_{144}, & \hat{c}_{123} &= c_{123}, \\
\hat{c}_{112} &= \frac{1}{2}c_{112}, & \hat{c}_{166} &= 2c_{166}, & \hat{c}_{456} &= 4c_{456}.
\end{aligned}
$$

Given any other direction $\mathbf{z}$ of wave propagation, we need to transform the formula (2.8) for the energy $W = W(\mathbf{E})$ according to the rule:

$$
(2.9)\qquad W(\mathbf{E}) \longrightarrow W(\mathbf{Q}_z\mathbf{E}\mathbf{Q}_z^T)
$$

where $\mathbf{Q}_z$ is the unitary matrix of the rotation that transforms the vector $\mathbf{z}_1 = [1, 0, 0]$ into the vector $\mathbf{z}$ and where the superscript T denotes matrix transposition.

In this paper we also consider the two other canonical directions of propagation: $\mathbf{z}_2 = [1, 1, 0]$ and $\mathbf{z}_3 = [1, 1, 1]$. The rotation matrix corresponding to the direction $\mathbf{z}_2$ is

$$
(2.10)\qquad \mathbf{Q}_{z_2} = \frac{1}{\sqrt{2}}\begin{bmatrix} 1 & -1 & 0 \\ 1 & 1 & 0 \\ 0 & 0 & \sqrt{2} \end{bmatrix}
$$

and to the direction $\mathbf{z}_3$ is

$$
(2.11)\qquad \mathbf{Q}_{z_3} = \begin{bmatrix} \frac{1}{\sqrt{3}} & \frac{1}{\sqrt{6}} & \frac{-1}{\sqrt{2}} \\ \frac{1}{\sqrt{3}} & \frac{1}{\sqrt{6}} & \frac{1}{\sqrt{2}} \\ \frac{1}{\sqrt{3}} & \frac{-\sqrt{2}}{\sqrt{3}} & 0 \end{bmatrix}.
$$

2.4. First order system in one dimensional-space

In the one-dimensional case ($\mathbf{x} = [x, 0, 0]$), making use of the formalism from Sec. 2.1, and under natural assumptions guaranteeing hyperbolicity, our nonlinear elasticity equations (2.1) lead to the *quasilinear hyperbolic system* of the form:

$$\frac{\partial \mathbf{w}}{\partial t} + \mathbf{A}(\mathbf{w}) \frac{\partial \mathbf{w}}{\partial x} = \mathbf{0}, \tag{2.12}$$

with the matrix $\mathbf{A}(\mathbf{w})$:

$$\mathbf{A}(\mathbf{w}) = - \begin{bmatrix} \mathbf{0} & \frac{1}{\rho_0}\mathbf{B}(\mathbf{w}) \\ \mathbf{I} & \mathbf{0} \end{bmatrix}, \tag{2.13}$$

where $\mathbf{I}$ is the 3×3 identity matrix and

$$\mathbf{w} = [\, \mathbf{v}(x,t), \mathbf{u}_{,x}(x,t) \,] = [\, w_1, w_2, w_3, w_4, w_5, w_6 \,].$$

The 3×3 matrix $\mathbf{B} = \{B_{ij}\}_{i,j=1}^{3}$ in (2.13) is derived from the equation of motion in (2.1) and is given by the general formula:

$$B_{ij} = \frac{\partial^2 \widetilde{W}}{\partial w_{i+3} \partial w_{j+3}} \qquad \text{with} \qquad \widetilde{W}(\mathbf{u}_{,x}) := W(\mathbf{E}(\mathbf{u}_{,x})). \tag{2.14}$$

The matrix $\mathbf{B}$ can be further specified after expanding the energy $W = W(\mathbf{E})$ up to the *third order* terms with respect to the strain matrix $\mathbf{E}$ (cf. Sec. 2.2).

In the final form of $\mathbf{B}$ obtained by using (2.14), we neglect higher than the first order terms in $\mathbf{w}$. The form of $\mathbf{B}$ depends on the direction $\mathbf{z}$ of the wave propagation in the cubic crystal, as the energy function W does (cf. Sec. 2.3, (2.8), (2.9)). The analytical form of the matrix $\mathbf{B}$ will be explicitly given later for three directions: $\mathbf{z}_1 = [1,0,0]$, $\mathbf{z}_2 = [1,1,0]$ and $\mathbf{z}_3 = [1,1,1]$.

3. WNGO approach

We are interested in the Cauchy problem for the quasilinear hyperbolic system (2.12) with periodic initial conditions

$$\begin{aligned} &\frac{\partial \mathbf{w}^\epsilon}{\partial t} + \mathbf{A}(\mathbf{w}^\epsilon) \frac{\partial \mathbf{w}^\epsilon}{\partial x} = \mathbf{0}, \\ &\mathbf{w}^\epsilon(x,0) = \mathbf{w}_0 + \epsilon\, \mathbf{w}_1(x, x/\epsilon), \end{aligned} \tag{3.1}$$

where ϵ is a small parameter and $\mathbf{w}_0$ is a constant state solution to the PDE system (2.12).

This problem can be solved by using asymptotic methods. The heuristic expansions, without proving their asymptotic correctness, were applied by physicists to study interactions of nonlinear waves already in the fifties. The modern, mathematically rigorous approach, called weakly nonlinear geometric optics (*WNGO*), was initiated by CHOQUET-BRUHAT [5], followed by HUNTER and KELLER [6]. In the eighties and nineties, many papers devoted to *WNGO* were published, e.g. [1, 2], several of them containing the rigorous proofs of the validity of *WNGO* [3, 7].

The *WNGO* method has been already applied to study resonances in different physical situations: gasdynamics [1], magnetohydrodynamics [8], isotropic elasticity [9], magnetoelasticity [10]. We have analyzed the resonances in nonlinear electrodynamics [11].

3.1. Asymptotics

A weakly *nonlinear geometric optics* asymptotic solution to the system (3.1) is sought for in the form:

$$\mathbf{w}^\epsilon(x,t) = \mathbf{w}_0 + \epsilon \sum_j a_j \left(x, t, \frac{x - \lambda_j t}{\epsilon} \right) \mathbf{r}_j + \mathcal{O}(\epsilon^2) \tag{3.2}$$

with the unknown amplitudes a_j. We assume here that a_j are periodic with zero mean.

Here λ_j is the eigenvalue of $\mathbf{A}(\mathbf{w}_0)$, $j = 1, \ldots, 6$, and $\mathbf{r}_j$ is the right eigenvector corresponding to λ_j:

$$(\mathbf{A}(\mathbf{w}_0) - \lambda_j \mathbf{I})\mathbf{r}_j = \mathbf{0}, \qquad \mathbf{l}_j\,(\mathbf{A}(\mathbf{w}_0) - \lambda_j \mathbf{I}) = \mathbf{0}, \qquad \mathbf{l}_i \cdot \mathbf{r}_j = \delta_{ij}$$

while $\mathbf{l}_j$ is the left eigenvector of $\mathbf{A}(\mathbf{w}_0)$ and δ_{ij} is the Kronecker delta.

Inserting (3.2) into (3.1), expanding $\mathbf{A}$ around $\mathbf{w}_0$, into Taylor's series, using multiple scale analysis and employing the solvability condition, we obtain the *transport evolution equations* for the amplitudes a_j of resonantly interacting waves.

In general, for strictly hyperbolic systems, these are integro-differential equations of the form [1]:

$$\frac{\partial a_j}{\partial t} + \lambda_j \frac{\partial a_j}{\partial x} + \Gamma^j_{jj} a_j \frac{\partial a_j}{\partial \eta} + {\sum_{p,q}}' \Gamma^j_{pq} \lim_{T\to\infty} \frac{1}{2T} \int_{-T}^{T} a'_p\, a_q\, ds = 0 \tag{3.3}$$

where

$$a_q = a_q(x, t, \eta + s(\lambda_j - \lambda_q)), \qquad a'_p = \frac{\partial a_p}{\partial \eta}(x, t, \eta + s(\lambda_j - \lambda_p)),$$

and $\sum'$ indicates summation avoiding repeated indices, while $\eta \equiv (x - \lambda_j t)\,\epsilon^{-1}$.

The *nonlinear resonance* takes place when at least one of the integro-differential terms with Γ^j_{pq} in (3.3), $j, p, q = 1, 2, \ldots, 6$, does not vanish.

3.2. Resonant interaction coefficients

The fundamental feature of a nonlinear resonance of waves is the generation of a new wave with a fixed wave number and a frequency being the combination of the componential wave numbers and frequencies [1, 3]. It is of great practical importance to investigate whether and when such nonlinear resonances take place.

The strength of the j-th wave produced through the nonlinear resonant interaction of p-th and q-th waves is represented by the coefficient Γ^j_{pq} in (3.3). It is called the *resonant interaction coefficient (RIC)*. It can be put into relatively simple form:

$$\Gamma^j_{pq}(\mathbf{w}_0) = \mathbf{l}_j \cdot (\nabla_{\mathbf{w}}\,\mathbf{A})\Big|_{\mathbf{w}=\mathbf{w}_0} \mathbf{r}_p \cdot \mathbf{r}_q \tag{3.4}$$

convenient for further manipulations with the help of the symbolic calculation program *Mathematica*.

The formula (3.4) for *RIC* involves right and left eigenvectors of the matrix $\mathbf{A}$ of our PDE set, and the derivatives of $\mathbf{A}$ with respect to the unknown vector $\mathbf{w}$, all evaluated at the constant state $\mathbf{w}_0$ around which we expand our asymptotics. In fact, the $(\nabla_{\mathbf{w}}\,\mathbf{A})$ is the Hessian of the matrix $\mathbf{A}$. Thus, together with the eigenvectors of $\mathbf{A}$ in the analytical form, the formula (3.4) can be quite lengthy and tedious. Nevertheless, it is in a suitable form for symbolic calculation programs like *Mathematica* or *Maple*.

Specially designed procedures have been developed in the *Mathematica* language. These procedures allow us to calculate analytically and efficiently simplify all the *RIC* of the system (3.3) for any given constant state $\mathbf{w}_0$.

4. Nonlinear resonances in a cubic crystal

The explicit form of *all* the *RIC* have been computed for system (2.12) of nonlinear elasticity equations for a cubic crystal, at the zero constant state ($\mathbf{w}_0 = \mathbf{0}$) for three different directions of wave propagation: $\mathbf{z}_1 = [1, 0, 0]$, $\mathbf{z}_2 = [1, 1, 0]$ and $\mathbf{z}_3 = [1, 1, 1]$.

In each case, apart from the analytical formulas for *RIC*, we present the particular analytical form of the matrix $\mathbf{B}$ (cf. (2.13)) and the eigenvalues of the matrix $\mathbf{A}(\mathbf{w}_0)$. All the formulas are presented as functions of the elastic material constants c_{ij}, c_{ijk}.

Moreover, in Fig. 1 we show a graphical representation of nonlinearly interacting waves. This representation can be interpreted as follows. Let us recall that a nonvanishing Γ^j_{pq} in (3.3) represents the strength of the j-th wave produced through the nonlinear resonant interaction of p-th and q-th waves. For each new j-th wave, $j = 1, ..., 6$, we show a 6×6 matrix of respectively shaded squares that represent the p-th and q-th waves, by interaction of which the new j-th wave is produced. The letters in the squares and the shades of the squares correspond to the analytical formulas for the respective *RIC*. They, in turn, are referred to the graphics by the letters in squares in the formulas.

Our graphical representation helps to determine all the nonvanishing *RIC* and to find the relations between them (e.g. which of them are equal) without presenting lengthy redundant equations. Such a visualization allows us to compare easily nonlinear resonant interaction of waves for different directions of propagation or for different constant states.

Let us notice that the structure of the eigensystem of our matrix $\mathbf{A}$ in (2.12) is preserved, irrespectively of the direction of the wave propagation $\mathbf{z}_j$. There are always three pairs of eigenvalues of opposite sign:

$$\lambda_1 = -\lambda_2, \qquad \lambda_3 = -\lambda_4, \qquad \lambda_5 = -\lambda_6, \tag{4.1}$$

with the degeneracy $\lambda_3 = \lambda_5$ in the cases 1 and 3. In each case, the calculated eigenvectors of $\mathbf{A}(\mathbf{w}_0)$ can be expressed in terms of the eigenvalues (4.1) and they take the following form:

$$\begin{aligned}
\mathbf{r}_1 &= [\lambda_1, 0, 0, 1, 0, 0], & \mathbf{l}_1 &= \frac{1}{2}[\lambda_1^{-1}, 0, 0, 1, 0, 0],\\
\mathbf{r}_2 &= [\lambda_2, 0, 0, 1, 0, 0], & \mathbf{l}_2 &= \frac{1}{2}[\lambda_2^{-1}, 0, 0, 1, 0, 0],\\
\mathbf{r}_3 &= [0, \lambda_3, 0, 0, 1, 0], & \mathbf{l}_3 &= \frac{1}{2}[0, \lambda_3^{-1}, 0, 0, 1, 0],\\
\mathbf{r}_4 &= [0, \lambda_4, 0, 0, 1, 0], & \mathbf{l}_4 &= \frac{1}{2}[0, \lambda_4^{-1}, 0, 0, 1, 0],\\
\mathbf{r}_5 &= [0, 0, \lambda_5, 0, 0, 1], & \mathbf{l}_5 &= \frac{1}{2}[0, 0, \lambda_5^{-1}, 0, 0, 1],\\
\mathbf{r}_6 &= [0, 0, \lambda_6, 0, 0, 1], & \mathbf{l}_6 &= \frac{1}{2}[0, 0, \lambda_6^{-1}, 0, 0, 1].
\end{aligned} \tag{4.2}$$

Formula (4.2) shows that in all the three cases analyzed we have a complete set of linearly independent eigenvectors satisfying $\mathbf{l}_i \cdot \mathbf{r}_j = \delta_{ij}$, in spite of the fact that our system (2.12) is not strictly hyperbolic at $\mathbf{w}_0$ in the cases 1 and 3. The completeness of the eigenvectors allows us to calculate *RIC* even in these degenerate cases.

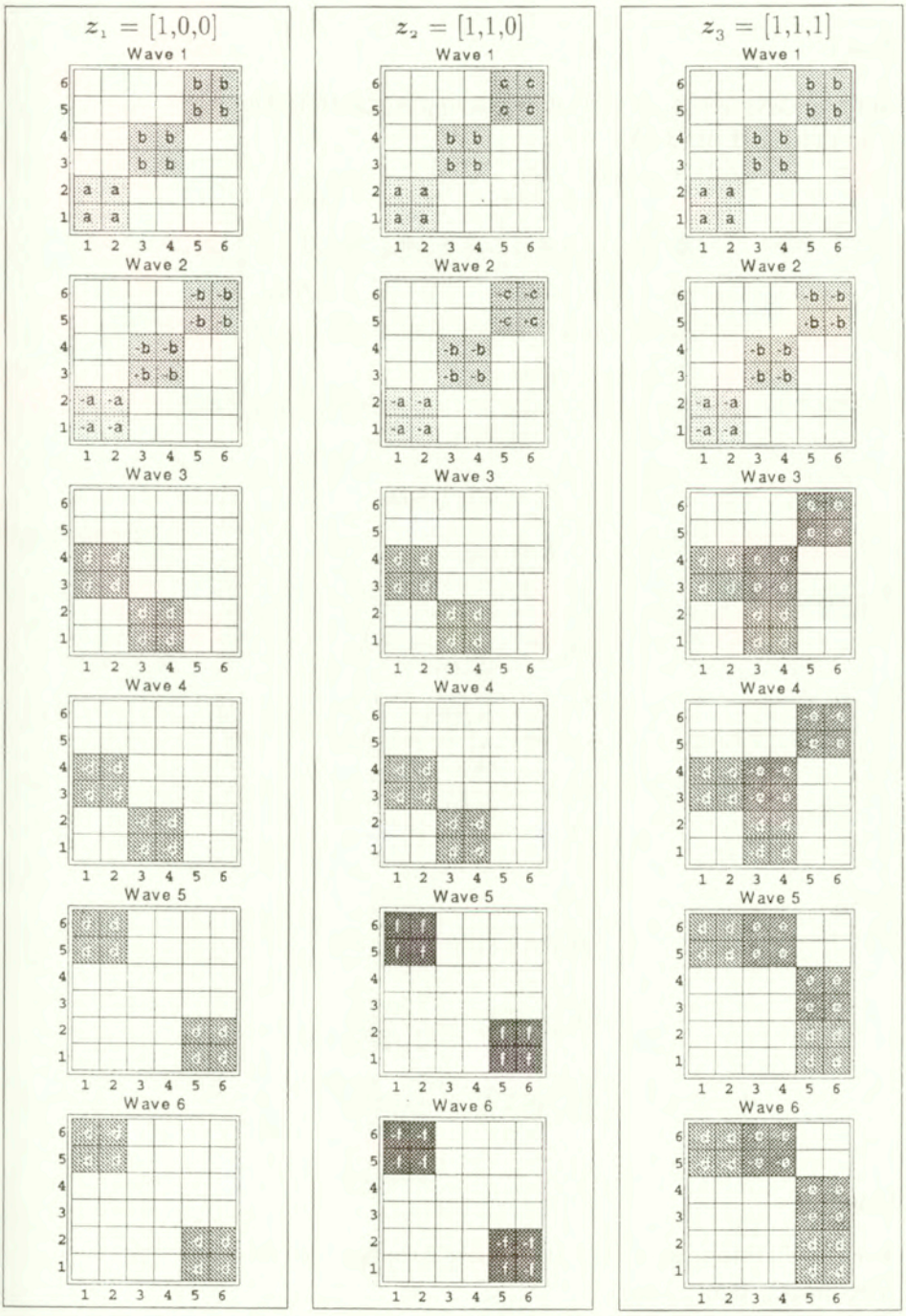

FIG. 1. Graphical representation of nonlinear resonances in a cubic crystal for different directions of wave propagation (see page 8).

4.1. Case 1

For the direction $\mathbf{z}_1 = [1,0,0]$ of wave propagation we have:
The matrix $\mathbf{B}$ in (2.13):

$$\mathbf{B} = \begin{bmatrix} \alpha + \beta w_4 & \gamma w_5 & \gamma w_6 \\ \gamma w_5 & \delta + \gamma w_4 & 0 \\ \gamma w_6 & 0 & \delta + \gamma w_4 \end{bmatrix}$$

with

$$\alpha = c_{11},$$

$$\beta = 3c_{11} + c_{111},$$

$$\gamma = c_{11} + c_{166},$$

$$\delta = c_{44}.$$

Eigenvalues:

$$\lambda_1 = -\sqrt{\frac{\alpha}{\rho_0}} = -\lambda_2,$$

$$\lambda_3 = -\sqrt{\frac{\delta}{\rho_0}} = -\lambda_4,$$

$$\lambda_5 = -\sqrt{\frac{\delta}{\rho_0}} = -\lambda_6.$$

RIC:

$$\boxed{\text{a}} \leftrightarrow \Gamma^1_{11} = \frac{-\beta}{2\sqrt{\rho_0\,\alpha}},$$

$$\boxed{\text{b}} \leftrightarrow \Gamma^1_{33} = \frac{-\gamma}{2\sqrt{\rho_0\,\alpha}},$$

$$\boxed{\text{d}} \leftrightarrow \Gamma^3_{13} = \frac{-\gamma}{2\sqrt{\rho_0\,\delta}}.$$

4.2. Case 2

For the direction $\mathbf{z}_2 = [1,1,0]$ of wave propagation we have:
The matrix $\mathbf{B}$ in (2.13):

$$\mathbf{B} = \begin{bmatrix} \alpha + \beta w_4 & \gamma w_5 & \gamma^* w_6 \\ \gamma w_5 & \delta + \gamma w_4 & 0 \\ \gamma^* w_6 & 0 & \delta^* + \gamma^* w_4 \end{bmatrix},$$

with

$$\alpha = \frac{1}{2}(c_{11} + c_{12} + 2c_{44}),$$

$$\beta = \frac{3}{2}(c_{11} + c_{12} + 2c_{44}) + \frac{1}{4}(c_{111} + 3c_{112} + 12c_{166}),$$

$$\gamma = \frac{1}{2}(c_{11} + c_{12} + 2c_{44}) + \frac{1}{4}(c_{111} - c_{112}),$$

$$\gamma^* = \frac{1}{2}(c_{11} + c_{12} + 2c_{44} + c_{144} + c_{166} + 2c_{456}),$$

$$\delta = \frac{1}{2}(c_{11} - c_{12}),$$

$$\delta^* = c_{44}.$$

Eigenvalues:

$$\lambda_1 = -\sqrt{\frac{\alpha}{\rho_0}} = -\lambda_2,$$

$$\lambda_3 = -\sqrt{\frac{\delta}{\rho_0}} = -\lambda_4,$$

$$\lambda_5 = -\sqrt{\frac{\delta^*}{\rho_0}} = -\lambda_6.$$

RIC:

$$\boxed{\text{a}} \leftrightarrow \Gamma^1_{11} = \frac{-\beta}{2\sqrt{\rho_0\,\alpha}},$$

$$\boxed{\text{b}} \leftrightarrow \Gamma^1_{33} = \frac{-\gamma}{2\sqrt{\rho_0\,\alpha}},$$

$$\boxed{\text{c}} \leftrightarrow \Gamma^1_{55} = \frac{-\gamma^*}{2\sqrt{\rho_0\,\alpha}},$$

$$\boxed{\text{d}} \leftrightarrow \Gamma^3_{13} = \frac{-\gamma}{2\sqrt{\rho_0\,\delta}},$$

$$\boxed{\text{f}} \leftrightarrow \Gamma^5_{15} = \frac{-\gamma^*}{2\sqrt{\rho_0\,\delta^*}}.$$

4.3. Case 3

For the direction $\mathbf{z}_3 = [1, 1, 1]$ of wave propagation we have:

The matrix $\mathbf{B}$ in (2.13):

$$\mathbf{B} = \begin{bmatrix} \alpha + \beta w_4 & \gamma w_5 & \gamma w_6 \\ \gamma w_5 & \delta + \gamma w_4 + \varepsilon w_5 & \varepsilon w_6 \\ \gamma w_6 & \varepsilon w_6 & \delta + \gamma w_4 + \varepsilon w_5 \end{bmatrix}$$

with

$$\alpha = \frac{1}{3}(c_{11} + 2c_{12} + 4c_{44}),$$

$$\beta = c_{11} + 2c_{12} + 4c_{44} + \frac{1}{9}(c_{111} + 6c_{112} + 12c_{144} + 24c_{166} + 2c_{123} + 16c_{456}),$$

$$\gamma = \frac{1}{3}(c_{11} + 2c_{12} + 4c_{44}) + \frac{1}{9}(c_{111} - 3c_{144} + 6c_{166} - c_{123} - 2c_{456}),$$

$$\delta = \frac{1}{3}(c_{11} - c_{12} + c_{44}),$$

$$\varepsilon = \frac{\sqrt{2}}{18}(c_{111} - 3c_{112} + 3c_{144} - 3c_{166} + 2c_{123} - 2c_{456}).$$

Eigenvalues:

$$\lambda_1 = -\sqrt{\frac{\alpha}{\rho_0}} = -\lambda_2,$$

$$\lambda_3 = -\sqrt{\frac{\delta}{\rho_0}} = -\lambda_4,$$

$$\lambda_5 = -\sqrt{\frac{\delta}{\rho_0}} = -\lambda_6.$$

RIC:

$$\boxed{\text{a}} \leftrightarrow \Gamma^1_{11} = \frac{-\beta}{2\sqrt{\rho_0\,\alpha}},$$

$$\boxed{\text{b}} \leftrightarrow \Gamma^1_{33} = \frac{-\gamma}{2\sqrt{\rho_0\,\alpha}},$$

$$\boxed{\text{d}} \leftrightarrow \Gamma^3_{13} = \frac{-\gamma}{2\sqrt{\rho_0\,\delta}},$$

$$\boxed{\text{e}} \leftrightarrow \Gamma^3_{33} = \frac{-\varepsilon}{2\sqrt{\rho_0\,\delta}}.$$

5. Conclusions

The coefficients of the transport evolution equations (3.3) of weakly nonlinear elastic waves in a homogeneous cubic crystal have been calculated explicitly in

a general *analytical* form. These coefficients, called *RIC*, represent resonant interactions of nonlinear waves and are expressed in terms of material constants of the medium. The *RIC* formulas have been analyzed for various crystalline directions of one-dimensional wave propagation.

The knowledge of the complete set of *RIC* for a given direction of propagation allows one to determine precisely which waves interact, how strong the nonlinear resonance is and what new waves are produced.

The analysis of the derived formulas shows that the most important factors influencing the resonant interactions are: the direction of wave propagation and the character of the nonlinearity of a crystal.

Closer examination of the Fig. 1 leads to the following observations:

- For all the three cases analyzed, the following formula holds true:

$$\Gamma^{j}_{pq} = -\Gamma^{j+1}_{pq}$$

for all p, q and $j = 1, 3, 5$. Let us also recall that $\lambda_j = -\lambda_{j+1}$. The physical interpretation is that resonant waves are produced always in pairs of waves propagating in opposite directions.

- The waves numbered 1 and 2 can only be produced by the interaction of waves in the same pair, namely: (1,2), (3,4) or (5,6).

- In the cases 1 and 2 there are the same nonvanishing *RIC* – meaning that the same resonances may occur in both cases; only the magnitudes of the nonlinear interactions differ.

- In the case 3 (propagation along the cubic diagonal) more nonzero *RIC* occur than in the other cases. All the additional *RIC* are expressed in terms of the third order material constants (cf. the definition of ε). Therefore, the *physical nonlinearity* is crucial here.

- All the nonvanishing *RIC* except those ε-dependent are not zero, even without the physical nonlinearity included in the energy formula expansion. Thus, nonlinear interactions manifest themselves already in the models with *geometrical nonlinearity* only. However, higher-order, *physical* nonlinearities influence substantially the *magnitude* of the resonances (cf. formulas for β and γ).

- Analytical formulas for *RIC* can be useful for determining elastic constants of a crystal in suitably designed measurements.

References

1. A. J. MAJDA and R. R. ROSALES, *Resonantly interacting weakly nonlinear hyperbolic waves, i. A single space variable*, Stud. Appl. Math., **71**, 149–179, 1984.

2. J. K. HUNTER, A. J. MAJDA and R. R. ROSALES, *Resonantly interacting weakly nonlinear hyperbolic waves, ii. Several space variables.* Stud. Appl. Math., **75**, 187–226, 1986.

3. J-L. JOLY, G. MÉTIVIER and J. RAUCH, *Resonant one dimensional nonlinear geometric optics*, J. Func. Anal., **114**, 106–231, 1993.

4. F. BIRCH, *Finite elastic strain of cubic crystals*, Phys. Rev., **71**, 11, 809–824, 1947.

5. Y. CHOQUET-BRUHAT, *Ondes asymptotique et approchées pour systèmes nonlineares d'equations aux derivèes partielles nonlinéaires*, J. Math. Pure et Appl., **48**, 117–158, 1969.

6. J. K. HUNTER and J. B. KELLER, *Weakly nonlinear high frequency waves*, Comm. Pure Appl. Math., **36**, 547–569, 1983.

7. R. DIPERNA and A. J. MAJDA, *The validity of geometric optics for weak solutions of conservation laws*, Comm. Math. Phys., **98**, 313–347, 1985.

8. P. CARBONARO, *Propagation and interaction of asymptotic waves in ideal magnetofluiddynamics*, ZAMP, **40**, 899–911, 1989.

9. J. K. HUNTER, *Interaction of elastic waves*, Stud. Appl. Math., **86**, 281–314, 1992.

10. W. DOMAŃSKI, *Weakly nonlinear magnetoelastic waves*, [In:] J. L. WEGNER and F. R. NORWOOD [Eds.], Proc. IUTAM Symposium on Nonlinear Waves in Solids, Victoria, Canada, 241–246, ASME, New Jersey 1995.

11. W. DOMAŃSKI and T. F. JABŁOŃSKI, *Resonant interaction coefficients for nonlinear electromagnetic waves in dielectrics and magnetics*, JSAEM Studies in Applied Electromagnetics, **4**, 68–72, 1996.

Received April 26, 2000; revised version October 27, 2000.

Arch. Mech., **53**, 2, pp. 105–122, Warszawa 2001

Thermodynamics of orientation discontinuity surface: small misorientation approach

P. DŁUŻEWSKI and G. MACIEJEWSKI

Institute of Fundamental Technological Research,
Polish Academy of Sciences
ul. Świętokrzyska 21, 00–049 Warsaw, Poland

THE THERMODYNAMICS of a crystal lattice reorientation process proceeding on low angle grain boundary is presented. In material science, the influence of lattice misorientation on the grain boundary energy is well established. On the other hand, in thermodynamics of discontinuity surface the influence of misorientation vector on the surface energy is usually ignored as yet. Therefore, in the present paper, attention is focused on this influence. To obtain the driving forces conjugate to relative grain reorientation, the continuum theory of dislocations has been applied. Starting from the energy balance law and assuming that the free energy of discontinuity surface depends strongly on the jump in crystal orientation field, the mathematical relations for the misorientation vector and the conjugated thermodynamic force are derived. The mentioned force contributes to the total driving force governing the grain boundary migration process. The problem of constitutive modelling of the surface motion is considered. The main result of this analysis is the incorporation of grain orientation jump into the thermodynamic description of driving forces of the grain reorientation process.

Key Words: Continuum theory of dislocations, misorientation, discontinuity of crystal surface.

1. Introduction

GRAIN REORIENTATION process plays an important role in mechanical behaviour of metals. Unfortunately, there are many factors, which may influence reorientation. To obtain a complete thermodynamic description of the reorientation process, the mechanical properties and geometry of individual grains (orientation, existing defects etc.) and boundary (its structure, defects existing on the boundary, possibility to move and glide, jump in respective thermodynamics parameters), interaction between defects in grains with the boundary should be incorporated. To avoid an extremely complex description in mathematical models of the polycrystal deformation, it is often assumed that the reorientation of grains depends only on the jump in the plastic deformation tensor. The influence of misorientation vector on the grain reorientation phenomenon is usually ignored, see Fig. 1.

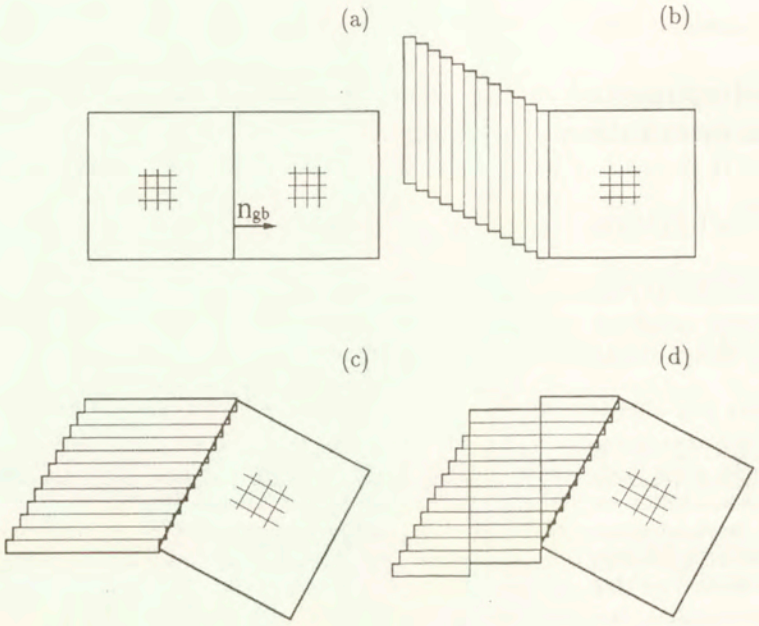

FIG. 1. Influence of slip orientation on grain reorientation: a) initial state; b) – d) state of deformed crystal.

The thermodynamic description of grain boundary motion considered in terms of the discontinuity surface has been considered in many papers [1, 3, 8, 13, 15]. However, in most of the papers a major premise is that driving traction originates from the balance of energy stored outside the boundary, cf. [1, 8, 13]. Additionally, the comparison of different thermodynamic approaches is difficult due to a variety of the used measures of crystal lattice defects, coordinate systems, tangent vector basis in which the position of measures are described, postulated deformation types (only elastic, elastoplastic etc.), cf. [2, 5, 6, 9, 18, 21, 24]. This is beyond our abilities to present most of them. In author's opinion, many of above approaches are not suitable for the considered type of discontinuity surface. For instance, the disclination theory can be a useful framework description of some of epitaxial layer interfaces [27] or defects in liquid crystals [16], while micropolar continuum description are much more complicated than the present framework. Therefore, we limit our references to the papers most representative for the approach developed here. Configurational forces play an important role in our analysis. Those forces are pivotal for the direction of the process evolution. For this reason, we distinguish the driving forces of the reorientation process originated from different grounds. Similar analysis based on a quite different axiomatic basis was presented by CERMELLI and SELLERS [2, 3]. They described the Bravais crystal with existence of the defects of lattice in the

form of dislocations, vacancies, interstitials and, contrary to our analysis, they did not use elastic-plastic decomposition. Additionally they discussed the widely used Born rule, see also [30]. Many other approaches have been formulated, e.g. [10, 11, 31], or more recently [15]. A common practice in the field of continuum mechanics is incorporation of internal variables to describe meso- or micro- proceses, which influence the macroscopic behaviour of the material. For the case of dislocation influence, the dislocation vector, dislocation tensor or lattice directors are incorporated into the constitutive equation, cf. [2, 12].

On the other hand, in the material science, the effect of lattice misorientation on the energy of low angle grain boundaries is well established, cf. [14, 28]. Moreover, the surface density of the free energy has been catalogued with respect to lattice misorientation vectors for given crystal lattices.

In this paper starting from the energy balance law and assuming that the free energy of discontinuity surface depends on the jump in orientation field, the relations for the misorientation vector and conjugate thermodynamical force are derived. This force contributes to the total driving force of the grain boundary migration process. The problem of constitutive modelling of the surface movement is considered. Due to the assumption of dislocation model of the grain boundary, the current analysis concerns only the low angle grain boundary. State of the dislocated crystal lattice near the boundary depends strongly on the exerted strain, cf. [28]. Thus in the first step, we have limited consideration to small deformation approach.

In the present analysis, incorporation of dislocation density tensor enables the description of the existence of dislocation in the bulk and on the grain boundary. The classical balance laws with symmetric stress tensor are used and no additional balance laws for couple stress are needed. To describe the orientation jump on the surface, the jump in the elastic and plastic deformation tensors are considered.

In the following section the kinematics of small deformation with continuous distribution of dislocations is presented. The notion of curvature tensor is introduced and its connection with the dislocation density tensor, which is a defect measure of the body, is considered. Particular attention is focused on the curvature measure of the dislocated continuum. The relation between the elastic, plastic and total curvature measure are also investigated. Section 3 concerns the compatibility conditions for deformation field on the grain boundary. The relations of the dislocation density to the grains misorientation are formulated. The importance of analysis in Sec. 4 consists in describing thermodynamics of the continuum theory of dislocations applied to the grain boundary reorientation process. Balance laws and the forms of driving forces are described explicitly. Proposition of a general form of the constitutive equation for grain boundary migration is proposed in Subsec. 4.3. Finally, in Sec. 5, summary of the analysis is presented.

2. Crystal lattice versus kinematics of the oriented continuum

In the case of small deformations, we assume an additive decomposition of the displacement gradient

$$\nabla \mathbf{u} = \mathbf{w} + \boldsymbol{\varepsilon}_{\mathrm{e}} + \boldsymbol{\varepsilon}_{\mathrm{p}}, \tag{2.1}$$

where $\mathbf{w}$, $\boldsymbol{\varepsilon}_{\mathrm{e}}$ and $\boldsymbol{\varepsilon}_{\mathrm{p}}$ denote the antisymmetric tensor of lattice rotation, symmetric tensor of elastic deformation, and generally unsymmetrical tensor of plastic deformation, respectively. Let us consider the conservative movement of dislocations (slips). Then, the plastic deformation tensor can be expressed as

$$\boldsymbol{\varepsilon}_{\mathrm{p}} = \sum_{i=1}^{n} \gamma_i \, \mathbf{s}_i \otimes \mathbf{m}_i,$$

where $\gamma_i, \mathbf{s}_i, \mathbf{m}_i$ denote the plastic slip value on the i-th slip system, vector parallel to the i-th slip system and vector perpendicular to the i-th slip system, respectively. The displacement integrability condition takes the following form:

$$\mathrm{curl}(\nabla \mathbf{u}) = \mathbf{0}. \tag{2.2}$$

Substituting (2.1), we obtain

$$-\boldsymbol{\alpha} + \boldsymbol{\alpha}_{\mathrm{e}} + \boldsymbol{\alpha}_{\mathrm{p}} = 0, \tag{2.3}$$

where

$$\boldsymbol{\alpha} \stackrel{df}{=} -\mathrm{curl}\mathbf{w}, \tag{2.4}$$

$$\boldsymbol{\alpha}_{\mathrm{e}} \stackrel{df}{=} \mathrm{curl}\boldsymbol{\varepsilon}_{\mathrm{e}}, \tag{2.5}$$

$$\boldsymbol{\alpha}_{\mathrm{p}} \stackrel{df}{=} \mathrm{curl}\boldsymbol{\varepsilon}_{\mathrm{p}}. \tag{2.6}$$

In the above equations $\boldsymbol{\alpha}$, $\boldsymbol{\alpha}_{\mathrm{e}}$, $\boldsymbol{\alpha}_{\mathrm{p}}$ denote measures of the continuum curvature, which originates from the total, elastic and plastic deformations, respectively. The close relation between elastic and plastic curvature in (2.3) is explained by the general deformation rule, i.e. elastic and plastic strains separately do not satisfy the compatibility relation (2.2), cf. [19]. There exists another group of curvature measures $\boldsymbol{\kappa}$, $\boldsymbol{\kappa}_{\mathrm{e}}$, $\boldsymbol{\kappa}_{\mathrm{p}}$. Tensors kappa are related with tensors alpha by the linear, mutually reversible relationships, noted by NYE, cf. [25],

$$\begin{aligned} \boldsymbol{\alpha}_{\ldots} &= -\boldsymbol{\kappa}_{\ldots}^{T} + \mathbf{1}\mathrm{tr}\,\boldsymbol{\kappa}_{\ldots}^{T}..., \\ \boldsymbol{\kappa}_{\ldots} &= -\boldsymbol{\alpha}_{\ldots}^{T} + \frac{1}{2}\mathrm{tr}\,\boldsymbol{\alpha}_{\ldots}^{T}. \end{aligned} \tag{2.7}$$

This relation is a consequence of geometrical nature of current consideration. The choice of measure depends on convenience in its application to particular cases. Burgers vector can be determined as an integral over a Burgers circuit c around a given dislocation

$$\mathbf{b}_{\mathrm{d}} = \oint_{c} \boldsymbol{\varepsilon}_{\mathrm{p}} d\mathbf{r}.$$

Using the Stokes theorem, we obtain

$$\mathbf{b}_{\mathrm{d}} = \int_{s} \mathrm{curl}\boldsymbol{\varepsilon}_{\mathrm{p}} d\mathbf{s}.$$

This means that from the mathematical point of view, we can define using Eqs. (2.1), (2.4), (2.5), (2.6), the following vectors:

$$\mathbf{b} \overset{df}{=} \int_{s} \boldsymbol{\alpha} d\mathbf{s},$$

$$\mathbf{b}_{\mathrm{e}} \overset{df}{=} \int_{s} \boldsymbol{\alpha}_{\mathrm{e}} d\mathbf{s},$$

$$\mathbf{b}_{\mathrm{p}} \overset{df}{=} \int_{s} \boldsymbol{\alpha}_{\mathrm{p}} d\mathbf{s},$$

where $\mathbf{b}_{\mathrm{p}} = \mathbf{b}_{d}$. By analogy to the classical Burgers vector, the above vectors can be called the total, elastic and plastic Burgers vectors. From Eq. (2.3) we find

$$\mathbf{b} = \mathbf{b}_{\mathrm{e}} + \mathbf{b}_{\mathrm{p}}.$$

Relationship between the dislocation density tensor and the curvature tensors were first introduced by NYE, cf. [25]. However, he didn't specify which of curvature tensor corresponded to the dislocation density tensor. According to the above consideration it is easy to note that the dislocation density tensor corresponds to a measure of plastic curvature similar to $\boldsymbol{\kappa}_{\mathrm{p}}$, cf. [7, 8].

In the case when in the continuum there exists a discontinuity surface of displacement gradient, on the basis of (2.4) we can assume the following relation for the total measure of continuum curvature

$$\int_{v} \boldsymbol{\alpha} dv = \int_{v^+} \boldsymbol{\alpha} dv + \int_{\partial v^{\pm}} \boldsymbol{\alpha}_s ds - \int_{v^-} \boldsymbol{\alpha} dv, \tag{2.8}$$

where $\int_{\partial v^{\pm}} \boldsymbol{\alpha}_s ds$ denotes the measure of continuum curvature due to existence of the discontinuity surface. The last equation may be expressed as

$$-\int_{v} \mathrm{curl}\mathbf{w} dv = -\int_{v^+} \mathrm{curl}\mathbf{w} dv + \int_{\partial v^{\pm}} \boldsymbol{\alpha}_s ds + \int_{v^-} \mathrm{curl}\mathbf{w} dv \tag{2.9}$$

and

$$-\int_{\partial v} \mathbf{w} \times d\mathbf{s} = -\int_{\partial v^+} \mathbf{w} \times d\mathbf{s} + \int_{\partial v^\pm} \alpha_s ds + \int_{\partial v^-} \mathbf{w} \times d\mathbf{s},$$

what leads to the following integral form:

$$\int_{\partial v^\pm} \alpha_s ds = -\int_{\partial v^\pm} \lceil \mathbf{w} \rceil \times d\mathbf{s}$$

and the local form, namely

$$\alpha_s = -\lceil \mathbf{w} \rceil \times \mathbf{n}. \tag{2.10}$$

Here $\lceil \cdot \rceil$ and $\mathbf{n}$ denote the jump in the respective quantity across the grain boundary, e.g. $\lceil \varepsilon_{\mathrm{p}} \rceil = \varepsilon_{\mathrm{p}}^+ - \varepsilon_{\mathrm{p}}^-$, and the unit normal to the surface. Relation (2.10) defines a curvature measure on the discontinuity surface of the displacement gradient. Now, we can define the curvature measure on the grain boundary corresponding to the jump in: the displacement gradient, the elastic deformation tensor and the plastic deformation tensor, namely

$$\alpha_{\mathrm{gb}} \overset{df}{=} -\lceil \mathbf{w} \rceil \times \mathbf{n}_{\mathrm{gb}}, \tag{2.11}$$

$$\alpha_{\mathrm{gb\,e}} \overset{df}{=} \lceil \varepsilon_{\mathrm{e}} \rceil \times \mathbf{n}_{\mathrm{gb}}, \tag{2.12}$$

$$\alpha_{\mathrm{gb\,p}} \overset{df}{=} \lceil \varepsilon_{\mathrm{p}} \rceil \times \mathbf{n}_{\mathrm{gb}}, \tag{2.13}$$

and

$$\kappa_{\mathrm{gb}} \overset{df}{=} -\alpha_{\mathrm{gb}}^T + \frac{1}{2}\mathrm{tr}, \quad \alpha_{\mathrm{gb}}^T = \lceil \varphi \rceil \otimes \mathbf{n}_{\mathrm{gb}}, \tag{2.14}$$

$$\kappa_{\mathrm{gb\,e}} \overset{df}{=} -\alpha_{\mathrm{gb\,e}}^T + \frac{1}{2}\mathrm{tr}\,\alpha_{\mathrm{gb\,e}}^T, \tag{2.15}$$

$$\kappa_{\mathrm{gb\,p}} \overset{df}{=} -\alpha_{\mathrm{gb\,p}}^T + \frac{1}{2}\mathrm{tr}\,\alpha_{\mathrm{gb\,p}}^T, \tag{2.16}$$

where $\varphi = -\mathbf{w} : \mathbf{e}$. The quantities φ, $\mathbf{e}$, $\mathbf{n}_{\mathrm{gb}}$ denote the vector of lattice orientation, alternating symbol and the unit vector normal to the grain boundary, respectively. It is worth emphasizing that equation (2.14) connects continuous curvature of the grain boundary with jump in the lattice orientation, cf. critical notes in [30]. Equations (2.11) to (2.16) visualize the correspondence between the classical measures of structure discontinuity and oriented continuum curvature measures. By analogy to the additive curvature decomposition (2.3), let us define the jump in the orientation caused by elastic and plastic deformation, respectively.

$$\lceil \varphi_{\mathrm{e}} \rceil \overset{df}{=} \kappa_{\mathrm{gb\,e}} \cdot \mathbf{n}_{\mathrm{gb}},$$

$$\lceil \varphi_{\mathrm{p}} \rceil \overset{df}{=} \kappa_{\mathrm{gb\,p}} \cdot \mathbf{n}_{\mathrm{gb}}.$$

From the above definitions, we get additional curvature measure relations on the grain boundary, namely

$$\alpha_{...}(\mathrm{x}) = -\alpha^{-}_{...}(\mathrm{x})\frac{H(x^3_{\mathrm{gb}} - x^3)}{\sqrt{g^{33}}} + \alpha_{\mathrm{gb}\,...}\frac{\delta(x^3{}_{\mathrm{gb}})}{\sqrt{g^{33}}} + \alpha^{+}_{...}(\mathrm{x})\frac{H(x^3 - x^3_{\mathrm{gb}})}{\sqrt{g^{33}}},$$
$$\kappa_{...}(\mathrm{x}) = -\kappa^{-}_{...}(\mathrm{x})\frac{H(x^3_{\mathrm{gb}} - x^3)}{\sqrt{g^{33}}} + \kappa_{\mathrm{gb}\,...}\frac{\delta(x^3{}_{\mathrm{gb}})}{\sqrt{g^{33}}} + \kappa^{+}_{...}(\mathrm{x})\frac{H(x^3 - x^3_{\mathrm{gb}})}{\sqrt{g^{33}}},$$

where by $H(\cdot)$, x^3, $x^3{}_{\mathrm{gb}}$, $\sqrt{g^{33}}$, $\delta(\cdot)$ we denote the Heaviside function, any curvilinear coordinate perpendicular to the surface, its value at the intersection point on the surface, the respective component of the metric tensor and the Dirac function, respectively.

3. Misorientation vector on the grain boundary

From the point of view of the oriented continuum mechanics, a grain boundary can be considered as a surface of jump in the orientation field. Non-zero misorientation vector $\Delta\boldsymbol{\varphi}$ ($\Delta\boldsymbol{\varphi} = \lceil\boldsymbol{\varphi}\rceil/\sqrt{g_{33}}$ for $x^3 = x^3_{\mathrm{gb}}$) can be attributed to all points on this surface. In such a case, the curvature tensor on grain boundary $\boldsymbol{\kappa}$ (Eq. (2.14)) can be restated in the form

$$\boldsymbol{\kappa} = \delta(x^3 - x^3_{\mathrm{gb}})\sqrt{g_{33}}\;\Delta\boldsymbol{\varphi}\otimes\mathbf{n}_{\mathrm{gb}},$$

and, by the NYE relation (2.7), the tensor alpha is determined

$$\boldsymbol{\alpha} = \delta(x^3 - x^3_{\mathrm{gb}})\sqrt{g_{33}}\,(-\mathbf{n}_{\mathrm{gb}}\otimes\Delta\boldsymbol{\varphi} + (\mathbf{n}_{\mathrm{gb}}\cdot\Delta\boldsymbol{\varphi})\mathbf{1})\,.$$

By making use of (2.3), we define the following misorientation vectors:

$$\Delta\boldsymbol{\varphi} = \left(+\lceil\mathbf{w}\rceil\times\mathbf{n}_{\mathrm{gb}} - \frac{1}{2}\mathrm{tr}(\lceil\mathbf{w}\rceil\times\mathbf{n}_{\mathrm{gb}})\right)\mathbf{n}_{\mathrm{gb}},$$

(3.1)
$$\Delta_{\mathrm{e}}\boldsymbol{\varphi} = \left(-\lceil\boldsymbol{\varepsilon}_{\mathrm{e}}\rceil\times\mathbf{n}_{\mathrm{gb}} + \frac{1}{2}\mathrm{tr}(\lceil\boldsymbol{\varepsilon}_{\mathrm{e}}\rceil\times\mathbf{n}_{\mathrm{gb}})\right)\mathbf{n}_{\mathrm{gb}},$$

$$\Delta_{\mathrm{p}}\boldsymbol{\varphi} = \left(-\lceil\boldsymbol{\varepsilon}_{\mathrm{p}}\rceil\times\mathbf{n}_{\mathrm{gb}} + \frac{1}{2}\mathrm{tr}(\lceil\boldsymbol{\varepsilon}_{\mathrm{p}}\rceil\times\mathbf{n}_{\mathrm{gb}})\right)\mathbf{n}_{\mathrm{gb}}.$$

The above relation shows that in the case of elastic-plastic crystal deformation, we can define elastic and plastic vectors of lattice misorientation. This implies that

representation of the dislocation density tensor in orthogonal base $\{\mathbf{n}_1, \mathbf{n}_2, \mathbf{n}_3\}$ takes the form

$$[\alpha_{\mathrm{gb}}] = \rho_{\mathrm{gb}} \begin{bmatrix} -b_3 & 0 & 0 \\ 0 & -b_3 & 0 \\ b_1 & b_2 & 0 \end{bmatrix},$$

where

$$\begin{aligned} \mathbf{n}_3 &= \mathbf{n}_{\mathrm{gb}}, \\ b_i &= -a\,(\Delta_{\mathrm{p}}\varphi \cdot \mathbf{n}_i), \\ \rho_{\mathrm{gb}} &= \frac{\delta(x^3 - x^3_{\mathrm{gb}})\sqrt{g_{33}}}{a}. \end{aligned}$$

Parameter a plays the role of the length scale, e.g. it corresponds to the length of crystal cell. It is easy to notice that the grain boundary dislocation tensor corresponds to a superposition of two families of dislocation lines lying on the considered surface. As an alternative, dislocation density vector can be included, cf. [12].

4. Thermodynamics

In order to obtain the form of driving forces of the process, we should complete the thermodynamical description. In Subsec. 4.1 we derive the constitutive relations for the body without discontinuity surface and next, in Subsec. 4.2, the discontinuity surface in continuum is described. From the viewpoint of balance equations, our approach differs from the classical elastic-plastic continuum thermodynamics only by the dislocation energy flux term included in the energy balance.

4.1. Continuum theory of dislocations

For a dislocated crystal, we postulate the balance equations in the form

$$\frac{d}{dt}\int\limits_v \rho dv = 0,$$

$$\frac{d}{dt}\int\limits_v \rho \mathbf{v} dv = \int\limits_s \boldsymbol{\sigma} d\mathbf{s} + \int\limits_v \rho \mathbf{j} dv,$$

$$\frac{d}{dt}\int\limits_v \mathbf{x} \times \rho \mathbf{v} dv = \int\limits_s \mathbf{x} \times \boldsymbol{\sigma} d\mathbf{s} + \int\limits_v \mathbf{x} \times \rho \mathbf{j} dv,$$

$$\frac{d}{dt}\int\limits_v \left(\rho u + \frac{1}{2}\rho \mathbf{v}\mathbf{v}\right) dv = \int\limits_s (\mathbf{v}\sigma - \mathbf{q}_T - \mathbf{q}) d\mathbf{s} + \int\limits_v (\rho \mathbf{j}\mathbf{v} + \rho h) dv,$$

$$\frac{d}{dt}\int\limits_v \rho\eta dv \geq -\int\limits_s \frac{\mathbf{q}_T}{T} d\mathbf{s} + \int\limits_v \frac{\rho h}{T} dv,$$

where ρ, σ, $\mathbf{j}$, $\mathbf{v}$, u, $\mathbf{q}_T$, h, η denote the mass density, Cauchy stress tensor, body force density, velocity, internal energy density, heat flux and heat source density, respectively, while $\mathbf{q}$ denotes the vector of the energy flux due to the relation between free energy and the dislocation density tensor. The above integral relations imply the following local form of balance equations:

$$\begin{aligned} \dot{\rho} + \rho \operatorname{div} \mathbf{v} &= 0, \\ \operatorname{div}\sigma + \rho \mathbf{j} - \rho \dot{\mathbf{v}} &= \mathbf{0}, \\ \sigma - \sigma^T &= \mathbf{0}, \\ -\rho \dot{u} + \sigma : \nabla \mathbf{v} - \operatorname{div}\mathbf{q} - \operatorname{div}\mathbf{q}_T + \rho h &= 0, \end{aligned} \tag{4.1}$$

$$\rho\dot{\eta} + \operatorname{div}\left(\frac{\mathbf{q}_T}{T}\right) - \frac{\rho h}{T} \geq 0. \tag{4.2}$$

Using the free energy function ($\psi = u - \eta T$), the last inequality can be expressed as

$$-\rho\dot{\psi} - \rho\eta\dot{T} + \sigma : \dot{\varepsilon}_{\mathrm{e}} + \sigma : \dot{\varepsilon}_{\mathrm{p}} - \operatorname{div}\mathbf{q} - \frac{\mathbf{q}_T}{T}\nabla T \geq 0. \tag{4.3}$$

To find the driving forces on the dislocation field, let us assume that the specific free energy of the dislocated crystal depends not only on the elastic strain and temperature, but also on the dislocation density tensor corresponding to the plastic curvature (induced by permanent rebuilding of the lattice by plastic deformation). Thus, let the free energy take the form

$$\psi = \psi(\varepsilon_{\mathrm{e}}, \alpha_{\mathrm{p}}, T). \tag{4.4}$$

The similar dependency were assumed by many other authors, e.g. [29]. Substituting this equation into (4.3) and making use of (2,6), we obtain

$$(\sigma - \sigma_{\mathrm{p}}) : \dot{\varepsilon}_{\mathrm{p}} - \frac{\mathbf{q}_T}{T}\nabla T \geq \mathbf{0}. \tag{4.5}$$

To hold this inequality for all processes, the Cauchy stress tensor resulting from elastic strain, the stress resulting from existence of dislocations (tending to minimize the free energy due to dislocation distribution), and the energy flux as

an effect of dislocation distribution and finally, the entropy have to satisfy the following equations:

$$
\begin{aligned}
\sigma &= \rho \frac{\partial \psi}{\partial \varepsilon_{\mathrm{e}}}, \\
\sigma_{\mathrm{p}} &= -\mathrm{curl}\left(\rho \frac{\partial \psi}{\partial \alpha_{\mathrm{p}}}\right), \\
\mathbf{q} &= -\left(\rho \frac{\partial \psi}{\partial \alpha_{\mathrm{p}}}\right) \dot{\times} \dot{\varepsilon}_{\mathrm{p}}, \\
\eta &= -\frac{\partial \psi}{\partial T}.
\end{aligned}
\tag{4.6}
$$

In (4.6) symbol $\dot{\times}$ denotes the double product: the scalar one over the first indices and the vector one over the second indices, i.e. $\dfrac{\partial \psi}{\partial \alpha_{\mathrm{p}ij}} \dot{\varepsilon}_{\mathrm{p}}^{ik} e^{j}{}_{kl}$. Fundamental equation describing the plastic flow in the continuum theory of dislocations takes the form

$$
\dot{\varepsilon}_{\mathrm{p}} = \alpha_{\mathrm{p}} \times \mathbf{v}_{\mathrm{p}}, \tag{4.7}
$$

where $\mathbf{v}_{\mathrm{p}}$ denotes the dislocation velocity vector, cf. [19, 23].

4.2. Driving forces on the dislocation field

The driving force is a sum of Peach-Koehler forces and the configuration force. Peach-Koehler force describes the influence of stress field on dislocation, cf. [26] and more general [10], while configuration force describes the influence of spatial configuration of all dislocation on each dislocation. The configuration force is responsible for minimization of the stored energy due to dislocations configuration. The favorable dislocations configurations are often called the low energy dislocation structures [20]. This force gives direct information on the direction of the reorientation process. Using (4.7), relations (4.5) and (4.6) can be rewritten in the form

$$
\begin{aligned}
(\mathbf{f} - \mathbf{f}_{\mathrm{p}})\mathbf{v}_{\mathrm{p}} + \frac{\mathbf{q}_T}{T} \nabla T &\geq 0, \\
\mathbf{q} &= k_{\mathrm{p}} \mathbf{v}_{\mathrm{p}},
\end{aligned}
$$

where

$$
\begin{aligned}
\mathbf{f} &= \sigma \dot{\times} \alpha_{\mathrm{p}}, \\
\mathbf{f}_{\mathrm{p}} &= \sigma_{\mathrm{p}} \dot{\times} \alpha_{\mathrm{p}}, \\
k_{\mathrm{p}} &= \frac{\partial \psi}{\partial \alpha_{\mathrm{p}}} : \alpha_{\mathrm{p}}.
\end{aligned}
\tag{4.8}
$$

In the above equations $\mathbf{f}$ denotes the elastic force acting on the dislocation field – the Peach-Koehler force, while $\mathbf{f}_{\mathrm{p}}$ denotes the configuration force. According to the obtained thermodynamic restrictions, the dislocation velocity constitutive equation (plastic flow equation) can be assumed in the following form:

$$\mathbf{v}_{\mathrm{p}} = \mathbf{v}_{\mathrm{p}}(\mathbf{f} - \mathbf{f}_{\mathrm{p}}, \alpha_{\mathrm{p}}, T). \tag{4.9}$$

The configuration force $\mathbf{f}_{\mathrm{p}}$ is responsible mainly for the self-reorganization of dislocation field towards formation of the grain boundaries. This force is parallel to the gradient of dislocation density field, but takes usually the opposite sign to the above gradient. Therefore, a continuous field of unbalanced (monomial) dislocation tends to concentrations in narrow regions, what in terms of the continuum theory of dislocations corresponds to the process of subgrain boundary formation. Similar role on discrete dislocations plays the Peach-Koehler force. The energy of local stress field around dislocations must be taken into account in the energy equation assumed on the continuum dislocation field level, see (4.4). The role of configuration force can be also considered in terms of the Baushinger force (by analogy to the Baushinger stress) induced e.g. by the pile-up of discrete dislocations on the existing grain boundaries.

4.3. Thermodynamics of the orientation discontinuity surface

Let us consider translational motion of the orientation discontinuity surface. Due to dislocation models of the grain boundary, we consider only a small angle discontinuity surface (e.g. up to 15° for germanium). For such a case we assume the following conditions:

1. The surface possesses densities of mass, energy and entropy, but the fluxes of the above quantities vanish on the surface.
2. The surface density of mass on the discontinuity surface is constant.
3. The displacement field is continuous with the piecewise continuous first and second-order derivatives, i.e. the grain boundary sliding is excluded.
4. The temperature field is continuous on the orientation discontinuity surface.

The attributes of such a surface allow to call it stationary discontinuity. Let us denote the discontinuity surface velocity by $\mathbf{w}_{\mathrm{gb}}$. Then the local velocity vector of the surface motion (grain boundary velocity) is $\mathbf{v}_{\mathrm{gb}} = \mathbf{w}_{\mathrm{gb}} - \mathbf{v}$. Additionally, we assume convection parameterization of the surface. The velocity of a material point lying on the discontinuity surface at a given time denoted by $\mathbf{v}$ can be decomposed into normal and tangential parts

$$\mathbf{v} = v_{\mathrm{n}}\mathbf{n}_{\mathrm{gb}} + v^{\alpha}\mathbf{i}_{\alpha},$$

where $\mathbf{i}_\alpha$ denotes the local base vectors tangent to the coordinates on the surface. This allows us to define the time derivative of arbitrarily chosen scalar density ω for points lying outside the surface and ω_{gb} for points inside the surface, see [17].

$$\dot{\omega} \equiv \frac{\partial \omega}{\partial t}|_{X=\mathrm{const}} + \mathrm{grad}\,\omega \cdot \mathbf{v},$$

$$\overset{\circ}{\omega}_{\mathrm{gb}} \equiv \frac{\partial \omega_{\mathrm{gb}}}{\partial t}|_{\mathrm{i}_\alpha=\mathrm{const}} + \omega_{\mathrm{gb},\alpha}\mathbf{v}^\alpha.$$

Due to the mass balance and the assumed zero surface flux of mass, the mass flux across the discontinuity surface satisfies the condition

$$\pi_{\mathrm{gb}} = \rho^+ \mathbf{v}^+_{\mathrm{gb}} \cdot \mathbf{n}_{\mathrm{gb}} = \rho^- \mathbf{v}^-_{\mathrm{gb}} \cdot \mathbf{n}_{\mathrm{gb}}. \tag{4.10}$$

With respect to the kinematical constraints, total velocity of the surface must assume the same value on both sides of this surface, i.e.

$$(\mathbf{v}^+_{\mathrm{gb}} + \mathbf{v}^+)\mathbf{n}_{\mathrm{gb}} = (\mathbf{v}^-_{\mathrm{gb}} + \mathbf{v}^-)\mathbf{n}_{\mathrm{gb}},$$

which implies the relation of jump in local velocity of the grain boundary to the jump in the continuum velocity, namely

$$\lceil \mathbf{v}_{\mathrm{gb}} \rceil \mathbf{n}_{\mathrm{gb}} = -\lceil \mathbf{v} \rceil \mathbf{n}_{\mathrm{gb}}. \tag{4.11}$$

Such restriction implies the following set of equations on the discontinuity surface, cf. (4.1) – (4.2),

$$\begin{aligned} \lceil \rho \mathbf{v}_{\mathrm{gb}} \rceil \mathbf{n}_{\mathrm{gb}} &= 0, \\ \lceil \boldsymbol{\sigma} + \rho \mathbf{v} \otimes \mathbf{v}_{\mathrm{gb}} \rceil \mathbf{n}_{\mathrm{gb}} &= \mathbf{0}, \end{aligned} \tag{4.12}$$

$$\lceil \rho u \mathbf{v}_{\mathrm{gb}} + \frac{1}{2}\rho(\mathbf{v}\cdot\mathbf{v})\mathbf{v}_{\mathrm{gb}} + \mathbf{v}\boldsymbol{\sigma} - \mathbf{q}_T - k_{\mathrm{p}}(\mathbf{v}_{\mathrm{p}} - \mathbf{v}_{\mathrm{gb}}) \rceil \mathbf{n}_{\mathrm{gb}} = \rho_{\mathrm{gb}} \overset{\circ}{u}_{\mathrm{gb}}, \tag{4.13}$$

$$\lceil -\rho\eta \mathbf{v}_{\mathrm{gb}} + \frac{\mathbf{q}_T}{T} \rceil \mathbf{n}_{\mathrm{gb}} + \rho_{\mathrm{gb}} \overset{\circ}{\eta}_{\mathrm{gb}} \geq 0, \tag{4.14}$$

where ρ_{gb} denotes the surface mass density. Substituting (4.10) and (4.11) into (4.13), inequality (4.14) takes the form

$$\pi_{\mathrm{gb}} \lceil \psi \rceil + \mathbf{n}_{\mathrm{gb}} \boldsymbol{\sigma} \lceil \mathbf{v} \rceil - \lceil k_{\mathrm{p}}(\mathbf{v}_{\mathrm{p}} - \mathbf{v}_{\mathrm{gb}}) \rceil \mathbf{n}_{\mathrm{gb}} - \rho_{\mathrm{gb}} \overset{\circ}{\psi}_{\mathrm{gb}} - \rho_{\mathrm{gb}} \eta_{\mathrm{gb}} \overset{\circ}{T} \geq 0, \tag{4.15}$$

where $\boldsymbol{\sigma} = \frac{1}{2}(\boldsymbol{\sigma}^+ + \boldsymbol{\sigma}^-)$. To determine the thermodynamical driving forces on the surface we must postulate the state variables on surface. Our approach is based

on the assumption that misorientation should be incorporated into constitutive modelling of the reorientation process. To do this let us assume, that the constitutive equation for the surface free energy density depends on misorientation and temperature, i.e.

$$\boxed{\psi_{\mathrm{gb}} = \psi_{\mathrm{gb}}(\Delta_{\mathrm{p}}\boldsymbol{\varphi}, T).} \tag{4.16}$$

If we take into account that in our formalism the Born rule holds, then the same restriction for the surface free energy density is obtained as those assumed by CERMELLI and SELLERS in [3]. This postulate is crucial for the analysis and it has strong consequences on the shape of driving forces. Substituting (4.16) to (4.15) we get

$$\pi_{\mathrm{gb}}\lceil\psi\rceil + \mathbf{n}_{\mathrm{gb}}\sigma\lceil\mathbf{v}\rceil - \lceil k_{\mathrm{p}}(\mathbf{v}_{\mathrm{p}} - \mathbf{v}_{\mathrm{gb}})\rceil\mathbf{n}_{\mathrm{gb}} - \mathbf{m}_{\mathrm{p}}\,\overset{\circ}{\Delta_{\mathrm{p}}\boldsymbol{\varphi}} - \rho_{\mathrm{gb}}\,\overset{\circ}{T}\left(\frac{\partial\psi_{\mathrm{gb}}}{\partial T} + \eta_{\mathrm{gb}}\right) \geq 0, \tag{4.17}$$

where

$$\mathbf{m}_{\mathrm{p}} = \rho_{\mathrm{gb}}\frac{\partial\psi_{\mathrm{gb}}}{\partial\Delta_{\mathrm{p}}\boldsymbol{\varphi}}. \tag{4.18}$$

To satisfy (4.17) for all possible process, we find

$$\eta_{\mathrm{gb}} = -\frac{\partial\psi_{\mathrm{gb}}}{\partial T}. \tag{4.19}$$

It is easy to realize that $\mathbf{m}_{\mathrm{p}}$ has the meaning of the misorientation vector driving force. Traditionally η_{gb} in (4.19) denotes entropy density of the grain boundary. Additionally, using (4.11) and (4.12), the jump in continuum velocity can be expressed as

$$\lceil\mathbf{v}\rceil = -\lceil\frac{1}{\rho}\rceil\mathbf{n}_{\mathrm{gb}}\pi_{\mathrm{gb}}. \tag{4.20}$$

Let us define the right and left dislocation flux vectors to the boundary, namely

$$\pi_{\mathrm{p}}^{\pm} = \mp\mathbf{n}_{\mathrm{gb}}\cdot(\mathbf{v}_{\mathrm{p}}^{\pm} - \mathbf{v}_{\mathrm{gb}}^{\pm}).$$

It can be established, that[1]

[1]Using (3.1) we find $\overset{\circ}{\Delta_{\mathrm{p}}\boldsymbol{\varphi}} = -\mathbf{n}_{\mathrm{gb}}\cdot\lceil\overset{\circ}{\boldsymbol{\varepsilon}_{\mathrm{p}}}\rceil\times\mathbf{n}_{\mathrm{gb}} + \frac{1}{2}\mathbf{n}_{\mathrm{gb}}\mathrm{tr}\left(\lceil\overset{\circ}{\boldsymbol{\varepsilon}_{\mathrm{p}}}\rceil\times\mathbf{n}_{\mathrm{gb}}\right)$
$= -\mathbf{n}_{\mathrm{gb}}\cdot\lceil\dot{\boldsymbol{\varepsilon}}_{\mathrm{p}} + \nabla\boldsymbol{\varepsilon}_{\mathrm{p}}\,\mathbf{v}_{\mathrm{gb}}\rceil\times\mathbf{n}_{\mathrm{gb}} + \frac{1}{2}\mathbf{n}_{\mathrm{gb}}\mathrm{tr}(\lceil\dot{\boldsymbol{\varepsilon}}_{\mathrm{p}} + \nabla\boldsymbol{\varepsilon}_{\mathrm{p}}\,\mathbf{v}_{\mathrm{gb}}\rceil\times\mathbf{n}_{\mathrm{gb}})$
$= -\mathbf{n}_{\mathrm{gb}}\cdot\lceil\dot{\boldsymbol{\varepsilon}}_{\mathrm{p}} + \nabla_{<}\boldsymbol{\varepsilon}_{\mathrm{p}>}\,\mathbf{v}_{\mathrm{gb}} + \nabla_{(}\boldsymbol{\varepsilon}_{\mathrm{p})}\,\mathbf{v}_{\mathrm{gb}}\rceil\times\mathbf{n}_{\mathrm{gb}}$
$+ \frac{1}{2}\mathbf{n}_{\mathrm{gb}}\mathrm{tr}\left(\lceil\dot{\boldsymbol{\varepsilon}}_{\mathrm{p}} + \nabla_{<}\boldsymbol{\varepsilon}_{\mathrm{p}>}\,\mathbf{v}_{\mathrm{gb}} + \nabla_{(}\boldsymbol{\varepsilon}_{\mathrm{p})}\,\mathbf{v}_{\mathrm{gb}}\rceil\times\mathbf{n}_{\mathrm{gb}}\right)$
$= -\mathbf{n}_{\mathrm{gb}}\cdot\lceil\boldsymbol{\alpha}_{\mathrm{p}}\times\mathbf{v}_{\mathrm{p}} + \nabla_{<}\boldsymbol{\varepsilon}_{\mathrm{p}>}\,\mathbf{v}_{\mathrm{gb}} + \nabla_{(}\boldsymbol{\varepsilon}_{\mathrm{p})}\,\mathbf{v}_{\mathrm{gb}}\rceil\times\mathbf{n}_{\mathrm{gb}}$
$+ \frac{1}{2}\mathbf{n}_{\mathrm{gb}}\mathrm{tr}\left(\lceil\boldsymbol{\alpha}_{\mathrm{p}}\times\mathbf{v}_{\mathrm{p}} + \nabla_{<}\boldsymbol{\varepsilon}_{\mathrm{p}>}\,\mathbf{v}_{\mathrm{gb}} + \nabla_{(}\boldsymbol{\varepsilon}_{\mathrm{p})}\,\mathbf{v}_{\mathrm{gb}}\rceil\times\mathbf{n}_{\mathrm{gb}}\right)$
$= -\mathbf{n}_{\mathrm{gb}}\cdot\lceil\boldsymbol{\alpha}_{\mathrm{p}}\times(\mathbf{v}_{\mathrm{p}} - \mathbf{v}_{\mathrm{gb}}) + \nabla_{(}\boldsymbol{\varepsilon}_{\mathrm{p})}\,\mathbf{v}_{\mathrm{gb}}\rceil\times\mathbf{n}_{\mathrm{gb}} + \frac{1}{2}\mathbf{n}_{\mathrm{gb}}\mathrm{tr}\left(\lceil\boldsymbol{\alpha}_{\mathrm{p}}\times(\mathbf{v}_{\mathrm{p}} - \mathbf{v}_{\mathrm{gb}}) + \nabla_{(}\boldsymbol{\varepsilon}_{\mathrm{p})}\,\mathbf{v}_{\mathrm{gb}}\rceil\times\mathbf{n}_{\mathrm{gb}}\right).$

$$\overset{\circ}{\Delta}_{\mathrm{p}}\varphi = \pi_{\mathrm{p}}^{+}\,\mathrm{angl}(\alpha_{\mathrm{p}}^{+}\times\mathbf{n}_{\mathrm{gb}}) + \pi_{\mathrm{p}}^{-}\,\mathrm{angl}(\alpha_{\mathrm{p}}^{-}\times\mathbf{n}_{\mathrm{gb}}) + \pi_{\mathrm{gb}}\,\mathrm{angl}\lceil\frac{\nabla(\varepsilon_{\mathrm{p}})\cdot\mathbf{n}_{\mathrm{gb}}}{\rho}\rceil, \tag{4.21}$$

where, for each tensor $\mathbf{t}$, operator $\mathrm{angl}\,\mathbf{t}$ is defined as

$$\mathrm{angl}\,\mathbf{t} \overset{df}{=} \mathbf{n}_{\mathrm{gb}}\cdot\mathbf{t}\times\mathbf{n}_{\mathrm{gb}} + \frac{1}{2}\mathbf{n}_{\mathrm{gb}}\mathrm{tr}\mathbf{t}.$$

By the use of (4.21), the entropy inequality (4.17) in the isothermal conditions can be rewritten in the form

$$t_{\mathrm{gb}}\pi_{\mathrm{gb}} + t_{\mathrm{p}}^{+}\pi_{\mathrm{p}}^{+} + t_{\mathrm{p}}^{-}\pi_{\mathrm{p}}^{-} \geq 0, \tag{4.22}$$

where

$$t_{\mathrm{gb}} = \lceil\psi\rceil - \mathbf{n}_{\mathrm{gb}}\cdot\sigma\cdot\mathbf{n}_{\mathrm{gb}}\lceil\frac{1}{\rho}\rceil - \mathbf{m}_{\mathrm{p}}\cdot\mathrm{angl}\lceil\frac{\nabla(\varepsilon_{\mathrm{p}})\cdot\mathbf{n}_{\mathrm{gb}}}{\rho}\rceil, \tag{4.23}$$

$$t_{\mathrm{p}}^{\pm} = k_{\mathrm{p}}^{\pm} - \mathbf{m}_{\mathrm{p}}\cdot\mathrm{angl}(\alpha_{\mathrm{p}}^{\pm}\times\mathbf{n}_{\mathrm{gb}}). \tag{4.24}$$

In above equations t_{gb} and t_{p} denote driving forces conjugate to: the jump in the respective quantities on the boundary and the existing dislocation around the boundary. In order to complete the thermodynamical formulation of the theory, the manner in which the grain boundary migrates, should be given.

Constitutive equation for a grain boundary migration. According to known experimental data i.e. [4], the mobility of grain boundary depends mainly on misorientation, temperature, concentration of precipitations and driving forces described by (4.23) and (4.24). According to the thermodynamic restrictions obtained in the previous subsection we can assume a constitutive equation for fluxes across the boundary. Taking into account the driving forces, misorientation and temperature, the constitutive equations for the mass and dislocation flux through the grain boundary can be stated in the form

$$\pi_{\mathrm{gb}} = \pi_{\mathrm{gb}}(t_{\mathrm{gb}}, \Delta_{\mathrm{p}}\varphi, T), \tag{4.25}$$

$$\pi_{\mathrm{p}}^{\pm} = \pi_{\mathrm{p}}^{\pm}(t_{\mathrm{p}}^{\pm}, \Delta_{\mathrm{p}}\varphi, T). \tag{4.26}$$

Equation (4.26) does not mean that a single dislocations have to overcome a grain boundary, but it means that the proportion between the annihilation of dislocations on one side and production of them on the second side subject to a limitation imposed on this process by energy of the grain boundary, according to (4.26) and (4.24). According to the thermodynamic balance we have determined

a thermodynamic force t_{p} yielding from the change of grain misorientation energy inherently related to the production and annihilation of dislocations on the grain boundary. For example, it is known that some orientations of grains in polycrystals are observed more often than others. Our paper is devoted to thermodynamic reasons of this effect obtained from thermodynamics of the grain reorientation process. It is worth emphasizing that in terms of the classical theory of crystal plasticity, this effect cannot be described as far as the grain misorientation energy will be incorporated into thermodynamic considerations on elastic-plastic deformations.

The constitutive equation (4.25) describes the mass flux over the grain boundary, what means that this equation describes nothing more than the migration of grain boundary. This is induced by the jump in the specific free energy on the opposite sides of boundary, cf. (4.25) and (4.23). In real crystals another component of the driving force often exists when the strongly dislocated structure on one side of the grain is recovered on the second side in the form of the nucleation and growth of new (undislocated) grain. So, the force t_{gb} can be treated here only as a part of the resulting driving force governing the migration of grain boundaries in real crystals. The main part of this force results from the difference of the free energy of dislocated and recovered grains on opposite sides of the grain boundary. Equation (4.23) describes a component induced by unbalanced dislocations, which bend crystal lattice within grains.

5. Final remarks

In this paper, a thermodynamical solution for the grain reorientation process and the conjugated driving forces has been derived. In the presented approach it has been assumed that the surface density of the free energy depends on the misorientation vector. It is worth emphasizing that in material science the influence of lattice misorientation on the energy of low angle grain boundaries is well established, cf. [14], while from the viewpoint of continuum thermodynamics of plastic deformation such a dependence is usually ignored.

According to the symmetry of crystal lattice, to a given boundary several vectors of jump in orientation can be attributed. Even in the case of asymmetric unit there exist two misorientation vectors with the lengths: $\Delta\varphi$ and $\Delta\varphi' = (2\pi - \Delta\varphi)$. In real crystal lattices e.g. for fcc crystal, we can assign 48 mutually different orientation vectors for a single boundary. The choice of real vector of jump in orientation corresponds to the choice of a certain inner grain boundary structure. This suggests that in oreder to describe properly the single-valued grain reorientation process, initial orientations of grains around boundary should be included.

The effect of grain reorientation has been described here in the spirit of the macroscopic dislocation theory. We have shown, how the influence of the grains misorientation on the reorientation process can be described in terms of continuum theory of dislocations. As a result of the dependence of surface energy on the misorientation vector, additional terms have been obtained in the equation of driving force of grain boundary motion.

On the other hand, from the viewpoint of the general continuum theory of defects our approach concerns only a thermodynamic solution obtained in terms of the dislocation theory. For example, in terms of the disclination theory we should assume that a constitutive dependence for surface energy takes into account not only the dependence on the misorientation vector, but also on its gradient along the boundary. This gradient corresponds to continuous distribution of disclinations along grain the boundary. For a discrete wedge disclination, understood as a line bounding the grain boundary within a crystal, the gradient will reduce to the delta distribution at the edge of the grain boundary identified with disclination line. Therefore the disclination model needs the determination of the discontinuity conditions of higher order than those considered in the present paper. It is most probable that to balance the energy, which is dependent on the misorientation gradient along the grain boundary, the polar elasticity could appear to be indispensable. Then the polar elasticity could play a similar role as the symmetric elasticity employed here to the dislocation theory. Thus, our approach concerns thermodynamics of crystal lattice misorientation considered in terms of a discontinuity surface analyzed in the framework of the dislocation theory and the symmetric elasticity. It is worth emphasizing that in real crystals the grain boundaries usually show a constant misorientation vector along the boundary; moreover, boundaries do not end within a crystal by disclinations – therefore, from the viewpoint of the authors, the dislocational model of the grain boundary seems to be much closer to thermodynamics of low-angle grain boundaries than the considerably more advanced disclination/dislocation model.

Acknowledgement

This research was supported by the State Committee for Scientific Research (KBN) in Poland under Grant No. 7T07A00416.

References

1. R. ABREYARATNE and J. KNOWLES, *On the driving traction acting on a surface of strain discontinuity in a continuum*, J. Mech. and Phys. of Solids, **38**, 3, 345–360, 1990.

2. P. CERMELLI and S. SELLERS, *On the nonlinear mechanics of Bravais crystals with continuous distributions of defects*, Mathematics and Mechanics of Solids, **3**, 3, 331–358, 1998.

3. P. CERMELLI and S. SELLERS, *Multi-phase equilibrium of crystalline solids*, J. Mech. and Phys. of Solids, **48**, 4, 765–796, 2000.

4. G. A. CHADWICK and D. A. SMITH, *Grain boundary structure and properties*, Academic Press, 1976.

5. C. DAVINI, *A proposal for a continuum theory of defective crystals*, Archive for Rational Mechanics and Analysis, **96**, 295–317, 1986.

6. R. DE WITT, *A view of the relation between the continuum theory of lattice defects and non-Euclidean geometry in the linear approximation*, Int. J. of Engng. Sci., **19**, 12, 1475–1506, 1981.

7. P. DŁUŻEWSKI, *Continuum theory of dislocations as a theory of constitutive modelling of finite elastic-plastic deformations*, Habilitations Thesis. IFTR Reports 13/1996, Warsaw 1996.

8. P. DŁUŻEWSKI, *On geometry and continuum thermodynamics of structural defect movement*, Mech. of Mat., **22**, 23–41, 1996.

9. A. C. ERINGEN and C. B. KAFADAR, *Polar field theories*, [In:] A. C. ERINGEN [Ed.], Continuum Physics, **4**, 1–73, Academic Press, New York 1976.

10. J. D. ESHELBY, *The force on an elastic singularity*, Philosophical Trans. of the Roy. Soc. of London, **A244**, 87, 112, 1951.

11. J. D. ESHELBY, *Energy relations and the energy-momentum tensor in continuum mechanics*, [In:] M. F. KANNINEN, W. F. ADLER, A. R. ROSENFIELD and R. I. JAFFEE [Eds.], Inelastic Behavior of Solids, 77–114, McGraw-Hill, New York 1970.

12. N. FOX, *A dislocation theory for oriented media*, [In:] M. F. KANNINEN, W. F. ADLER, A. R. ROSENFIELD and R. I. JAFFEEE [Eds.], Inelastic Behavior of Solids, 349–377, McGraw-Hill, New York 1970.

13. N. A. GJOSTEIN, *Short circuit diffusion*, [In:] Diffusion, Metals Park, Ohio 1973.

14. M. GRABSKI, *Structure of grain boundaries in metals* [in Polish], BFM Śląsk, Katowice 1969.

15. M. E. GURTIN, *The nature of configurational forces*, Archive for Rational Mechanics and Analysis, **131**, 1–66, 1995.

16. M. KLÉMAN, *Dislocation, disclinations and magnetisms*, [In:] F. R. N. NABARRO [Ed.], Dislocations in solids, **5**, 349, North-Hollands 1980.

17. W. KOSIŃSKI, *Field singularities and wave propagation analysis in continuum mechanics*, PWN, Warsaw 1986.

18. E. KOSSECKA and R. de WITT, *Disclination kinematics*, Arch. Mech., **29**, 5, 633–651, 1977.

19. E. KRÖNER, *Continuum theory of defects*, [In:] J. P. BALIAN, M. KLEMAN [Eds.], Physics if Defects, 215–315, Nord-Holland, Amsterdam 1981.

20. D. KUHLMANN-WILSDORF, *Theory of plastic deformation – properties of low energy dislocation*, Mat. Sci. and Engng., **A113**, 1–41, 1989.

21. K. C. LE and H. STUMPF, *nonlinear continuum theory of dislocations*, Int. J. of Engng. Sci., **57**, 3, 255–280, 1974.

22. G. P. MOECKEL, *Thermodynamics of an interface*, Archive for Rational Mechanics and Analysis, **57**, 3, 255–280, 1974.

23. T. MURA, *Method of continuously distributed dislocations*, [In:] T. MURA [Ed.], Mathematical Theory of Dislocations, The American Society of Mechanical Engineers, 25–48, New York 1969.

24. P. M. NAGHDI and A. R. SRINIVASA, *Characterisation of dislocations and their influence on plastic deformation in single crystals*, Int. J. of Engng. Sci., **32**, 7, 1157–1182, 1994.

25. J. F. NYE, *Some geometrical relations for dislocated crystals*, Acta Metall., **1**, 153–162, 1953.

26. M. O. PEACH and J. S. KOEHLER, *The forces exerted on dislocations and the stress fields produced by them*, Phys. Rev., **80**, 436, 1950.

27. R. C. POND, *Line defects in interfaces*, [In:] F. R. N. NABARRO [Ed.], Dislocations in solifs, **8**, 1–67, North-Holland 1989.

28. S. SUN, B. l. ADAMS and W. E. KING, *Observations of lattice curvature near the interface of a deformed aluminium bicrystal*, Philosophical Magazine A, **80**, 1, 9–25, 2000.

29. C. TEODOSIU, *A dynamic theory of dislocations and its applications to the theory of the elastic plastic continuum*, [In:] A. SIMMONDS [Ed.], Fundamental Aspects of Dislocation Theory, Nat. Bur. Stand. Spec. Publ., **317**, 2, 1–36, 1970.

30. G. ZANZOTTO, *On the material symetry group of elastic crystal and the Born rule*, Archive for Rational Mechanics and Analysis, **121**, 1, 1–36, 1992.

31. H. ZORSKI, *Force on a defect in nonlinear elastic medium*, Int. J. of Engng. Sci., **19**, 1573, 1980.

Received May 26, 2000; revised version December 6, 2000.

Arch. Mech., **53**, 2, pp. 123–150, Warszawa 2001

Laminar dispersed two-phase flows at low concentration III Pseudo-turbulence

J. L. ACHARD and A. CARTELLIER

Laboratoire des Écoulements Géophysiques et Industriels
CNRS-UJF-INPG, B.P. 53X, 38041 Grenoble Cedex, France
e-mail: Jean-Luc.Achard@hmg.inpg.fr

TWO PRECEDING PAPERS (Parts I and II) present a generalised system of equations to describe non-turbulent flows of inclusion-fluid mixtures. The two first-order equations for each phase correspond to equations of the standard two-fluid models. The closure problem, consisting in the derivation of constitutive laws for unknown quantities (mainly interaction terms between phases) is not encountered in our approach; these quantities are provided by two infinite sequences of higher order equations controlling more and more conditioned "disturbance fields". The difficulty is then to truncate in a consistent way these sequences using a dilutness assumption. Agitation terms are also unknowns, both in first and higher orders equations. These terms, which result from various types of micro-motions of both phases (the so-called pseudo-turbulence phenomena), have not been related to disturbance fields at the end of the two preceding papers; they just came out as unclosed correlation functions. This paper gives each correlation function a specific expression; some of them must be approximated due to dilutness in order to be effectively computed.

1. Introduction

VERY EARLY IN THE DERIVATION of averaged two-phase flows models, BUYEVICH [3, 4] was one of a few authors to discuss agitation terms which influence the bulk momentum transfer of both the inclusions and the continuous phase, as soon as inertia effects are important. Even if they appear as formally similar unknown correlations, they represent six (at least) different types of phenomena. It is worth to start a preliminary discussion of the physical origin of these types which renews that proposed by BUYEVICH and SHCHELCHKOVA [5]. Recall that two-phase flows considered in our analysis must be dilute since otherwise the collisions between inclusions become an essential and quite distinct mechanism of agitation.

The first case to adress corresponds to turbulent motions of the carrying phase modified by inclusions; turbulence would even exist in the absence of inclusions. Particle-turbulence interactions have been experimentally investigated in a number of situations. Among these, let us quote bubbly flows in basic tur-

bulence fields studied by LANCE and collaborators [6 – 9], and bubbly flows in ducts [10, 11]. Interactions with solid particles have been considered notably by TSUJI *et al.* [12] and by FAETH and coworkers [13, 14]. Even under turbulent conditions, the role of the particle-induced turbulence has been emphasized, but it is experimentally quite difficult to distinguish this contribution from that of the shear-induced turbulence. On the other hand, DNS has thrown some light on the turbulence modulation by small rigid inclusions of variable inertia [15, 16, 17]. To illustrate the complex coupling between phases occuring even at low concentrations, let us mention the occurence of a preferential accumulation of inert particles in regions of low vorticity or high strain rate, a phenomena first identified from simulations [18, 19, 20]. The case of bubbles has also been adressed [21]. More practical and more versatile models are also extracted from all these fundamental studies [22].

The second possibility is that correlation functions may result from the turbulent motion of the carrying phase solely induced by inclusions. The very presence of inclusions may trigger the hydrodynamic unstability of the fluid flow which would be otherwise laminar. This case seems to be beyond our present analysis capabilities (cf. Sec. 3 – Part I).

Surface tension is unable to maintain spherical bubbles and drops against various forces (gravity, inertia, viscosity...) beyond some size. Then, inclusion shapes result from interactions with the ambient fluid, causing generally highly complex free boundary value problems. Interfaces are subjected to various instabilities generating pulsations in both phases. Inclusion trajectories themselves can be spiraling, pulsating, zig-zagging (CLIFT *et al.* [23]) due to shape oscillations or simply modifications (i.e. sphere to ellipsoid) associated to vortex shedding. The ensuing determination of agitation terms due to this third mechanism in the bulk equations is still in infancy, but progress can be expected in the near future from DNS undertaken on bubbly flows [24].

Very small suspended particles (colloidal particles) may be affected by translational (or rotational if they are non-spherical) Brownian motion (RUSSEL *et al.* [25]). To describe this constant state of random motion, a particle velocity autocorrelation function is first calculated from the Langevin equation and then the time change of the variance in position follows; finally, the diffusion coefficients useful for a "population balance" approach (first kinetic equation) can be estimated. An exhaustive study of the influence of Brownian motion is now available. This mechanism of agitation (restricted here to inclusions) as well as the three preceding ones (affecting both phases) are excluded from our analysis. We are left with the two last ones which will be adressed now.

Any local technique for continuous phase velocity measurements in two-phase flows, records inevitably pulsations caused by the local distortions in the fluid flow streamlines caused by the submerged inclusions. They occur in the potential

fields at the fore-part, possibly in the viscous boundary layers and mainly in the wake regions. To understand the origin and to have the first estimate of the corresponding fluid velocity variance tensors, it is possible to refer to a deterministic approach. Then, one considers a given dispersed two-phase flow characterized by a configuration of particles having an idealised order: for instance, the particles can be equal-sized spheres arranged in periodic arrays (see the pioneering work of HASIMOTO [26]); at zero or low Reynolds numbers, the corresponding hydrodynamic fields can be solved exactly. The method of homogenisation, which is basically a two-scale method, falls also into this category, when at least it is effectively implemented (MIKSIS and TING, [27]). The result is a macroscopic system of equations for the hydrodynamical variables and the coefficients in this system are given by solving a microscopic problem for a cell to close all unknown terms, and among them, the agitation tensor. This is in essence the approach of NIGMATULIN [28] which proposed an expression for such a tensor based on a potential flow cellular scheme. To our knowledge, there are very few attemps in the literature to calculate variance tensors in various flows conditions (complete range of volume fraction of solid spheres, spherical bubbles, high Reynolds number flows...) having a "frozen configuration", though the corresponding models exist.

In turns out that configurations of particles seldom (if ever) maintain a regular order (CARTELLIER *et al.* [29]); they are very unstable for increasing dispersed phase concentration and decreasing continuous phase viscosity. The time evolution of any configuration of particles which interact together via the suspending fluid, constitutes a highly nonlinear multibody process. The interparticle interaction is accomplished through random pressure and velocity fields in the ambient fluid; this induces lateral and longitudinal pulsations of the particles with respect to a preferred direction and, second, to pulsations in the fluid itself. This so-called "pseudo-turbulence" of both phases which is anisotropic, causes the initiation of additional stresses at the bulk level. This is the last mechanism of agitation we describe. The relevant literature will be evoked in Sec. 4.4.

We will see in our paper that we can pass on in a continuous way from the fourth mechanism description to the fifth one as the concentration Θ increases. To point out the whole process, we restrict our interest to the same type of idealised dispersed two-phase flows which have been selected in the preceding papers [1, 2] (referred to as Parts I and II); e.g. these flows carry spherical inclusions having a radius a small compared to the length scale L of the averaged flows. The concentration Θ or averaged dispersed phase volume fraction is defined by $\Theta = N(a/\mathrm{L})^3$, where N is the total number (assumed to be very large) of inclusions in the studied system, is supposed to be small. Finally, recall that at the end of the Sec. 4 of Part II, all equations of the Lundgren Hierarchy and of the B.B.G.K.Y. hierarchy and, besides, boundary conditions between these

two sets of equations at any order but the first one, have been transformed into equations for averaged disturbance flows. The only unclosed terms are agitation terms of various types.

The first three sections adress the velocity variance tensors (agitation or pseudo-turbulent tensors) involving dispersed or continuous phase fluctuations. These tensors differ by their order since they involve fluctuations conditioned by one, two, three inclusions. To get the clue to express any of these tensors in terms of the disturbance fields defined in Part II, we show first in Sec. 2 that any tensor can be expanded in a finite sequence of terms gradually bringing out the contribution of groups of inclusions more and more numerous with respect to the conditioning number characterizing the considered tensor. These expansions open the way to an effective scheme of calculations and two approximation procedures have been devised to simplify them. In Sec. 3, a first approximation based on a preliminary scale analysis exploits diluteness ($\Theta \ll 1$). This assumption precisely permits to extract the leading order terms from the contribution of each group. An extra approximation in Sec. 4 exploits a weak deviation from homogeneity by using a multipole expansion: then only the lowest order multipoles are retained via an asymptotic expansion in terms of $\beta = a/\mathrm{L}$; at the end of this section, proposals available in the literature, concerning some velocity variance tensors we have derived, are briefly compared. In the following two sections, we consider cross-correlations combining properties relative to both phases. In Sec. 5, new terms which correlate the continuous phase presence at one location with the inclusion (s) velocity(ies) at a neighbouring point(s) are expressed in terms of the disturbance fields, while in Sec. 6, fluid-particles velocity covariance tensors (composite agitation tensors) are treated as the above single-phase tensors are. We conclude in Sec. 7 by giving a perspective of this work which will come in a future paper.

2. Expansions of pseudo-turbulent tensors

Pseudo-turbulent tensors appear in momentum equations relative to both phases at any order.

2.1. The dispersed phase pseudo-turbulent tensors

To expand a variance tensor of any order in a finite sequence of contributions relative to groups having an increasing number of test inclusions, we develop a procedure which is based on a property of fine-grained densities introduced in Part I. Given an arbitrary random scalar process $\mathrm{y}(s,t)$, introducing the spiky field of realisations $\delta[\mathrm{y} - \mathrm{y}(s,t)]$ has offered in Part I the possibility to obtain

the standard pdf $\mathcal{P}(\mathrm{y})$ by taking its ensemble average i.e. $\mathcal{P}(\mathrm{y}) = E[\delta\{\mathrm{y} - \mathrm{y}(s,t)\}]$. But if δ is a functional of the random process $\mathrm{y}(s,t)$, it is also, for a given realization, a simple pdf of y having the normalization property $\int \delta\{\mathrm{y} - \mathrm{y}(s,t)\}dy = 1$ by definition of the delta function. Extensions of this property for a vectorial random process $\mathrm{y}(s,t)$ are obvious. For instance, the first order tensor, $\mathbb{A}^1_{\mathrm{uu}}(\mathbf{x})$ defined by (4.24 – Part I) can be cast in the following form:

$$(2.1)\qquad \mathbb{A}^1_{\mathrm{uu}}(\mathbf{x}) = \sum_{i=1}^{N} E[\varphi_i \mathbf{u}'_i \mathbf{u}'_i] = NE[\varphi_1 \mathbf{u}'_1 \mathbf{u}'_1]$$

$$= NE\left[\int \varphi_2(\mathbf{x}^\circ)\varphi_1(\mathbf{x})\mathbf{u}'_1\mathbf{u}'_1(\mathbf{x})d\mathbf{x}^\circ\right] = N\int E[\varphi_2(\mathbf{x}^\circ)\varphi_1(\mathbf{x})\mathbf{u}'_1\mathbf{u}'_1(\mathbf{x})]d\mathbf{x}^\circ,$$

where the integration is performed, for each $\mathbf{x}$, over the sole domain accessible to the single inclusion centred at $\mathbf{x}^\circ$, knowing that another one is located at $\mathbf{x}$, (non-overlapping condition). Note that throughout this paper, the ensemble average operator $E[\ ]$ applied to integrals involving fine-grained quantities (as φ_1, the first order density) is transformed according to the rules established in Sec. 3 – Part I which result from the definition of $E[\ ]$. By means of the definition of the first fluctuation field (i.e. $\varphi_1\mathbf{u}_1 = \varphi_1\overline{\mathbf{u}}^1 + \varphi_1\mathbf{u}'_1$, see Sec. 4.4 – Part I), the integrand of the r.h.s. may in turn be broken down into three parts:

$$(2.2)\qquad NE[\varphi_2(\mathbf{x}^\circ)\varphi_1(\mathbf{x})\mathbf{u}'_1\mathbf{u}'_1(\mathbf{x})] = NE[\varphi_2(\mathbf{x}^\circ)\varphi_1(\mathbf{x})(\mathbf{u}_1 - \overline{\mathbf{u}}^1)(\mathbf{u}_1 - \overline{\mathbf{u}}^1)]$$

$$= NE[\varphi_2(\mathbf{x}^\circ)\varphi_1(\mathbf{x})\mathbf{u}_1\mathbf{u}_1] + NE[\varphi_2(\mathbf{x}^\circ)\varphi_1(\mathbf{x})]\overline{\mathbf{u}}^1\overline{\mathbf{u}}^1$$

$$- 2\overline{\mathbf{u}}^1 E[\varphi_2(\mathbf{x}^\circ)\varphi_1(\mathbf{x})\mathbf{u}_1]$$

and further can be related to a second-order unsymmetrical (with respect to $\mathbf{x}$ and $\mathbf{x}^\circ$) tensor $\mathbb{A}^2_{\mathrm{uu}}(\mathbf{x}|\mathbf{x}^\circ)$, conditional upon the presence at $\mathbf{x}^\circ$ of another inclusion, by introducing the second fluctuation field defined by $\varphi_1\varphi_2\mathbf{u}_1 = \varphi_1\varphi_2\overline{\mathbf{u}}^2 + \varphi_1\varphi_2\mathbf{u}''_1$ (see Sec. 4.4 – Part I):

$$(2.3)\qquad NE[\varphi_2(\mathbf{x}^\circ)\varphi_1(\mathbf{x})\mathbf{u}'_1\mathbf{u}'_1(\mathbf{x})] = \frac{1}{(N-1)}\Big\{\phi^{(2)}\overline{\mathbf{u}}^2\overline{\mathbf{u}}^2 + N(N-1)$$

$$E[\varphi_2(\mathbf{x}^\circ)\varphi_1(\mathbf{x})\mathbf{u}''_1\mathbf{u}''_1(\mathbf{x})] + \phi^{(2)}\overline{\mathbf{u}}^1\overline{\mathbf{u}}^1 - 2\phi^{(2)}(\mathbf{x},\mathbf{x}^\circ)\overline{\mathbf{u}}^1\overline{\mathbf{u}}^2\Big\}$$

$$= \frac{1}{(N-1)}\Big\{\phi^{(2)}\left[\overline{\mathbf{u}}^2(\mathbf{x}|\mathbf{x}^\circ) - \overline{\mathbf{u}}^1(\mathbf{x})\right]\left[\overline{\mathbf{u}}^2(\mathbf{x}|\mathbf{x}^\circ) - \overline{\mathbf{u}}^1(\mathbf{x})\right] + \mathbb{A}^2_{\mathrm{uu}}(\mathbf{x}|\mathbf{x}^\circ)\Big\}.$$

Inserting this result into (2.1) we get:

$$(2.4)\qquad \mathbb{A}^1_{\mathrm{uu}}(\mathbf{x}) = NE[\varphi_1\mathbf{u}'_1\mathbf{u}'_1] = \frac{1}{(N-1)}\int d\mathbf{x}^\circ\Big\{\phi^{(2)}[\overline{\mathbf{u}}^2(\mathbf{x}|\mathbf{x}^\circ) - \overline{\mathbf{u}}^1(\mathbf{x})]$$

$$[\overline{\mathbf{u}}^2(\mathbf{x}|\mathbf{x}^\circ) - \overline{\mathbf{u}}^1(\mathbf{x})] + \mathbb{A}^2_{\mathrm{uu}}(\mathbf{x}|\mathbf{x}^\circ)\Big\}.$$

Likewise, the second order tensor, $\mathbb{A}^2_{\mathrm{uu}}(\mathbf{x}|\mathbf{x}^\circ)$ can be related to an integral for each $\mathbf{x}$ and $\mathbf{x}^\circ$ of $E[\varphi_3(\mathbf{x}^{\circ\circ})\varphi_2(\mathbf{x}^\circ)\varphi_1(\mathbf{x})\mathbf{u}_1''\mathbf{u}_2''(\mathbf{x})]$ over the domain accessible to the single inclusion centred at $\mathbf{x}^{\circ\circ}$ taking into account the non-overlapping condition:

$$\mathbb{A}^2_{\mathrm{uu}}(\mathbf{x}|\mathbf{x}^\circ) = N(N-1)E[\varphi_2(\mathbf{x}^\circ)\varphi_1(\mathbf{x})\mathbf{u}_1''\mathbf{u}_1''(\mathbf{x})] \tag{2.5}$$

$$= N(N-1)E\left[\int \varphi_3(\mathbf{x}^{\circ\circ})\varphi_2(\mathbf{x}^\circ)\varphi_1(\mathbf{x})\mathbf{u}_1''\mathbf{u}_1''(\mathbf{x})d\mathbf{x}^{\circ\circ}\right]$$

$$= \frac{1}{(N-2)}\int d\mathbf{x}^{\circ\circ}\{\phi^{(3)}[\overline{\mathbf{u}}^3(\mathbf{x}|\mathbf{x}^\circ,\mathbf{x}^{\circ\circ}) - \overline{\mathbf{u}}^2(\mathbf{x}|\mathbf{x}^\circ)]$$

$$[\overline{\mathbf{u}}^3(\mathbf{x}|\mathbf{x}^\circ,\mathbf{x}^{\circ\circ}) - \overline{\mathbf{u}}^2(\mathbf{x}|\mathbf{x}^\circ)] + \mathbb{A}^3_{\mathrm{uu}}(\mathbf{x}|\mathbf{x}^\circ,\mathbf{x}^{\circ\circ})\}$$

Clearly we have:

$$\mathbb{A}^3_{\mathrm{uu}}(\mathbf{x}|\mathbf{x}^\circ,\mathbf{x}^{\circ\circ}) = \frac{1}{(N-3)}\int d\mathbf{x}^{\circ\circ\circ}\{\phi^{(4)}[\overline{\mathbf{u}}^4(\mathbf{x}|\mathbf{x}^\circ,\mathbf{x}^{\circ\circ},\mathbf{x}^{\circ\circ\circ}) \tag{2.6}$$

$$-\overline{\mathbf{u}}^3(\mathbf{x}|\mathbf{x}^\circ,\mathbf{x}^{\circ\circ})][\overline{\mathbf{u}}^4(\mathbf{x}|\mathbf{x}^\circ,\mathbf{x}^{\circ\circ},\mathbf{x}^{\circ\circ\circ}) - \overline{\mathbf{u}}^3(\mathbf{x}|\mathbf{x}^\circ,\mathbf{x}^{\circ\circ})]$$

$$+\mathbb{A}^4_{\mathrm{uu}}(\mathbf{x}|\mathbf{x}^\circ,\mathbf{x}^{\circ\circ},\mathbf{x}^{\circ\circ\circ})\}.$$

It is straightforward to derive a recurrent relation in which $\mathbb{A}^j_{\mathrm{uu}}$ is related to $\mathbb{A}^{j+1}_{\mathrm{uu}}$ where j varies from 1 to $N-1$, and where the various domains of integration must take into account a more and more stringent non-overlapping condition. Thus, one property of the above relation is that it can provide in the same shot $\mathbb{A}^1_{\mathrm{uu}}$, $\mathbb{A}^2_{\mathrm{uu}}$ as well as any higher tensor in terms of a sequence involving all the subsequent tensors.

Of course, a similar recurrent relation holds for mixed agitation tensors of the first kind, which are conditional upon the presence around $\mathbf{x}$ (say $\mathbf{x}^\circ$, $\mathbf{x}^{\circ\circ}$, $\mathbf{x}^{\circ\circ\circ}$,...) of various inclusions; e.g. $\mathbb{A}^1_{\mathrm{u}\omega}(\mathbf{x})$ is expressible in terms of $\mathbb{A}^2_{\omega}(\mathbf{x}|\mathbf{x}^\circ)$ which is itself related to $\mathbb{A}^3_{\omega}(\mathbf{x}|\mathbf{x}^\circ,\mathbf{x}^{\circ\circ})$ and so on...

Equations ((4.29) and (4.30) – Part I) require also symmetrical (with respect to $\mathbf{x}$ and $\mathbf{x}^\circ$) agitation tensors as $\mathbb{A}^2_{\mathrm{uu}^\circ}$. We can give it an expression in terms of the third order agitation tensor relative to two positions by decomposing properly $\mathbf{u}''$ and $\mathbf{u}^{\circ\prime\prime}$ thanks to (Sec. 4.4 – Part I) evaluated respectively at $\mathbf{x}$ and at $\mathbf{x}^\circ$:

$$\mathbb{A}^2_{\mathrm{uu}^\circ}(\mathbf{x},\mathbf{x}^\circ) = \frac{1}{(N-2)}\int d\mathbf{x}^{\circ\circ}\{\phi^{(3)}[\overline{\mathbf{u}}^3(\mathbf{x}|\mathbf{x}^\circ,\mathbf{x}^{\circ\circ}) - \overline{\mathbf{u}}^2(\mathbf{x}|\mathbf{x}^\circ)] \tag{2.7}$$

$$\cdot[\overline{\mathbf{u}^\circ}^3(\mathbf{x}^\circ|\mathbf{x},\mathbf{x}^{\circ\circ}) - \overline{\mathbf{u}^\circ}^2(\mathbf{x}^\circ|\mathbf{x})] + \mathbb{A}^3_{\mathrm{uu}^\circ}\}.$$

The second kind of mixed agitation tensor $\mathbb{A}^2_{\omega u^\circ}$ becomes similarly:

$$\mathbb{A}^2_{\omega u^\circ}(\mathbf{x},\mathbf{x}^\circ) = \frac{1}{(N-2)}\int d\mathbf{x}^{\circ\circ}\{\phi^{(3)}[\overline{\omega}^3(\mathbf{x}|\mathbf{x}^\circ,\mathbf{x}^{\circ\circ}) - \overline{\omega}^2(\mathbf{x}|\mathbf{x}^\circ)] \cdot[\overline{\mathbf{u}^\circ}^3(\mathbf{x}^\circ|\mathbf{x},\mathbf{x}^{\circ\circ})) - \overline{\mathbf{u}^\circ}^2(\mathbf{x}^\circ|\mathbf{x})] + \mathbb{A}^3_{\omega u^\circ}\}. \tag{2.8}$$

We have thus shown that any kind of inclusion velocity (linear and rotational) variance tensors could be expressed as finite sums of integrals implying higher and higher pseudo-turbulent tensors. The physical interpretation of the various terms comprised in, say the first order tensor $\mathbb{A}^1_{uu}(\mathbf{x})$, is the following. Each extra term in the infinite sequence gradually brings out the influence of more and more important groups of inclusions upon the first-order agitation tensor. This influence is expressed via increasingly complex space integrals showing definitely its non-local character.

2.2. The continuous phase pseudo-turbulent tensors

There is no basic difference between the ways to expand the velocity variance tensors whether they arise from velocity fluctuations in the dispersed phase or from velocity fluctuations in the continuous phase. For instance, by introducing the presence of an inclusion at $\mathbf{x}^\circ$, the first tensor $\mathbb{A}^1_{vv}$, which involves fluctuations in the continuous phase defined by $X^c\mathbf{v}^c = X^c\overline{\mathbf{v}^c}^1 + X^c\mathbf{v}^{c'}$ (see Sec. 5.4 – Part I), can be cast, in a quite general way, in the following form:

$$\mathbb{A}^1_{vv}(\mathbf{x}) = E[X^c\mathbf{v}^{c'}\mathbf{v}^{c'}](\mathbf{x}) = E\left[\int \varphi_1(\mathbf{x}^\circ)X^c_1\mathbf{v}^{c'}\mathbf{v}^{c'}(\mathbf{x})d\mathbf{x}^\circ\right] = \int E[\varphi_1(\mathbf{x}^\circ)X^c_1\mathbf{v}^{c'}\mathbf{v}^{c'}(\mathbf{x})]d\mathbf{x}^\circ, \tag{2.9}$$

where the integration is performed, for each $\mathbf{x}$, so that the first inclusion centred at $\mathbf{x}^\circ$ does not overlap $\mathbf{x}$ which must be occupied by the continuous phase; following the same line of reasoning as that giving (2.2) and (2.3), the integrand of the r.h.s. of (2.9) may be related to the second order unsymmetrical (with respect to $\mathbf{x}$ and $\mathbf{x}^\circ$) tensor $\mathbb{A}^2_{vv}(\mathbf{x}|\mathbf{x}^\circ)$, conditional upon the presence at $\mathbf{x}^\circ$ of an inclusion:

$$E[\varphi_1X^c_1\mathbf{v}^{c'}\mathbf{v}^{c'}] = E[\varphi_1X^c_1(\overline{\mathbf{v}^c}^2 - \overline{\mathbf{v}^c}^1)(\overline{\mathbf{v}^c}^2 - \overline{\mathbf{v}^c}^1)] + E[\varphi_1X^c_1\mathbf{v}^{c''}\mathbf{v}^{c''}]$$
$$= \frac{1}{N}[\phi^{(1)}(\mathbf{x}^\circ)\alpha^{c2}(\mathbf{x}|\mathbf{x}^\circ)(\overline{\mathbf{v}^c}^2 - \overline{\mathbf{v}^c}^1)(\overline{\mathbf{v}^c}^2 - \overline{\mathbf{v}^c}^1)(\mathbf{x}|\mathbf{x}^\circ) + \mathbb{A}^2_{vv}(\mathbf{x}|\mathbf{x}^\circ), \tag{2.10}$$

where the fluctuation field $\mathbf{v}^{c''}$ defined in Sec. 5.4. – Part I fulfils $\varphi_1X^c_1\mathbf{v}^c(\mathbf{x}^\circ) =$

$\varphi_1 X_1^c \overline{\mathbf{v}^c}^2(\mathbf{x}^\circ|\mathbf{x}) + \varphi_1 X_1^c \mathbf{v}^{c''}(\mathbf{x}^\circ|\mathbf{x})$. The second order tensor $\mathbb{A}^2_{\mathrm{vv}}(\mathbf{x}|\mathbf{x}^\circ)$ in turn becomes:

$$\mathbb{A}^2_{\mathrm{vv}} = NE[\varphi_1 X^c \mathbf{v}^{c''} \mathbf{v}^{c''}] = N \int E[\varphi_1(\mathbf{x}^\circ)\varphi_2(\mathbf{x}^{\circ\circ}) X^c_{1,2} \mathbf{v}^{c''} \mathbf{v}^{c''}(\mathbf{x})] d\mathbf{x}^{\circ\circ}, \tag{2.11}$$

where the integration domain must satisfy two conditions at $\mathbf{x}$ and at $\mathbf{x}^\circ$. The integrand in the r.h.s. of (2.11) can be in turn broken down into two parts as in (2.10) and so on... We realise that a finite (up to N) recurrent relation can be derived. The first terms of this relation are:

$$\mathbb{A}^1_{\mathrm{vv}}(\mathbf{x}) = \frac{1}{N} \int d\mathbf{x}^\circ \{\phi^{(1)} \alpha^{c2} [\overline{\mathbf{v}^c}^2(\mathbf{x}|\mathbf{x}^\circ) - \overline{\mathbf{v}^c}^1(\mathbf{x})]$$

$$\cdot [\overline{\mathbf{v}^c}^2(\mathbf{x}|\mathbf{x}^\circ) - \overline{\mathbf{v}^c}^1(\mathbf{x})] + \mathbb{A}^2_{\mathrm{vv}}(\mathbf{x}|\mathbf{x}^\circ)\},$$

$$\mathbb{A}^2_{\mathrm{vv}}(\mathbf{x}|\mathbf{x}^\circ) = \frac{1}{(N-1)} \int d\mathbf{x}^{\circ\circ} \{\phi^{(2)} \alpha^{c3} [\overline{\mathbf{v}^c}^3(\mathbf{x}|\mathbf{x}^\circ, \mathbf{x}^{\circ\circ}) - \overline{\mathbf{v}^c}^2(\mathbf{x}|\mathbf{x}^\circ)]$$

$$\cdot [\overline{\mathbf{v}^c}^3(\mathbf{x}|\mathbf{x}^\circ, \mathbf{x}^{\circ\circ}) - \overline{\mathbf{v}^c}^2(\mathbf{x}|\mathbf{x}^\circ)] + \mathbb{A}^3_{\mathrm{vv}}(\mathbf{x}|\mathbf{x}^\circ, \mathbf{x}^{\circ\circ})\}, \tag{2.12}$$

$$\mathbb{A}^3_{\mathrm{vv}}(\mathbf{x}|\mathbf{x}^\circ, \mathbf{x}^{\circ\circ}) = \frac{1}{(N-2)} \int d\mathbf{x}^{\circ\circ\circ} \{\phi^{(3)} \alpha^{c4} [\overline{\mathbf{v}^c}^4(\mathbf{x}|\mathbf{x}^\circ, \mathbf{x}^{\circ\circ}, \mathbf{x}^{\circ\circ\circ})$$

$$-\overline{\mathbf{v}^c}^3(\mathbf{x}|\mathbf{x}^\circ, \mathbf{x}^{\circ\circ})][\overline{\mathbf{v}^c}^4(\mathbf{x}|\mathbf{x}^\circ, \mathbf{x}^{\circ\circ}, \mathbf{x}^{\circ\circ\circ}) - \overline{\mathbf{v}^c}^3(\mathbf{x}|\mathbf{x}^\circ, \mathbf{x}^{\circ\circ})]$$

$$+\mathbb{A}^4_{\mathrm{vv}}(\mathbf{x}|\mathbf{x}^\circ, \mathbf{x}^{\circ\circ}, \mathbf{x}^{\circ\circ\circ})\}.$$

The expressions (3.5) will be used to analyse their order of magnitude as it will be shown in the next section.

The closure problem is not solved yet for any of the above variance tensors. To see this point, consider $\mathbb{A}^2_{\mathrm{uu}}(\mathbf{x}|\mathbf{x}^\circ)$ which can be expressed in terms of variables of the whole hierarchy as $\overline{\mathbf{u}}^1(\mathbf{x})$, $\overline{\mathbf{u}}^2(\mathbf{x}|\mathbf{x}^\circ)$, $\phi^{(2)}(\mathbf{x}, \mathbf{x}^\circ)$, $\overline{\mathbf{u}}^3(\mathbf{x}|\mathbf{x}^\circ, \mathbf{x}^{\circ\circ})$, $\phi^{(3)}(\mathbf{x}, \mathbf{x}^\circ, \mathbf{x}^{\circ\circ})$... or the corresponding disturbance velocities. What would be necessary is to account for a few terms of this sum; more precisely, these terms must be preponderant according to some small parameter and involve variables which appear in equations of order less or equal to two. This aim is reached in the next section where it will be seen that the influence of each group of test inclusions must be broken down in subclasses effects.

3. Approximation of pseudo-turbulent tensors

3.1. Breaking down the contribution of each group

To break down the influence of each group of inclusions into subclasses effects, it suffices to express conditional velocities differences appearing in the recurrence relations, in terms of disturbance fields. For instance, consider the one-position agitation tensors, relative to the dispersed phase. Our treatement is based on the definition of disturbance fields given in Part II which are repeated for convenience: the first disturbance is $\mathbf{u}^*(\mathbf{x}|\mathbf{x}^\circ) = \overline{\mathbf{u}}^2(\mathbf{x}|\mathbf{x}^\circ) - \overline{\mathbf{u}}^1(\mathbf{x})$, the second order disturbance is given by $\mathbf{u}^{**}(\mathbf{x}|\mathbf{x}^\circ, \mathbf{x}^{\circ\circ}) = \overline{\mathbf{u}}^3(\mathbf{x}|\mathbf{x}^\circ, \mathbf{x}^{\circ\circ}) - \overline{\mathbf{u}}^2(\mathbf{x}|\mathbf{x}^\circ) - \overline{\mathbf{u}}^2(\mathbf{x}|\mathbf{x}^{\circ\circ}) + \overline{\mathbf{u}}^1(\mathbf{x})$ and the third order one obeys $\mathbf{u}^{***}(\mathbf{x}|\mathbf{x}^\circ, \mathbf{x}^{\circ\circ}, \mathbf{x}^{\circ\circ\circ}) = \overline{\mathbf{u}}^4(\mathbf{x}|\mathbf{x}^\circ, \mathbf{x}^{\circ\circ}, \mathbf{x}^{\circ\circ\circ}) - \overline{\mathbf{u}}^3(\mathbf{x}|\mathbf{x}^\circ, \mathbf{x}^{\circ\circ}) - \overline{\mathbf{u}}^3(\mathbf{x}|\mathbf{x}^\circ, \mathbf{x}^{\circ\circ\circ}) - \overline{\mathbf{u}}^3((\mathbf{x}|\mathbf{x}^{\circ\circ}, \mathbf{x}^{\circ\circ\circ}) + \overline{\mathbf{u}}^2(\mathbf{x}|\mathbf{x}^\circ) + \overline{\mathbf{u}}^2(\mathbf{x}|\mathbf{x}^{\circ\circ}) + \overline{\mathbf{u}}^2(\mathbf{x}|\mathbf{x}^{\circ\circ\circ}) - \overline{\mathbf{u}}^1(\mathbf{x})$. Combining these definitions leads to the following identities:

$$
\begin{aligned}
\overline{\mathbf{u}}^2(\mathbf{x}|\mathbf{x}^\circ) - \overline{\mathbf{u}}^1(\mathbf{x}) &= \mathbf{u}^*(\mathbf{x}|\mathbf{x}^\circ), \\
\overline{\mathbf{u}}^3(\mathbf{x}|\mathbf{x}^\circ, \mathbf{x}^{\circ\circ}) - \overline{\mathbf{u}}^2(\mathbf{x}|\mathbf{x}^\circ) &= \mathbf{u}^{**}(\mathbf{x}|\mathbf{x}^\circ, \mathbf{x}^{\circ\circ}) + \mathbf{u}^*(\mathbf{x}|\mathbf{x}^{\circ\circ}), \\
\overline{\mathbf{u}}^4(\mathbf{x}|\mathbf{x}^\circ, \mathbf{x}^{\circ\circ}, \mathbf{x}^{\circ\circ\circ}) - \overline{\mathbf{u}}^3(\mathbf{x}|\mathbf{x}^\circ, \mathbf{x}^{\circ\circ}) &= \mathbf{u}^{***}(\mathbf{x}|\mathbf{x}^\circ, \mathbf{x}^{\circ\circ}, \mathbf{x}^{\circ\circ\circ}) \\
&\quad + \mathbf{u}^{**}(\mathbf{x}|\mathbf{x}^\circ, \mathbf{x}^{\circ\circ\circ}) + \mathbf{u}^{**}(\mathbf{x}|\mathbf{x}^{\circ\circ}, \mathbf{x}^{\circ\circ\circ}) + \mathbf{u}^*(\mathbf{x}|\mathbf{x}^{\circ\circ\circ}).
\end{aligned} \tag{3.1}
$$

$$\cdots$$

Inserting the above first relation into (2.4) leads to:

$$
\mathbb{A}^1_{\mathrm{uu}}(\mathbf{x}) = \frac{1}{(N-1)} \int d\mathbf{x}^\circ [\phi^{(2)} \mathbf{u}^* \mathbf{u}^*(\mathbf{x}|\mathbf{x}^\circ) + \mathbb{A}^2_{\mathrm{uu}}(\mathbf{x}|\mathbf{x}^\circ)]. \tag{3.2}
$$

The second order tensor in the r.h.s. becomes, using (2.5) and the second relation (3.1):

$$
\begin{aligned}
\frac{1}{(N-1)} \int d\mathbf{x}^\circ \mathbb{A}^2_{\mathrm{uu}}(\mathbf{x}|\mathbf{x}^\circ) &= \frac{1}{(N-1)} \int d\mathbf{x}^\circ [\phi^{(2)} \mathbf{u}^* \mathbf{u}^*(\mathbf{x}|\mathbf{x}^\circ)] \\
&\quad + \frac{1}{(N-1)(N-2)} \int d\mathbf{x}^\circ \int d\mathbf{x}^{\circ\circ} \{\phi^{(3)} [\mathbf{u}^{**} \mathbf{u}^{**}(\mathbf{x}|\mathbf{x}^\circ, \mathbf{x}^{\circ\circ}) \\
&\quad + 2\mathbf{u}^*(\mathbf{x}|\mathbf{x}^{\circ\circ}) \mathbf{u}^{**}(\mathbf{x}|\mathbf{x}^\circ, \mathbf{x}^{\circ\circ})] + \mathbb{A}^3_{\mathrm{uu}}(\mathbf{x}|\mathbf{x}^\circ, \mathbf{x}^{\circ\circ})\}.
\end{aligned} \tag{3.3}
$$

Using (2.6) and the third relation (3.1), the third order tensor in the r.h.s. of (3.3) can be expressed, in its turn, as:

$$
\frac{1}{(N-1)(N-2)} \int d\mathbf{x}^\circ \int d\mathbf{x}^{\circ\circ} \mathbb{A}^3_{\mathrm{uu}}(\mathbf{x}|\mathbf{x}^\circ, \mathbf{x}^{\circ\circ}) \tag{3.4}
$$

(3.4) [cont.]

$$= \frac{1}{(N-1)} \int d\mathbf{x}^{\circ} [\phi^{(2)} \mathbf{u}^{*} \mathbf{u}^{*}(\mathbf{x}|\mathbf{x}^{\circ})]$$

$$+ \frac{1}{(N-1)(N-2)} \int d\mathbf{x}^{\circ} \int d\mathbf{x}^{\circ\circ} \{\phi^{(3)} [2\mathbf{u}^{**}\mathbf{u}^{**}(\mathbf{x}|\mathbf{x}^{\circ}, \mathbf{x}^{\circ\circ}) + 4\mathbf{u}^{*}(\mathbf{x}|\mathbf{x}^{\circ})\mathbf{u}^{**}(\mathbf{x}|\mathbf{x}^{\circ}, \mathbf{x}^{\circ\circ})]\}$$

$$+ \frac{1}{(N-1)(N-2)(N-3)} \int d\mathbf{x}^{\circ} \int d\mathbf{x}^{\circ\circ} \int d\mathbf{x}^{\circ\circ\circ} \{\phi^{(4)} [\mathbf{u}^{***}\mathbf{u}^{***}(\mathbf{x}|\mathbf{x}^{\circ}, \mathbf{x}^{\circ\circ}, \mathbf{x}^{\circ\circ\circ}) + 2\mathbf{u}^{**}(\mathbf{x}|\mathbf{x}^{\circ}, \mathbf{x}^{\circ\circ\circ})\mathbf{u}^{**}(\mathbf{x}|\mathbf{x}^{\circ\circ}, \mathbf{x}^{\circ\circ\circ}) + 2\mathbf{u}^{***}(\mathbf{x}|\mathbf{x}^{\circ}, \mathbf{x}^{\circ\circ}, \mathbf{x}^{\circ\circ\circ})\mathbf{u}^{*}(\mathbf{x}|\mathbf{x}^{\circ\circ\circ}) + 2\mathbf{u}^{***}(\mathbf{x}|\mathbf{x}^{\circ}, \mathbf{x}^{\circ\circ}, \mathbf{x}^{\circ\circ\circ})\mathbf{u}^{**}(bfx|\mathbf{x}^{\circ}, \mathbf{x}^{\circ\circ\circ}) + 2\mathbf{u}^{***}(\mathbf{x}|\mathbf{x}^{\circ}, \mathbf{x}^{\circ\circ}, \mathbf{x}^{\circ\circ\circ})\mathbf{u}^{**}(\mathbf{x}|\mathbf{x}^{\circ\circ}, \mathbf{x}^{\circ\circ\circ})] + \mathbb{A}^{4}_{\mathrm{uu}}(\mathbf{x}|\mathbf{x}^{\circ}, \mathbf{x}^{\circ\circ}, \mathbf{x}^{\circ\circ\circ})\}.$$

Such a process can be continued by expanding $\mathbb{A}^{4}_{\mathrm{uu}}(\mathbf{x}|\mathbf{x}^{\circ}, \mathbf{x}^{\circ\circ}, \mathbf{x}^{\circ\circ\circ})$ and so on, as far as $\mathbb{A}^{N-1}_{\mathrm{uu}}$ is reached. Collecting in each expression identical terms, we obtain:

$$\mathbb{A}^{1}_{\mathrm{uu}}(\mathbf{x}) = \int d\mathbf{x}^{\circ} [\phi^{(2)}(\mathbf{x}^{\circ}, \mathbf{x})\mathbf{u}^{*}\mathbf{u}^{*}(\mathbf{x}|\mathbf{x}^{\circ})] + \frac{1}{2} \int d\mathbf{x}^{\circ} \int d\mathbf{x}^{\circ\circ} \{\phi^{(3)}(\mathbf{x}|\mathbf{x}^{\circ}, \mathbf{x}^{\circ\circ})[\mathbf{u}^{**}\mathbf{u}^{**}(\mathbf{x}|\mathbf{x}^{\circ}, \mathbf{x}^{\circ\circ}) + 2\mathbf{u}^{*}(\mathbf{x}|\mathbf{x}^{\circ})\mathbf{u}^{**}(\mathbf{x}|\mathbf{x}^{\circ}, \mathbf{x}^{\circ\circ})]\} + \ldots \tag{3.5}$$

where the $2\sum_{i=1}^{N-2} i = (N-1)(N-2)$ has been used. Thus we have succeded in breaking down the influence of each group of inclusions into one-inclusion, two-inclusions, ... effects. There's nothing surprising about that; for example, contributions of two, three... test inclusions contain cases where a single neighbouring inclusion at $\mathbf{x}^{\circ}$ is close to the first one at $\mathbf{x}$. These cases feed what will be the leading order of an asymptotic sequence in terms of Θ which will be derived from all these series in the next section.

Note that we can also deduce expressions for $\mathbb{A}^{2}_{\mathrm{u}^{\circ}\mathrm{u}^{\circ}}(\mathbf{x}^{\circ}|\mathbf{x})$ and $\mathbb{A}^{2}_{\mathrm{u}^{\circ}\mathrm{u}}(\mathbf{x}^{\circ}, \mathbf{x})$ which are required in (4.16 – Part II):

$$\mathbb{A}^{2}_{\mathrm{u}^{\circ}\mathrm{u}^{\circ}}(\mathbf{x}^{\circ}|\mathbf{x}) = \int d\mathbf{x}^{\circ\circ} \phi^{(3)}(\mathbf{x}, \mathbf{x}^{\circ}, \mathbf{x}^{\circ\circ})\mathbf{u}^{*}\mathbf{u}^{*}(\mathbf{x}^{\circ}|\mathbf{x}^{\circ\circ}) + \int d\mathbf{x}^{\circ\circ} \{\phi^{(3)}(\mathbf{x}, \mathbf{x}^{\circ}, \mathbf{x}^{\circ\circ})[\mathbf{u}^{**}\mathbf{u}^{**}(\mathbf{x}^{\circ}|\mathbf{x}, \mathbf{x}^{\circ\circ}) + 2\mathbf{u}^{*}(\mathbf{x}^{\circ}|\mathbf{x}^{\circ\circ})\mathbf{u}^{**}(\mathbf{x}^{\circ}|\mathbf{x}, \mathbf{x}^{\circ\circ})]\} + \ldots \tag{3.6}$$

$$\mathbb{A}^2_{\mathbf{u}^\circ\mathbf{u}}(\mathbf{x}^\circ,\mathbf{x}) = \int d\mathbf{x}^{\circ\circ}\phi^{(3)}(\mathbf{x},\mathbf{x}^\circ,\mathbf{x}^{\circ\circ})\mathbf{u}^*(\mathbf{x}^\circ|\mathbf{x}^{\circ\circ})\mathbf{u}^*(\mathbf{x}|\mathbf{x}^{\circ\circ}) \tag{3.7}$$

$$+ \int d\mathbf{x}^{\circ\circ}\{\phi^{(3)}(\mathbf{x},\mathbf{x}^\circ,\mathbf{x}^{\circ\circ})[\mathbf{u}^{**}(\mathbf{x}|\mathbf{x}^\circ,\mathbf{x}^{\circ\circ})\mathbf{u}^{**}(\mathbf{x}^\circ|\mathbf{x},\mathbf{x}^{\circ\circ})$$

$$+ \int d\mathbf{x}^{\circ\circ}\{\phi^{(3)}(\mathbf{x},\mathbf{x}^\circ,\mathbf{x}^{\circ\circ})[\mathbf{u}^{**}(\mathbf{x}|\mathbf{x}^\circ,\mathbf{x}^{\circ\circ})\mathbf{u}^{**}(\mathbf{x}^\circ|\mathbf{x},\mathbf{x}^{\circ\circ})$$

$$+ \mathbf{u}^*(\mathbf{x}|\mathbf{x}^{\circ\circ})\mathbf{u}^{**}(\mathbf{x}^\circ,\mathbf{x}^{\circ\circ}) + \mathbf{u}^*(\mathbf{x}^\circ|\mathbf{x}^{\circ\circ})\mathbf{u}^{**}(\mathbf{x}|\mathbf{x}^\circ,\mathbf{x}^{\circ\circ})]\} + ...$$

An expression for $\mathbb{A}^1_{\omega\mathbf{u}}(\mathbf{x})$ appearing in ((4.11) – Part II) as well as expressions for $\mathbb{A}^2_{\omega^\circ\mathbf{u}^\circ}(\mathbf{x}^\circ|\mathbf{x})$ and $\mathbb{A}^2_{\omega^\circ\mathbf{u}}(\mathbf{x}^\circ,\mathbf{x})$ in ((4.17) – Part II) are required. It is straightforward to derive them from (3.5), (3.6) and (3.7), respectively.

A treatment of any kind of tensor seen in Sec. 2.1 as well as agitation tensors relative to the continuous phase parallels exactly the above analysis. We find for example:

$$\mathbb{A}^1_{\mathbf{vv}}(\mathbf{x}) = \int d\mathbf{x}^\circ[\phi^{(1)}(\mathbf{x}^\circ)\alpha^{c2}\mathbf{v}^*\mathbf{v}^*(\mathbf{x}|\mathbf{x}^\circ)] \tag{3.8}$$

$$+ \frac{1}{2}\int d\mathbf{x}^\circ \int d\mathbf{x}^{\circ\circ}\{\phi^{(2)}(\mathbf{x}^\circ,\mathbf{x}^{\circ\circ})\alpha^{c3}[\mathbf{v}^{**}\mathbf{v}^{**}(\mathbf{x}|\mathbf{x}^\circ,\mathbf{x}^{\circ\circ})$$

$$+ 2\mathbf{v}^*(\mathbf{x}|\mathbf{x}^\circ)\mathbf{v}^{**}(\mathbf{x}|\mathbf{x}^\circ,\mathbf{x}^{\circ\circ})]\},$$

$$\ldots$$

$$\mathbb{A}^2_{\mathbf{v}^\circ\mathbf{v}^\circ}(\mathbf{x}^\circ|\mathbf{x}) = \int d\mathbf{x}^{\circ\circ}\phi^{(2)}(\mathbf{x},\mathbf{x}^{\circ\circ})\alpha^{c3}\mathbf{v}^*\mathbf{v}^*(\mathbf{x}^\circ|\mathbf{x}^{\circ\circ}) \tag{3.9}$$

$$+ \int d\mathbf{x}^{\circ\circ}\{\phi^{(2)}(\mathbf{x},\mathbf{x}^{\circ\circ})\alpha^{c3}[\mathbf{v}^{**}\mathbf{v}^{**}(\mathbf{x}^\circ|\mathbf{x},\mathbf{x}^{\circ\circ})$$

$$+2\mathbf{v}^*(\mathbf{x}^\circ|\mathbf{x}^{\circ\circ})\mathbf{v}^{**}(\mathbf{x}^\circ|\mathbf{x},\mathbf{x}^{\circ\circ})]\}.$$

$$\ldots$$

We first observe that $\mathbb{A}^1_{\mathbf{vv}}$, $\mathbb{A}^2_{\mathbf{vv}}$... have not the same dimension as the corresponding order dispersed phase agitation tensors $\mathbb{A}^1_{\mathbf{uu}}$, $\mathbb{A}^2_{\mathbf{uu}}$ ... since, at a given order, they do not involve the same p.d.f. in their integrand. On the other hand, contrary to the disturbance interfacial force densities which only imply the next order variables, we also observe that all higher order disturbance velocities are requested. Now, it remains to show that all the expansions we have devised can be considered as expansions in terms of the averaged concentration Θ. Only after that, the closure problem will be claimed to be solved.

3.2. Expansion in terms of Θ

To set an example of our procedure, we will consider the above one-point agitation tensor (3.8), relative to the continuous phase. To put this tensor in a dimensionless form, some scales will be specified in a very general way:

(i) The length scale of the first order averaged fields is L as it has been pointed out in Sec. 2.1. – Part II; it is given by the specification of some boundary or initial conditions. The length scale of all the disturbance averaged fields is expected to be a function of a single inclusion dynamics. In the first approximation, it will be set equal to the inclusion radius a. These two scales hold for both phases.

(ii) There are representative scales for the various densities in physical space, ϕ_1, ϕ_2, ...; they are simply $1/\mathrm{L}^3$, $1/\mathrm{L}^6$... The reason of this normalisation is that $\phi_1\mathrm{L}^3$, $\phi_2\mathrm{L}^6$,... have an order of magnitude of 1 since they are probabilities.

(iii) The first order averaged disturbance field, $\mathbf{v}^*$, has a scale denoted V_2, the possible values of which will be given in a future paper. The same scale can be maintained for higher-order disturbance fields. In relation to our present concern, theses values are irrelevant. Furthermore, it will be shown that disturbance fields of higher order have at most the same scale V_2.

Takin into account all these assumptions which are not restrictive, we obtain:

$$\mathbb{A}^1_{\mathrm{vv}}(\mathbf{x}) = \Theta V_2^2 \int d\mathbf{x}^\circ [\phi_1 \alpha^{c2} \mathbf{v}^* \mathbf{v}^* (\mathbf{x}|\mathbf{x}^\circ)] + \Theta^2 V_2^2 \int d\mathbf{x}^\circ \int d\mathbf{x}^{\circ\circ} \{\phi_2 \alpha^{c3} [\mathbf{v}^{**}\mathbf{v}^{**}(\mathbf{x}|\mathbf{x}^\circ, \mathbf{x}^{\circ\circ})/2 + \mathbf{v}^*(\mathbf{x}|\mathbf{x}^\circ)\mathbf{v}^{**}(\mathbf{x}|\mathbf{x}^\circ, \mathbf{x}^{\circ\circ})]\} + O[\Theta^3] + O[1/N], \tag{3.10}$$

where all the variables in the r.h.s. are dimensionless. Asymptotic sequences can also be derived for any agitation tensor by using the same (or very close) nondimensionalisation process.

However, it is expected that integrals at the r.h.s. may be not convergent in many cases, especially when disturbance flows are creeping and have long-range hydrodynamic interactions (CAFLISCH and LUKE [30]). This means that the above scaling and especially, the length scale of the disturbance averaged fields, is by far too naive and ought to be reconsidered. The role of the above expansion which appears, to the order $O(1/N)$, as an asymptotic sequence in terms of Θ, is to start a necessary truncation procedure based on dilutness. In this way asymptotic expansions of any unknowns in terms of Θ are sought; investigating the source of nonconverging integrals will amount to determining the regions of nonuniformities for the above expansions. These critical problems will be adressed in a future paper.

4. Expansions in multipoles

Pseudo-turbulent (or agitation) tensors for both phases and interfacial force densities for the continuous phase share common features: they involve some hydrodynamic fields, velocity fluctuations for the former, interfacial stresses for the latter, which result from multipole contributions at a given observation point $\mathbf{x}$, brought by inclusions placed at various positions in the neighborhood of $\mathbf{x}$. To be calculated more easily, all these quantities need to be treated by a multipole expansion method. As explained in Sec. 5.2. – Part II, this amounts to muster the causes of multipole contributions at one location. However, there is a difference between force densities and agitation tensors: hydrodynamic fields are picked off at the interface for the former while they are selected in the bulk for the latter. In the following, we will restrict to expand terms in tensors which involve two-inclusions interactions.

4.1. Slow and fast independant spatial variables

Pseudo-turbulent tensors for both phases have been expressed in Sec. 3.1. in terms of velocity disturbance flows. These fields are solutions of problems which explicitly depend on both fast-varying and slow-varying independent spatial variables. All consequences of this property will be envisaged in a future paper. Here, only some elementary considerations necessary to estimate the order of magnitude of various terms in the obtained multipoles expansions are introduced. They are based on the change of variable:

$$\mathbf{x} = \mathbf{x} \quad \text{and} \quad \mathbf{r} = \mathbf{x}^\circ - \mathbf{x}. \tag{4.1}$$

consider a typical first order disturbance, say $\mathbf{u}^*$; we will be led in the future to let

$$\hat{\mathbf{u}}(\mathbf{r}, \mathbf{x}) = \mathbf{u}^*(\mathbf{x} + \mathbf{r}|\mathbf{x}) = \mathbf{u}^*(\mathbf{x}^\circ|\mathbf{x})$$

be the new unknown. The entire two-inclusions problem can be expressed in scaling the first coordinate $\mathbf{r}$ with a and the second coordinate $\mathbf{x}$ with L. All these new small-scale functions are defined throughout an (usually) unbounded region denoted $\mathcal{V}^d_{\mathbf{x},\mathbf{r}}$ which replace $\mathcal{V}^d_{\mathbf{x},\mathbf{x}^\circ}$. Likewise, a similar change of variables for the second-order disturbance fields:

$$\mathbf{x} = \mathbf{x}, \quad \mathbf{r} = \mathbf{x}^\circ - \mathbf{x} \quad \text{and} \quad \mathbf{r}^\circ = \mathbf{x}^{\circ\circ} - \mathbf{x}^\circ \tag{4.2}$$

gives rise to $\hat{\hat{\mathbf{u}}}(\mathbf{r}, \mathbf{r}^\circ, \mathbf{x})$.

All the concerned velocity disturbance field equations of the continuous phase can be made dimensionless in the same way as above as $\mathbf{v}^{\circ *}$ which becomes:

$$\hat{\mathbf{v}}(\mathbf{r}, \mathbf{x}) = \mathbf{v}^{\circ *}(\mathbf{x} + \mathbf{r}|\mathbf{x}) = \mathbf{v}^{\circ *}(\mathbf{x}^\circ|\mathbf{x}).$$

4.2. The pseudo-turbulent tensors in the dispersed phase

The leading term of the agitation tensor $\mathbb{A}^1_{uu}(\mathbf{x})$ which is defined in (3.5) can be transformed by (4.1):

$$\mathbb{A}^1_{uu}(\mathbf{x}) = \int d\mathbf{x}^\circ[\phi^{(2)}\mathbf{u}^*(\mathbf{x}|\mathbf{x}^\circ)] = \int d\mathbf{r}[\phi^{(2)}(\mathbf{x},\mathbf{x}+\mathbf{r})\mathbf{u}^*\mathbf{u}^*(\mathbf{x}|\mathbf{x}+\mathbf{r}]. \tag{4.3}$$

The integrand is denoted by:

$$f(\mathbf{r},\mathbf{x}) = \phi^{(2)}(\mathbf{x},\mathbf{x}+\mathbf{r})\mathbf{u}^*\mathbf{u}^*(\mathbf{x}|\mathbf{x}+\mathbf{r}). \tag{4.4}$$

Expanding $\mathbf{f}$ with the respect to the second argument around $\mathbf{x}-\mathbf{r}$ according to the formula ((2.5) – Part II) gives:

$$f(\mathbf{r},\mathbf{x}) = \sum_{m=0}^{\infty} \frac{(-1)^m}{m!}\mathbf{r}^m \boxed{m} \frac{\partial^m}{\partial \mathbf{x}^m} f(\mathbf{r},\mathbf{x}-\mathbf{r}). \tag{4.5}$$

The resulting expansion for the leading term of the agitation tensor can be written:

$$\int d\mathbf{x}^\circ[\phi^{(2)}\mathbf{u}^*\mathbf{u}^*(\mathbf{x}|\mathbf{x}^\circ)] = (N-1)\sum_{m=0}^{\infty} \frac{\partial^m}{\partial \mathbf{x}^m} \boxed{m} \phi^{(1)}(\mathbf{x})\mathbb{N}^1_{uu,m}(\mathbf{x}), \tag{4.6}$$

where the m^{th} agitation multipole of the first-order for the dispersed phase is:

$$\mathbb{N}^1_{uu,m}(\mathbf{x}) = \frac{1}{m!}\int d\mathbf{r}\mathbf{r}^m \chi_2 \mathbf{u}^*\mathbf{u}^*(\mathbf{x}+\mathbf{r}|\mathbf{x}). \tag{4.7}$$

In this multipole $\mathbf{r}^m$ denotes an m-fold tensor product of $\mathbf{r}$. It describes the agitation due to the first-order disturbance flow of the dispersed phase over a test inclusion centred at $\mathbf{x}$. It is a tensor of rank $m+2$, symmetric in its first m indices.

In the first-order dispersed-phase linear momentum equation ((4.10) – Part II), the above agitation tensor appears under a divergence term which becomes, using (4.6):

$$\rho^d(\phi^{(1)})^{-1}\frac{\partial}{\partial \mathbf{x}}\cdot\mathbb{A}^1_{uu} = \Theta[\rho^d U_2^2/L]\left\{\phi_1^{-1}\frac{\partial}{\partial \mathbf{x}}\cdot\phi_1\mathbb{N}^1_{uu,0} + \beta\phi_1^{-1}\frac{\partial}{\partial \mathbf{x}} \cdot\left[\frac{\partial}{\partial \mathbf{x}}\cdot\phi_1\mathbb{N}^1_{uu,1}\right] + O(\beta^2)\right\} + O(1/N), \tag{4.8}$$

where all the variables of the r.h.s. have been made dimensionless; note that U_2 is the uknown representative linear velocity scale for $\mathbf{u}^*$. It has been shown that the agitation tensor contribution is of $O(\Theta)$ compared to the classical bulk flow convective term (see Eq. (4.10) – Part II).

The agitation tensor $\mathbb{A}^1_{\omega u}(\mathbf{x})$ can obtain an expression similar to (4.6) in which U_2/a is chosen as the unknown representative angular velocity scale for ω^*. This tensor appears in ((4.11) – Part II) under a divergence term and a formula similar to (4.8) can be derived.

4.3. The pseudo-turbulent tensors in the continuous phase

The two leading terms of the agitation tensor $\mathbb{A}^1_{vv}(\mathbf{x})$ which is defined in (3.8) can be transformed by the change of variables (4.1):

$$\mathbb{A}^1_{vv}(\mathbf{x}) = \int d\mathbf{r} \left[\phi^{(1)}(\mathbf{x}+\mathbf{r})\alpha^{c2}\mathbf{v}^*\mathbf{v}^*(\mathbf{x}|\mathbf{x}+\mathbf{r}\right] + \frac{1}{2}\int d\mathbf{x}^{oo}\int d\mathbf{r}\left\{\phi^{(2)}(\mathbf{x}+\mathbf{r},\mathbf{x}^{oo})\alpha^{c3}[\mathbf{v}^{**}\mathbf{v}^{**}(\mathbf{x}|\mathbf{x}+\mathbf{r},\mathbf{x}^{oo}) + 2\mathbf{v}^*(\mathbf{x}|\mathbf{x}+\mathbf{r})\mathbf{v}^{**}(\mathbf{x}|\mathbf{x}+\mathbf{r},\mathbf{x}^{oo})]\right\} + \ldots \tag{4.9}$$

Expanding the two integrands with respect to the variable $\mathbf{x}$ around $\mathbf{x}-\mathbf{r}$ accotding to the formula ((2.5) – Part II) provides:

$$\mathbb{A}^1_{vv}(\mathbf{x}) = \sum_{m=0}^{\infty}\frac{\partial^m}{\partial\mathbf{x}^m}\boxed{m}\,\phi^{(1)}(\mathbf{x})\mathbb{N}^1_{vv,m}(\mathbf{x}) + 1/2\sum_{m=0}^{\infty}\frac{\partial^m}{\partial\mathbf{x}^m}\int d\mathbf{x}^{oo}\phi^{(2)}(\mathbf{x},\mathbf{x}^{oo})\mathbb{N}^2_{vv,m}(\mathbf{x},\mathbf{x}^{oo}) + \ldots \tag{4.10}$$

where the m^{th} agitation multipole of the first- and second-order for the continuous phase have been defined by:

$$\mathbb{N}^1_{vv,m}(\mathbf{x}) = \frac{1}{m!}\int d\mathbf{r}\mathbf{r}^m\alpha^{c2}\mathbf{v}^*\mathbf{v}^*(\mathbf{x}+\mathbf{r}|\mathbf{x}) \tag{4.11}$$

$$\mathbb{N}^2_{vv,m}(\mathbf{x},\mathbf{x}^{oo}) = \frac{1}{m!}\int d\mathbf{r}\{\mathbf{r}^m\alpha^{c3}[\mathbf{v}^{**}\mathbf{v}^{**}(\mathbf{x}+\mathbf{r}|\mathbf{x},\mathbf{x}^{oo}) + 2\mathbf{v}^*(\mathbf{x}+\mathbf{r}|\mathbf{x})\mathbf{v}^{**}(\mathbf{x}+\mathbf{r}|\mathbf{x},\mathbf{x}^{oo})]\}. \tag{4.12}$$

The m^{th} agitation multipole of order 1 and 2 describe the agitation due to the first and the second disturbance flows of the continuous phase over a test inclusion centred at $\mathbf{x}$. It is a tensor of rank m+2, symmetric in its first m indices. Observe that $\mathbb{N}^2_{vv,m}(\mathbf{x},\mathbf{x}^{oo})$ is not symmetrical.

In the first-order continuous-phase momentum Eq. (4.1) – Part II, the above agitation tensor appears under a divergence term which becomes, using (4.10):

$$(4.13)\qquad (\alpha^{c1})^{-1}\frac{\partial}{\partial \mathbf{x}}\cdot \mathbb{A}^1_{\mathrm{vv}}(\mathbf{x}) = \frac{\Theta V_2^2}{L\alpha^{c1}}\left\{\frac{\partial}{\partial \mathbf{x}}\cdot \phi_1 \mathbb{N}^1_{\mathrm{vv},0}(\mathbf{x}) + \beta\frac{\partial}{\partial \mathbf{x}}\cdot\frac{\partial}{\partial \mathbf{x}}\phi_1\mathbb{N}^1_{\mathrm{vv},1}(\mathbf{x}) + O(\beta^2)\right\} + \frac{\Theta^2 V_2^2}{2L\alpha^{c1}}\left\{\frac{\partial}{\partial \mathbf{x}}\cdot\left[\int d\mathbf{x}^{\circ\circ}\phi_2\mathbb{N}^2_{\mathrm{vv},0}(\mathbf{x},\mathbf{x}^{\circ\circ})\right] + \beta\frac{\partial}{\partial \mathbf{x}}\cdot\left[\frac{\partial}{\partial \mathbf{x}}\int d\mathbf{x}^{\circ\circ}\phi_2\mathbb{N}^2_{\mathrm{vv},1}(\mathbf{x},\mathbf{x}^{\circ\circ})\right] + O(\beta^2)\right\} + O(1/N),$$

where all the variables in the r.h.s. are dimensionless and where (4.2) have been used. Note that V_2 is the uknown representative linear velocity scale for $\mathbf{v}^*$ and $\mathbf{v}^{**}$.

The same arguments as those leading to (4.10) show that the agitation tensor for the field with one fixed inclusion which is defined in (3.9), can be expanded according to:

$$(4.14)\qquad \mathbb{A}^2_{\mathrm{v}^\circ\mathrm{v}^\circ}(\mathbf{x}^\circ|\mathbf{x}) = \sum_{\mathrm{m}=0}^{\infty}\frac{\partial^{\mathrm{m}}}{\partial \mathbf{x}^{\circ\mathrm{m}}}\boxed{\mathrm{m}}\,\phi^{(2)}(\mathbf{x},\mathbf{x}^\circ)\mathbb{N}^1_{\mathrm{vv,m}}(\mathbf{x}^\circ) + \sum_{\mathrm{m}=0}^{\infty}\frac{\partial^{\mathrm{m}}}{\partial \mathbf{x}^{\circ\mathrm{m}}}\boxed{\mathrm{m}}\,\phi^{(2)}(\mathbf{x},\mathbf{x}^\circ)\mathbb{N}^2_{\mathrm{vv,m}}(\mathbf{x}^\circ,\mathbf{x}) + \ldots$$

In the second-order continuous-phase momentum equation ((4.3) – Part II), the above agitation tensor appears under a divergence term combined with $(\alpha^{c1})^{-1}\dfrac{\partial}{\partial \mathbf{x}^\circ}\cdot\mathbb{A}^1_{\mathrm{v}^\circ\mathrm{v}^\circ}$. The leading order of this combination is:

$$(4.15)\qquad \frac{\partial}{\partial \mathbf{x}^\circ}\cdot\mathbb{A}^1_{\mathrm{v}^\circ\mathrm{v}^\circ}/\alpha^{c1} - \frac{\partial}{\partial \mathbf{x}^\circ}\cdot\mathbb{A}^2_{\mathrm{v}^\circ\mathrm{v}^\circ}/\alpha^{c2}\phi^{(1)} = -N\frac{\partial}{\partial \mathbf{x}^\circ}\cdot\chi^*(\mathbf{x}^\circ|\mathbf{x})\int d\mathbf{r}^\circ[\mathbf{v}^*\mathbf{v}^*(\mathbf{x}^\circ+\mathbf{r}^\circ|\mathbf{x}^\circ)].$$

4.4. Comparison with previous work

The first-order agitation tensors $\mathbb{A}^1_{\mathrm{vv}}(\mathbf{x})$ and $\mathbb{A}^1_{\mathrm{uu}}(\mathbf{x})$ are the only quantities for which comparison with previous work can be envisaged. Other pseudo-turbulent quantities appearing in this paper are specific to our approach. Even so restricted, a comparison is not an easy task for several reasons. Various authors apply different averaging techniques, e.g. they take volume average of the two phases separately; they take volume or ensemble average of the whole mixture as well;

some of them even mix two types of averaging. Concerning our method, only phasic ensemble averaging is used. Secondly, they consider at the outset very specific types of carrier flows: mostly incompressible potential or creeping flows; their way to process the equations takes advantage of the specific properties they have selected. Moreover, in the limit of creeping flows, many studies which use kinetic theory concepts, focus on the first-order averaged field and do not even consider the agitation tensors [31, 32]. Our approach is marked off by being based on general Navier-Stokes equations. Finally they provide explicit closure relations, generally based on specified local distribution of inclusions (periodic arrays or uniform distributions); although the above expressions of the agitation tensors $\mathbb{A}^1_{vv}(\mathbf{x})$ and $\mathbb{A}^1_{uu}(\mathbf{x})$ are presented in the form of computable quantities, we have up to now not furnished such explicit results. To get them, higher order disturbance equations (e.g. $\mathbf{v}^*$ and $\mathbf{u}^*$ equations) have to be simplified according to a given particular approximation of disturbance flows and then truncated due to dilution; this will only be achieved in the next paper (Part IV). However, we can anticipate somehow and obtain some straightforward results concerning $\mathbb{A}^1_{vv}(\mathbf{x})$ which can precisely be found in the literature.

Concerning $\mathbb{A}^1_{uu}(\mathbf{x})$, the available studies mentioning this quantity are fairly recent [33, 34, 35, 36]. All these authors derived average equations for a suspension of spherical inclusions (possibly massless bubbles) carried by an incompressible irrotational flow. They propose expressions of a quantity they term kinetic (or translational) part of the dispersed-phase stress, which are mainly formal while they compute explicitly the interaction terms (they call it "potential part" of the stress) in both phases momentum equations. Moreover, they introduce a new dispersed phase momentum equation controlling the apparent momentum that can be attributed to an inclusion, i.e. including the impulse of the fluid surrounding each inclusion. In conclusion, we were unable to compare (4.8) with any analytical result.

Let us return to $\mathbb{A}^1_{vv}(\mathbf{x})$ for which there are plenty of studies. First, we will restrict ourselves to a quasi-homogeneous ($\beta \ll 1$) and dilute ($\Theta \ll 1$) mixture of spherical inclusions non-rotating and non-pulsating. In this case, the leading order of the agitation tensor given in (3.10) is, rewritten in a dimensional form:

$$\mathbb{A}^1_{vv}(\mathbf{x}) = \phi^{(1)}(\mathbf{x}) \int d[\mathbf{v}^*\mathbf{v}^*(\mathbf{x}+\mathbf{r}|\mathbf{x})] + \ldots \tag{4.16}$$

The agitation results from the superimposition of fluctuations due to each inclusion. The above formula has been used by KOCH [37] for moderate inclusion Reynolds numbers, $\mathrm{Re}^d \approx O(1-10)$. For very low particle Reynolds number, within the point-particle approximation, and in the dilute limit, KOCH and SHAQFEH [38] based their analysis upon a similar formula; they also included an extra contribution which formally corresponds to the second term at the r.h.s.

of (3.8). Albeit they did not define averaged disturbance flows as we did, the likeness of our results is even closer if we refer to the expression they derived in the Appendix (see their Eq. (A3)). Here, the result (3.8) has been obtained under very general conditions granted that the scale analysis made in Sec. 3.2. is relevant.

Consider now specific carrier phase flows. A simple way to evaluate the integral in the r.h.s. of (4.16) is to consider the disturbance velocity $\mathbf{v}^*(\mathbf{x}+\mathbf{r}|\mathbf{x})$ as that of a pure fluid set in motion by the presence of a single test inclusion moving with the relative velocity $\overline{\mathbf{u}}^1$ (cf. (4.12) – Part II), and to integrate $\mathbf{v}^*\mathbf{v}^*(\mathbf{x}+\mathbf{r}|\mathbf{x})$ over the fluid volume outside the test inclusion. This corresponds to the simplest approximation of the one-inclusion problem ((4.3) and (4.7) – Part II). Two models of carrier phase flows can be considered: irrotational flows and Stokes flows.

When $\mathbf{v}^*(\mathbf{x}+\mathbf{r}|\mathbf{x})$ is assumed as irrotational, it decays as $1/r^3$, r being the distance from the centre of the test inclusion. Computation of the integral in the r.h.s. of (4.16) is straigthforward:

$$\mathbb{A}^1_{vv}(\mathbf{x}) = \alpha^{d1}(\mathbf{x})[k_1\overline{\mathbf{u}}^1\cdot\overline{\mathbf{u}}^1(\mathbf{x})\mathbb{I} + k_2\overline{\mathbf{u}}^1\overline{\mathbf{u}}^1(\mathbf{x})] \tag{4.17}$$

where $k_1 = 3/20$ and $k_2 = 1/20$. BIESHEUVEL and VAN WIJNGAARDEN [39] considered the more general case of compressible bubbles; employing ensemble averaging and introducing at certain stages volume averaging which holds for a statistically homogeneous medium, they found the same coefficients. For ellipsoidal bubbles, LANCE [6] obtain an expression similar to (4.17) with a multiplicative coefficient which, for linear trajectories, increases almost linearly with the eccentricity. Besides, he has experimentally confirmed the validity of (4.17), at least over a limited range of void fraction. The cell model which is used as an ad-hoc approximation of the conditionaly-averaged micro-problem around a given test inclusion has allowed many investigators to produce results having the same structure. GARIPOV [40] even found the same coefficients. NIGMATULIN [28] obtained the above formula with $k_1 = 1/6$ and $k_2 = -1/2$. ARNOLD, DREW and LAHEY [41] extended the concept of cell averaging technique to acommodate gradients in the phase distributions and in the discrete phase velocity. In this limiting case, their results are the same as ours.

The Stokes limit, although extensively treated, is still much debated. Early, CAFLISCH and LUKE [30] have evaluated the integral in (4.16) for a random structure of monodispersed particles in an infinite medium, and pointed out the aforementioned divergent behaviour since $\mathbf{v}^*(\mathbf{x}+\mathbf{r}|\mathbf{x})$ decays as the velocity induced by a Stokeslet, i.e. as $1/r$. These foundings have been corroborated by direct simulations [42] but not by experiments (at least not in an unambiguous way). Various arguments have been put forward to solve this issue, and it is worth to briefly recall them in order to illustrate the difficulties encountered when using

(4.16). The first type of arguments is associated with the existence of screening effects which damp the $1/r$ behaviour at infinity. Various screening mechanisms have been proposed. One would be due to a departure from equilibrium of the microstructure of the suspension. For example, considering the interaction of a pair of particles with a third one, KOCH and SHAQFEH [38] predicted a deficit of the pair probability which decreases as $1/r$ at long range, leading to a screening distance of order a/Θ and a variance $v'^2 U_\infty^2 \approx O(1)$, where U_∞ denotes the terminal velocity. So far, the existence of such a microstructure has not been confirmed. On the contrary, the pair density near contact has been found to be significantly higher than the equilibrium one, both in experiments [43, 44], and in simulations (LADD [42]). A second screening effect which was first propounded by KOCH [37] and recently discussed by BRENNER [45], occurs if the inclusions diffusivity becomes strong enough to hamper the momentum transfer in the carrier phase. This "inertial" screening leads to a scaling v'^2/U_∞^2 as $(\Theta/\mathrm{Re}^{\mathrm{d}})^{2/3}$ whose validity remains to be checked. The third mechanism would result from long-range interactions, either with walls [45] or with a large ensemble of particles (SEGRÉ, HERBOLZHEIMER and CHAIKIN [46]). The presence of walls not only induces a decay of the perturbation velocity faster than $1/r$ beyond some distance, but modifies the concentration distribution along a direction transverse to the sedimentation. The axial agitation v'^2/U_∞^2 may then evolve as Θ for the weak interaction regime, or as $\Theta^{2/3}$ for the strong interaction regime [45]. The latter scaling seems also to apply when correlated regions of large extent (10 to 20 times the mean interparticle distance) exist in the flow [46]. However, the conditions under which such "blobs" occur are still not understood.

At intermediate Re^{d}, similar questions arise. Accounting for the inertia brings additional complexity, and the only model we are aware of is due to KOCH [37]. For a slightly polydispersed suspension, a buoyancy screening is proposed which is controlled by pair interactions. The resulting microstructure exibits a pair density deficit in the wake of the test bubble up to a distance of the order $a/(\Theta \mathrm{Re}^{\mathrm{d}})$, and the velocity variance scales $v'^2/U_\infty^2 \approx \Theta \ln(1/\Theta)/\mathrm{Re}^{\mathrm{d}}$ for Re^{d} close to unity. Although the existence of the pair probability deficit in the near wake has been confirmed experimentally [47], the validity of the above scaling has not been clearly established.

This brief overview shows that at low Reynolds numbers, the sole equations controlling the one-inclusion problem ((4.3) and (4.7) – Part II) may be insufficient to devise consistent approximations and to provide a correct estimate for the carrier phase agitation tensor; if some of the above damping mechanisms of $\mathbf{v}^*(\mathbf{x}+\mathbf{r}|\mathbf{x})$ as r tends to infinity are correct, the one-inclusion problem must be connected somehow to the next multi-inclusion (two or even three) problems. This is probably so at intermediate particle Reynolds numbers (20 – 40) for which recent experiments have shown that the deviation from the pure fluid problem

can be surprisingly strong and the pair density structure is highly anisotropic (CARTELLIER and RIVIÈRE, [48]).

5. Cross-correlation terms of the first type

5.1. New averaged dispersed phase velocities

New terms C_α^* and C_α^{**} which correlate the continuous phase presence at one location with the inclusion(s) velocity(ies) at a neighbouring point(s) appear in the conditioned continuity equations of the continuous phase ((4.7) and (4.8) – Part II). They consist in divergence-type sources which involve specific conditionally-averaged velocities which result from $E[X_1^c\varphi_1\mathbf{u}_1]$, $E[X_2^c\varphi_2\mathbf{u}_2]$, $E[X_{1,2}^c\varphi_1\varphi_2\mathbf{u}_1]$ and $E[X_{1,2}^c\varphi_1\varphi_2\mathbf{u}_2]$.

$$
\begin{aligned}
E[X_1^c\varphi_1\mathbf{u}_1] &= \alpha^{c2}(\mathbf{x}^\circ|\mathbf{x})\phi_1\overline{\mathbf{u}^c}^2(\mathbf{x}|\mathbf{x}^\circ),\\
E[X_2^c\varphi_2\mathbf{u}_2] &= \alpha^{c2}(\mathbf{x}|\mathbf{x}^\circ)\phi_1(\mathbf{x}^\circ)\overline{\mathbf{u}^c}^2(\mathbf{x}^\circ|\mathbf{x}),\\
E[X_{1,2}^c\varphi_1\varphi_2\mathbf{u}_1] &= \alpha^{c3}(\mathbf{x}^{\circ\circ}|\mathbf{x},\mathbf{x}^\circ)\phi_2(\mathbf{x},\mathbf{x}^\circ)\overline{\mathbf{u}^c}^3(\mathbf{x}|\mathbf{x}^{\circ\circ},\mathbf{x}^\circ),\\
E[X_{1,2}^c\varphi_1\varphi_2\mathbf{u}_2] &= \alpha^{c3}(\mathbf{x}^{\circ\circ}|\mathbf{x},\mathbf{x}^\circ)\phi_2(\mathbf{x},\mathbf{x}^\circ)\overline{\mathbf{u}^c}^3(\mathbf{x}^\circ|\mathbf{x}^{\circ\circ},\mathbf{x}).
\end{aligned}
\tag{5.1}
$$

To interpret these new dispersed phase velocities, some simple transformations based on ((2.6) – Part I) are used, as $NE[X_1^c\varphi_1\mathbf{u}_1] = \phi^{(1)}\overline{\mathbf{u}}^1 - NE[X_1^d\varphi_1\mathbf{u}_1]$ and further:

$$
\alpha^{c2}(\mathbf{x}^\circ|\mathbf{x})\overline{\mathbf{u}^c}^2(\mathbf{x}|\mathbf{x}^\circ) = \overline{\mathbf{u}}^1(\mathbf{x}) - (N-1)\int\limits_{|\tilde{\mathbf{x}}-\mathbf{x}^\circ|\le a}\chi_2(\tilde{\mathbf{x}}|\mathbf{x})\overline{\mathbf{u}}^2(\mathbf{x}|\tilde{\mathbf{x}})d\tilde{\mathbf{x}}. \tag{5.2}
$$

It can be observed that when $\mathbf{x}^\circ$ increases to infinity, $\mathbf{x}$ being fixed, $\overline{\mathbf{u}}^2(\mathbf{x}|\tilde{\mathbf{x}}) \to \overline{\mathbf{u}}^1(\mathbf{x})$ and using ((2.2) – Part II), we conclude that $\overline{\mathbf{u}^c}^2(\mathbf{x}|\mathbf{x}^\circ) \to \overline{\mathbf{u}}^1(\mathbf{x})$. By commuting $\mathbf{x}^\circ$ and $\mathbf{x}$, a similar expression can be obtained for $\overline{\mathbf{u}^c}^2(\mathbf{x}^\circ|\mathbf{x})$.

Likewise, the relation $N(N-1)E[X^c\varphi_1\varphi_2\mathbf{u}_1] = \phi^{(2)}\overline{\mathbf{u}}^2 - N(N-1)E[X^d\varphi_1\varphi_2\mathbf{u}_1]$ holds and gives:

$$
\begin{aligned}
\alpha^{c3}(\mathbf{x}^{\circ\circ}|\mathbf{x},\mathbf{x}^\circ)\overline{\mathbf{u}^c}^3(\mathbf{x}|\mathbf{x}^{\circ\circ},\mathbf{x}^\circ) &= \overline{\mathbf{u}}^2(\mathbf{x}|\mathbf{x}^\circ)\\
&\quad -(N-2)\int\limits_{|\tilde{\mathbf{x}}-\mathbf{x}^{\circ\circ}|\le a}\chi_3(\tilde{\mathbf{x}}|\mathbf{x}^\circ,\mathbf{x})\overline{\mathbf{u}}^3(\mathbf{x}|\tilde{\mathbf{x}},\mathbf{x}^\circ)d\tilde{\mathbf{x}}.
\end{aligned}
\tag{5.3}
$$

By commuting $\mathbf{x}^\circ$ and $\mathbf{x}$, a similar expression can be obtained for $\overline{\mathbf{u}^c}^3(\mathbf{x}^\circ|\mathbf{x}^{\circ\circ},\mathbf{x})$.

Of course, we also have $\overline{\mathbf{u}^{c}}^{3}(\mathbf{x}^{\circ}|\mathbf{x},\mathbf{x}^{\circ\circ}) \to \overline{\mathbf{u}}^{2}(\mathbf{x}^{\circ}|\mathbf{x})$ and $\overline{\mathbf{u}^{c}}^{3}(\mathbf{x}|\mathbf{x}^{\circ},\mathbf{x}^{\circ\circ}) \to \overline{\mathbf{u}}^{2}(\mathbf{x}|\mathbf{x}^{\circ})$ when $\mathbf{x}^{\circ\circ}$ increases to infinity, $\mathbf{x}$ and $\mathbf{x}^{\circ}$ being fixed.

5.2. Continuity equations for the continuous phase

The above dispersed phase velocities, as given by (5.2) and (5.3), will be expressed in terms of disturbance flows, before calculating C_{α}^{*} and C_{α}^{**} in the conditioned continuity equations of the continuous phase. The equation (5.2) can be written:

$$\overline{\mathbf{u}^{c}}^{2}(\mathbf{x}|\mathbf{x}^{\circ}) = \overline{\mathbf{u}}^{1}(\mathbf{x}) - \frac{N-1}{\alpha^{c2}(\mathbf{x}^{\circ}|\mathbf{x})} \int\limits_{|\tilde{\mathbf{x}}-\mathbf{x}^{\circ}|\leq a} \chi_{2}(\tilde{\mathbf{x}}|\mathbf{x})\mathbf{u}^{*}(\mathbf{x}|\tilde{\mathbf{x}})d\tilde{\mathbf{x}} \tag{5.4}$$

leading to the following first-order continuity (Eq. (4.7) – Part II):

$$\frac{\partial \alpha^{\circ *}}{\partial t} + \frac{\partial}{\partial \mathbf{x}^{\circ}} \cdot \left[\alpha^{\circ *}(\overline{\mathbf{v}^{c}}^{1} + \mathbf{v}^{\circ *}) - \alpha^{c1}\mathbf{v}^{\circ *}\right] \tag{5.5}$$

$$= -\overline{\mathbf{u}}^{1} \cdot \frac{\partial}{\partial \mathbf{x}}\alpha^{\circ *} - \frac{N-1}{\phi_{1}}\frac{\partial}{\partial \mathbf{x}} \cdot \phi_{1} \int\limits_{|\tilde{\mathbf{x}}-\mathbf{x}^{\circ}|\leq a} \chi_{2}(\tilde{\mathbf{x}}|\mathbf{x})\mathbf{u}^{*}(\mathbf{x}|\tilde{\mathbf{x}})d\tilde{\mathbf{x}}.$$

The equation (5.3) can also be expressed in terms of disturbance flows:

$$\overline{\mathbf{u}^{c}}^{3}(\mathbf{x}|\mathbf{x}^{\circ},\mathbf{x}^{\circ\circ}) = \overline{\mathbf{u}}^{2}(\mathbf{x}|\mathbf{x}^{\circ}) \tag{5.6}$$

$$- \frac{N-2}{\alpha^{c3}(\mathbf{x}^{\circ\circ}|\mathbf{x}^{\circ},\mathbf{x})} \int\limits_{|\tilde{\mathbf{x}}-\mathbf{x}^{\circ\circ}|\leq a} \chi_{3}(\tilde{\mathbf{x}}|\mathbf{x}^{\circ},\mathbf{x})[\mathbf{u}^{**}(\mathbf{x}|\tilde{\mathbf{x}},\mathbf{x}^{\circ}) + \mathbf{u}^{*}(\mathbf{x}|\tilde{\mathbf{x}})]d\tilde{\mathbf{x}},$$

and a second one is obtained by commuting $\mathbf{x}^{\circ}$ and $\mathbf{x}$. The second-order continuity (Eq. (4.8) – Part II) becomes then:

$$\frac{\partial \alpha^{\circ\circ **}}{\partial t} + \frac{\partial}{\partial \mathbf{x}^{\circ\circ}} \cdot \{\alpha^{\circ\circ **}[\overline{\mathbf{v}^{c}}^{1}(\mathbf{x}^{\circ\circ}) + \mathbf{v}^{*}(\mathbf{x}^{\circ\circ}|\mathbf{x}) + \mathbf{v}^{*}(\mathbf{x}^{\circ\circ}|\mathbf{x}^{\circ}) + \mathbf{v}^{\circ\circ **}] \tag{5.7}$$

$$- \alpha^{c1}(\mathbf{x}^{\circ\circ})\mathbf{v}^{\circ\circ **}\} + \frac{\partial}{\partial \mathbf{x}^{\circ\circ}} \cdot \{\alpha^{*}(\mathbf{x}^{\circ\circ}|\mathbf{x}^{\circ})[\mathbf{v}^{*}(\mathbf{x}^{\circ\circ}|\mathbf{x}) + \mathbf{v}^{\circ\circ **}]$$

(5.7) [cont.)

$$+\ \alpha^*(\mathbf{x}^{\circ\circ}|\mathbf{x})[\mathbf{v}^*(\mathbf{x}^{\circ\circ}|\mathbf{x}^\circ)+\mathbf{v}^{\circ\circ**}]\}=+\overline{\mathbf{u}}^1\cdot\frac{\partial}{\partial\mathbf{x}}\alpha^{\circ*}+\overline{\mathbf{u}^\circ}^1\cdot\frac{\partial}{\partial\mathbf{x}^\circ}\alpha^*$$

$$-\overline{\mathbf{u}}^2\cdot\frac{\partial}{\partial\mathbf{x}}[\alpha^{\circ\circ**}+\alpha^*(\mathbf{x}^{\circ\circ}|\mathbf{x})]-\overline{\mathbf{u}^\circ}^2\cdot\frac{\partial}{\partial\mathbf{x}^\circ}[\alpha^{\circ\circ**}+\alpha^*(\mathbf{x}^{\circ\circ}|\mathbf{x}^\circ)]$$

$$+\frac{N-1}{\phi_1}\frac{\partial}{\partial\mathbf{x}}\cdot\phi_1\int\limits_{|\tilde{\mathbf{x}}-\mathbf{x}^\circ|\le a}\chi_2(\tilde{\mathbf{x}}|\mathbf{x})\mathbf{u}^*(\mathbf{x}|\tilde{\mathbf{x}})d\tilde{\mathbf{x}}$$

$$+\frac{N-1}{\phi_1^\circ}\frac{\partial}{\partial\mathbf{x}^\circ}\cdot\phi_1^\circ\int\limits_{|\tilde{\mathbf{x}}-\mathbf{x}|\le a}\chi_2(\tilde{\mathbf{x}}|\mathbf{x}^\circ)\mathbf{u}^*(\mathbf{x}^\circ|\tilde{\mathbf{x}})d\tilde{\mathbf{x}}$$

$$-\frac{N-2}{\phi_2}\frac{\partial}{\partial\mathbf{x}}\cdot\phi_2\int\limits_{|\tilde{\mathbf{x}}-\mathbf{x}^{\circ\circ}|\le a}\chi_3(\tilde{\mathbf{x}}|\mathbf{x},\mathbf{x}^\circ)[\mathbf{u}^{**}(\mathbf{x}|\tilde{\mathbf{x}},\mathbf{x}^\circ)+\mathbf{u}^*(\mathbf{x}|\tilde{\mathbf{x}})]d\tilde{\mathbf{x}}$$

$$-\frac{N-2}{\phi_2}\frac{\partial}{\partial\mathbf{x}^\circ}\cdot\phi_2\int\limits_{|\tilde{\mathbf{x}}-\mathbf{x}^{\circ\circ}|\le a}\chi_3(\tilde{\mathbf{x}}|\mathbf{x},\mathbf{x}^\circ)[\mathbf{u}^{**}(\mathbf{x}^\circ|\mathbf{x},\tilde{\mathbf{x}})+\mathbf{u}^*(\mathbf{x}^\circ|\tilde{\mathbf{x}})]d\tilde{\mathbf{x}}.$$

6. Cross-correlation terms of the second type: composite pseudo-turbulent tensors

6.1. Definitions

The second part of the program concerning cross-correlations between properties relative to each phase, deals with C_{v}^* and C_{v}^{**}; they appear in the conditioned momentum equations of the continuous phase ((4.3) and (4.5) – Part II). They collect terms which have already been seen in Sec. 5.1 and two new types of cross-correlations as $E[X_1^c\varphi_1\mathbf{u}_1\mathbf{v}^c]$ and $E[X_{1,2}^c\varphi_1\varphi_2\mathbf{u}_2\mathbf{v}^c]$; these correlate the continuous phase velocity at one point and the inclusions(s) velocity(ies) at a neighbouring point(s). To break down each cross-correlation into a mean flow convection term and an agitation term, we need to define several new fluctuation fields. To begin with, consider:

$$X_1^c(\mathbf{x}^\circ)\varphi_1(\mathbf{x})\mathbf{u}_1=X_1^c(\mathbf{x}^\circ)\varphi_1(\mathbf{x})\overline{\mathbf{u}^c}^2(\mathbf{x}|\mathbf{x}^\circ)+X_1^c(\mathbf{x}^\circ)\varphi_1(\mathbf{x})\mathbf{u}_1^{c''}. \tag{6.1}$$

This first fluctuation field is different from those defined in Sec. 4.4 – Part I. Combining this new field and the standard one $\varphi_1(\mathbf{x})X^c\mathbf{v}^{c''}(\mathbf{x}^\circ)$, defined in Sec. 5.4 –

Part I, yields:

$$(6.2)\quad \sum_{i=1}^{N} E[X_1^c(\mathbf{x}^\circ)\varphi_i(\mathbf{x})\mathbf{u}_i^{c''}\mathbf{v}^{c''}(\mathbf{x}^\circ)] = NE[X_1^c(\mathbf{x}^\circ)\varphi_1(\mathbf{x})\mathbf{u}_1^{c''}\mathbf{v}^{c''}(\mathbf{x}^\circ)]$$

$$= NE[X_1^c(\mathbf{x}^\circ)\varphi_1(\mathbf{x})(\mathbf{u}_1 - \overline{\mathbf{u}^c}^2)(\mathbf{v}^c - \overline{\mathbf{v}^c}^2)]$$

$$= \phi^{(1)}(\mathbf{x})\alpha^{c2}(\mathbf{x}^\circ|\mathbf{x})\overline{\mathbf{u}^c}^2(\mathbf{x}|\mathbf{x}^\circ)\overline{\mathbf{v}^c}^2(\mathbf{x}^\circ|\mathbf{x})$$

$$-NE[X_1^c\varphi_1\mathbf{u}_1]\overline{\mathbf{v}^c}^2 - N\overline{\mathbf{u}^c}^2E[X_1^c\varphi_1\mathbf{v}^c] + NE[X_1^c(\mathbf{x}^\circ)\varphi_1(\mathbf{x})\mathbf{u}_1\mathbf{v}^c]$$

$$= NE[X_1^c(\mathbf{x}^\circ)\varphi_1(\mathbf{x})\mathbf{u}_1\mathbf{v}^c(\mathbf{x}^\circ)] - \phi^{(1)}(\mathbf{x})\alpha^{c2}(\mathbf{x}^\circ|\mathbf{x})\overline{\mathbf{u}^c}^2(\mathbf{x}|\mathbf{x}^\circ)\overline{\mathbf{v}^c}^2(\mathbf{x}^\circ|\mathbf{x}).$$

Thus it is shown that the first above cross-correlation function $NE[X_1^c\varphi_1\mathbf{u}_1\mathbf{v}^c]$, which appears in C_{v}^*, is the sum of a mean composite convection term and of a composite pseudo-turbulent tensor of second-order which is defined by:

$$(6.3)\quad \mathbb{A}^2_{\mathrm{uv}^\circ}(\mathbf{x}^\circ,\mathbf{x}) = \sum_{i=1}^{N} E[X_i^c(\mathbf{x}^\circ)\varphi_i(\mathbf{x})\mathbf{u}_i^{c''}\mathbf{v}^{c''}(\mathbf{x}^\circ)].$$

Similar cross-correlation function appear in C_{v}^{**}. They are broken down in the same way and generate pseudo-turbulent tensors as $\mathbb{A}^2_{\mathrm{uv}^{\circ\circ}}(\mathbf{x}^{\circ\circ},\mathbf{x})$ and $\mathbb{A}^2_{\mathrm{u}^\circ\mathrm{v}^{\circ\circ}}(\mathbf{x}^{\circ\circ},\mathbf{x}^\circ)$ whose definitions are obvious.

The next fluctuation field is defined by:

$$(6.4)\quad X_{1,2}^c(\mathbf{x}^{\circ\circ})\varphi_1(\mathbf{x})\varphi_2(\mathbf{x}^\circ)\mathbf{u}_1 = X_{1,2}^c(\mathbf{x}^{\circ\circ})\varphi_1(\mathbf{x})\varphi_2(\mathbf{x}^\circ)\overline{\mathbf{u}^c}^3(\mathbf{x}|\mathbf{x}^\circ,\mathbf{x}^{\circ\circ})$$

$$+ X_{1,2}^c(\mathbf{x}^{\circ\circ})\varphi_1(\mathbf{x})\varphi_2(\mathbf{x}^\circ)\mathbf{u}_1^{c'''}.$$

It is used to break down the cross-correlation $N(N-1)E[X_{1,2}^c\varphi_1\varphi_2\mathbf{u}_1\mathbf{v}^c]$ of the second type, via the following equalities:

$$(6.5)\quad \sum_{i}^{N}\sum_{j\neq i} E[X_{i,j}^c(\mathbf{x}^{\circ\circ})\varphi_i(\mathbf{x})\varphi_j(\mathbf{x}^\circ)\mathbf{u}_i^{c'''}\mathbf{v}^{c'''}(\mathbf{x}^{\circ\circ})]$$

$$= N(N-1)E[X_{1,2}^c(\mathbf{x}^{\circ\circ})\varphi_1(\mathbf{x})\varphi_2(\mathbf{x}^\circ)\mathbf{u}_1^{c'''}\mathbf{v}^{c'''}(\mathbf{x}^{\circ\circ})]$$

$$= N(N-1)E[X_{1,2}^c(\mathbf{x}^{\circ\circ})\varphi_1(\mathbf{x})(\mathbf{u}_1 - \overline{\mathbf{u}^c}^3)(\mathbf{v}^c - \overline{\mathbf{v}^c}^3)]$$

$$+ \varphi^{(2)}(\mathbf{x},\mathbf{x}^\circ)\alpha^{c3}(\mathbf{x}^{\circ\circ})|\mathbf{x},\mathbf{x}^\circ)\overline{\mathbf{v}^c}^3(\mathbf{x}^{\circ\circ}|\mathbf{x},\mathbf{x}^\circ)\overline{\mathbf{u}^c}^3(\mathbf{x}|\mathbf{x}^\circ,\mathbf{x}^{\circ\circ})$$

$$- \overline{\mathbf{v}^c}^3N(N-1)E[X_{1,2}^c\varphi_1\varphi_2\mathbf{u}_1] - \overline{\mathbf{u}^c}^3N(N-1)E[X_{1,2}^c\varphi_1\varphi_2\mathbf{v}^c]$$

$$+ N(N-1)E[X_{1,2}^c(\mathbf{x}^{\circ\circ})\varphi_1(\mathbf{x})\varphi_2(\mathbf{x}^\circ)\mathbf{u}_1\mathbf{v}^c]$$

(6.5) [cont.]
$$= N(N-1)E[X^c_{1,2}(\mathbf{x}^{oo})\varphi_1(\mathbf{x})\varphi_2(\mathbf{x}^o)\mathbf{u}_1\mathbf{v}^c(\mathbf{x}^{oo})]$$
$$- \phi^{(2)}(\mathbf{x},\mathbf{x}^o)\alpha^{c3}(\mathbf{x}^{oo}|\mathbf{x},\mathbf{x}^o)\overline{\mathbf{v}^c}^3(\mathbf{x}^{oo}|\mathbf{x},\mathbf{x}^o)\overline{\mathbf{u}^c}^3(\mathbf{x}|\mathbf{x}^o,\mathbf{x}^{oo}),$$

and we are led to define the corresponding composite pseudo-turbulent tensor of third order by:

$$\mathbb{A}^3_{\mathrm{uv}^{oo}}(\mathbf{x}^{oo},\mathbf{x}|\mathbf{x}^o) = \sum_i^N \sum_{j\neq i} E[X^c_{i,j}(\mathbf{x}^{oo})\varphi_i(\mathbf{x})\varphi_j(\mathbf{x}^o)\mathbf{u}_i^{c'''}\mathbf{v}^{c'''}(\mathbf{x}^{oo})]. \tag{6.6}$$

A second one, $\mathbb{A}^3_{\mathrm{u}^o\mathrm{v}^{oo}}(\mathbf{x}^{oo},\mathbf{x}^o|\mathbf{x})$, is obtained by commuting $\mathbf{x}^o$ and $\mathbf{x}$; it is used to break down the similar cross-correlation function $N(N-1)E[X^c_{1,2}\varphi_1\varphi_2\mathbf{u}_2\mathbf{v}^c]$.

6.2. Expression of C^*_{v} in the second-order momentum equations for the continuous phase

The calculation of the composite pseudo-turbulent tensors is based on the procedure already used in Secs. 2.1 and 2.2, i.e. it begins by expanding them in terms expressing the contribution of each group, and goes on to break down the contribution of each group. This procedure will not be repeated here in detail. Moreover, we will restrict ourselves to the second order, i.e. to $\mathbb{A}^2_{\mathrm{uv}^o}(\mathbf{x}^o,\mathbf{x})$. Thus, we will not be able at the end to present an expression for C^{**}_{v}. The fluctuating part of such an expression is very complicated, much more than the corresponding one for C^{**}_{α} we have present above (see Eq. (5.6)). Moreover, our general strategy of finding solutions in the diluteness limit which will be presented in the next paper does not generally require the fluctuating part of this term: it suffices to know that it is an $O(\Theta)$ contribution.

We obtain first:

$$\mathbb{A}^2_{\mathrm{uv}^o}(\mathbf{x}^o,\mathbf{x}) = NE[X^c_1(\mathbf{x}^o)\varphi_1(\mathbf{x})\mathbf{u}_1^{c''}\mathbf{v}^{c''}(\mathbf{x}^o)] \tag{6.7}$$
$$= \frac{1}{N-1}\int d\mathbf{x}^{oo}\{\phi^{(2)}(\mathbf{x},\mathbf{x}^{oo})\alpha^{c3}(\mathbf{x}^o|\mathbf{x},\mathbf{x}^{oo})[\overline{\mathbf{u}^c}^3(\mathbf{x}|\mathbf{x}^o,\mathbf{x}^{oo}) - \overline{\mathbf{u}^c}^2(\mathbf{x}|\mathbf{x}^o)]$$
$$\cdot[\overline{\mathbf{v}^c}^3(\mathbf{x}^o|\mathbf{x},\mathbf{x}^{oo}) - \overline{\mathbf{v}^c}^2(\mathbf{x}^o|\mathbf{x})] + \mathbb{A}^3_{\mathrm{uv}^o}(\mathbf{x}^o,\mathbf{x}|\mathbf{x}^{oo})\}.$$

Note that similar computations can be used to express the next third-order composite correlation functions i.e. $\mathbb{A}^3_{\mathrm{uv}^{oo}}(\mathbf{x}^{oo},\mathbf{x}|\mathbf{x}^o)$ and $\mathbb{A}^3_{\mathrm{u}^o\mathrm{v}^{oo}}(\mathbf{x}^{oo},\mathbf{x}^o|\mathbf{x})$. Using (5.4), (5.6), and the definition of the second-order disturbances, the above expression leads to the following result valid up to $O(\Theta)$:

$$\mathbb{A}^2_{\mathrm{uv}^o}(\mathbf{x}^o,\mathbf{x}) = \int d\mathbf{x}^{oo}\{\phi^{(2)}(\mathbf{x},\mathbf{x}^{oo})\alpha^{c3}(\mathbf{x}^o|\mathbf{x}\mathbf{x}^{oo})\mathbf{u}^*(\mathbf{x}|\mathbf{x}^o) \tag{6.8}$$
$$\cdot[\mathbf{v}^*(\mathbf{x}^o|\mathbf{x}) + \mathbf{v}^{**}(\mathbf{x}^o|\mathbf{x},\mathbf{x}^{oo})]\} + \ldots$$

Having at our disposal $\mathbb{A}^2_{\mathrm{uv}^\circ}$ as well as the cross-correlation of the second type (see Sec. 5), the source term C^*_{v} appearing in the conditioned momentum equation ((4.7) – Part II) can be completely expressed in terms of disturbance flows.

$$
\begin{aligned}
(6.9) \qquad C^*_{\mathrm{v}}(\mathbf{x}^\circ|\mathbf{x}) &= \overline{\mathbf{v}^c}^2(\mathbf{x}^\circ|\mathbf{x}) \cdot \frac{\partial}{\partial \mathbf{x}} E[\varphi_1 X_1^c \mathbf{u}_1]/\alpha^{c2}\phi_1 \\
&- \frac{\partial}{\partial \mathbf{x}} \cdot E[\varphi_1 X_1^c \mathbf{u}_1 \mathbf{v}^c]/\alpha^{c2}\phi_1 = \overline{\mathbf{v}^c}^2 \cdot \frac{\partial}{\partial \mathbf{x}} \overline{\mathbf{u}^c}^2 - \frac{\partial}{\partial \mathbf{x}} \cdot \overline{\mathbf{u}^c}^2 \overline{\mathbf{v}^c}^2 \\
&+ [\overline{\mathbf{u}^c}^2 \overline{\mathbf{v}^c}^2 - \overline{\mathbf{v}^c}^2 \overline{\mathbf{u}^c}^2] \cdot \frac{\partial}{\partial \mathbf{x}} \mathrm{Log}(\alpha^{c2}\phi_1) - \frac{\partial}{\partial \mathbf{x}} \cdot \mathbb{A}^2_{\mathrm{uv}^\circ}/\alpha^{c2}\phi^{(1)}.
\end{aligned}
$$

7. Conclusions

To describe laminar flows carrying spherical inclusions, we succeeded to obtain at the end of Part I, two infinite sets of equations; the revisited BBGKY hierarchy for the dispersed phase and the revisited Lundgren hierarchy (LUNDGREN [49]) for the continuous phase. The first-order or bulk flow equations issued from both hierarchies constitute the basic building blocks of our two-fluid approach. Higher-order equations, which do not appear in usual two-fluid models, have to be retained as a rule up to some order depending on whether the mixture is more or less dilute. It happens that these higher-order equations are very complicated; as matters stand, they cannot easily be simplified nor truncated. The purpose of the second part was to transform these equations into equations controlling new conditional disturbance fields which are much more tractable.

Whatever their number or form may be, the disturbance flow equations have to be treated on an equal footing as the bulk flow equations in the final resulting model. At any time and at any location, they appear as the natural frame to specify the micro-problems, the solution of which provides the missing information to close the bulk flow equations. Among this information, the most delicate piece concerns pseudo-turbulence. This whole article part has been devoted to show that solution of the above micro-problems can effectively be used to estimate various pseudo-turbulent tensors and correlation functions.

Comparison with other similar studies is difficult. First of all, having regard to most of our correlations, it is simply impossible since usual models do not include these quantities: they are specific of our approach and have been ignored so far (i.e. second and higher-order pseudo-turbulent tensors, correlations and cross-correlations of the first and of the second type). The first-order pseudo-turbulent tensor for the continuous phase is an exception to this rule since it has given rise to many studies. Observe first that analogy with single-phase turbulent momentum transport is not allowed and that it is difficult to model this tensor in a standard approach since fluctuations are only generated by the flow around

individual inclusions. As a consequence, some micro-problems corresponding to schools of thought evoked in the introduction of Part I come inevitably to the assistance of modellers. Among various proposals, a formula derived by KOCH and SHAQFEY [38], in a more restricted framework, has been compared to our results; the two leading order terms of their formula correspond to the first two terms of a multipole expansion of the expression we have found for the first-order pseudo-turbulent tensor.

It might be pointed out that first-order pseudo-turbulent tensors we have proposed are not expressed in terms of bulk-flow variables and cannot be directly used in ordinary two-phase models. As the other unknowns terms met in the previous parts, they are explicitly related to the first-order disturbance flow equations. Thus, they are awaiting a closure relationship which results in our approach from solving specific micro-problems described by higher-order disturbance flow equations. The exact form of these extra equations, the way (one-way or two-way) they are coupled with bulk-flow equations depend on each considered physical situation (e.g. low or high inclusion Reynolds number). So does the ultimate number of equations in the final closed model which is given by the afore-mentioned truncation procedure, based on diluteness, which will be developped in the next Part IV.

References

1. J. L. ACHARD and A. CARTELLIER, *Laminar dispersed two-phase flows at low concentration. Part I. Generalised system of equations*, Arch. Mech., **52**, 1, 25–53, 2000.
2. J. L. ACHARD and A. CARTELLIER, *Laminar dispersed two-phase flows at low concentration. Part II. Disturbance equations*, Arch. Mech., **52**, 2, 275–302, 2000.
3. YU. A. BUYEVICH, *Statistical hydromechanics of disperse systems. Part 1. Physical background and general equations*, J. Fluid Mech., **49**, 489–507, 1971.
4. YU. A. BUYEVICH, *Statistical hydromechanics of disperse systems. Part 2. Solution of the kinetic equation for suspended particles*, J. Fluid Mech., **52**, 345–355, 1972.
5. YU. A. BUYEVICH and I. N. SHCHELCHKOVA, *Flow of dense suspensions*, Prog. Aerospace Sci., **18**, 121–150, 1978.
6. M. LANCE, *Étude de la turbulence dans les écoulements diphasiques dispersés*, Thèse d'état, Univ. Cl. Bernard, Lyon, France 1986.
7. M. LANCE and J. BATAILLE, *Turbulence in the liquid phase of a uniform bubbly air-waterflow*, J. Fluid Mech., **222**, 95–118, 1991.
8. M. LANCE, J. L. MARIÉ and J. BATAILLE, *Homogeneous turbulence in bubbly flow*, J. Fluid Engng., **113**, 295–300, 1991.
9. M. LANCE, J. L. MARIÉ and J. BATAILLE, C. SUZANNE, V. ROIG, R. BEL FADHILA and L. MASBERNAT, *Experimental study of turbulent bubbly shear flows*, Chem. Engng. Comm., **141–142**, 51–70, 1996.
10. I. MICHIYOSHI and A. SERIZAWA, *Turbulence in two-phase bubbly flow*, Nuclear Engng. Design, **95**, 253–267, 1986.

11. A. SERIZAWA and I. KATAOKA, *Turbulence suppressions in bubbly two-phase flows*, Nuclear Engng. Design, **122**, 1–16, 1990.

12. Y. TSUJI, Y. MORIKAWA and H. SHIOMI, *LDV measurements of an air-solid two-phase flow in a vertical pipe*, J. Fluid Mech., **139**, 417–434, 1984.

13. R. N. PARTHASARATHY and G. M. FAETH, *Turbulence modulation in homogeneous dilute particle-laden flows*, J. Fluid Mech., **220**, 485–514, 1990.

14. M. MIZUKAMI, R. N. PARTHASARATHY, G. M. FAETH, *Particle-generated turbulence in homogeneous dilute dispersed flows*, Int. J. Multiphase Flow., **18**, 3, 397–412, 1992.

15. K. SQUIRES and J. EATON, *Particle response and turbulence modification in isotropic turbulence* , Phys. Fluids, **A2**, 7, 130, 1990.

16. S. ELGOBASHI and G. C. TRUESDELL, *Direct simulation of particle dispersion in a decaying isotropic turbulence*, J. Fluid Mech., **242**, 655, 1992.

17. M. BOIVIN, O. SIMONIN and K. D. SQUIRES, *Direct numerical simulation of turbulence modulation by particles in isotropic turbulence*, J. Fluid Mech., **375**, 235–263, 1998.

18. K. SQUIRES and J. EATON, *Preferential concentration of particles by turbulence*, Phys. Fluids, **A3**, 130, 1991.

19. WANG and M. MAXEY, *Setting velocity and concentration distribution of heavy particles in homogeneous isotropic turbulence*, J. Fluid Mech., **256**, 27–68, 1993.

20. S. ELGOBASHI and G. C. TRUESDELL, *On the two-way interaction between homogeneous turbulence and dispersed solid particles I: turbulence modulation*, Phys. Fluids, **A5**, 1790, 1993.

21. O. A. DRUZHININ and S. ELGOBASHI, *Direct numerical simulation of bubbles laden turbulent flows using the two-fluid formulation*, Phys. Fluids, **A10**, 3, 685–697, 1998.

22. M. LANCE, J. L. MARIÉ and J. BATAILLE, *Turbulence in bubbly flows: from experiments to numerical modelling*, [In:] Proc. 2nd International Symposium on two-phase flow modelling and experimentation, Vol. I, 17–18, Roma 1999.

23. R. CLIFT, J. R. GRACE and M. E. WEBER, *Bubbles, drops and particles*, Academic Press, New York, San Francisco, London 1978.

24. A. ESMAEELI and G. TRYGGVASON, *Direct numerical simulations of bubbly flows.Part 1. Low Reynolds number arrays*, J. Fluid Mech., **377**, 313–345, 1998.

25. W. B. RUSSEL, D. A. SAVILLE and W. R. SCHOWALTER, *Colloidal dispersions*, Cambridge University Press, 1989.

26. H. HASIMOTO, *On the periodic fundamental solutions of the stokes equations and their application to viscous flow past a cubic array of spheres*, J. Fluid Mech., **5**, 317–328, 1959.

27. M. J. MIKSIS and L. TING, *Wave propagation in a bubbly liquid with finite-amplitude asymmetric bubble oscillations*, Phys. Fluids, **29**, 603–618, 1986.

28. R. I. NIGMATULIN, *Spatial averaging in the mechanics of heterogeneous and dispersed systems*, Int. J. Multiphase Flow, **5**, 353–385, 1979.

29. A. CARTELLIER, L. TIMKIN and N. RIVIÈRE, *New structures of Poiseuille bubbly flows due to clustering*, [In:] Proc. of ASME-FEDSM 97 and 6th Int. Symp. on Gas-liquid Two-phase Flows, paper 3528, June 22–26, Vancouver 1997.

30. R. E. CAFLISCH and J. H. C. LUKE, *Variance in the sedimentation speed of a suspension*, Phys. Fluids, **28**, 759–760, 1985.

31. R. JACKSON, *Locally averaged equations of motion for a mixture of identical spherical particles and a Newtonian fluid*, Chem. Engng. Sci., **52**, 15, 2457–2469, 1997 and Addena Chem. Engng. Sci., **52**, 23, 4437, 1997, and Chem. Engng. Sci., **53**, 10, 1955, 1998.

32. J. RUBINSTEIN and J. B. KELLER, *Particle distribution functions in suspensions*, Phys. Fluids, **A1**, 10, 1632–1641, 1989.

33. A. BIESHEUVEL and W. C. M. GORISSEN, *Two-phase flow equations for a dilute dispersion of gas bubbles in liquid*, Int. J. Multiphase Flow, **21**, 107–117, 1990.

34. A. S. SANGANI and A. K. DIDWANIA, *Dispersed-phase stress tensor in flows of bubbly liquid at large Reynolds number*, J. Fluid Mech., **248**, 27–54, 1993.

35. D. Z. ZHANG and A. PROSPERETTI, *Ensemble phase-averaged equations for bubbly flows*, Phys. Fluids, **6**, 2956–2970, 1994.

36. H. F. BULTHUIS, A. PROSPERETTI and A. S. SANGANI, *'Particle stress' in disperse two-phase potential flow*, J. Fluid Mech., **294**, 1–16, 1995.

37. D. L. KOCH, *Hydrodynamic diffusion in dilute sedimenting suspensions at moderate Reynolds numbers*, Phys. Fluids, **5**, 1141–1155, 1993.

38. D. L. KOCH and E. S. SHAQFEH, *Screening in sedimenting suspensions*, J. Fluid Mech., **224**, 275–303, 1991.

39. A. BIESHEUVEL and L. VAN WIJNGAARDEN, *Two-phase flow equations for a dilute dispersion of gas bubbles in liquid*, J. Fluid Mech., **148**, 301–318, 1984.

40. R. M. GARIPOV, *Closed system of equations for the motion of a liquid with gas bubbles*, Zh. Prikl. Mekh. Tekhn. Fiz., **6**, 3–24, 1973.

41. G. S. ARNOLD, D. A. DREW and R. T. LAHEY Jr., *Derivation of constitutive equations for interfacial force and Reynolds stress for a suspension of spheres using ensemble cell averaging*, Chem. Engng. Comm., **86**, 43–54, 1986.

42. A. J. C. LADD, *Sedimentation of homogeneous suspensions of non-Brownian sphere*, Phys. Fluids, **9**, 3, 491–499, 1997.

43. F. FEUILLEBOIS, L. TALINI and J. LEBLOND, *Sedimentation phenomena and structure in suspensions*, [In:] *Continuum models and discrete systems*, Proc. of the 9th Int. Symp., June 29–July 3, Istanbul, Turkey 1998.

44. F. ROUYER, *Structure et dynamique de suspensions modèles à 2 et 3 dimensions*, Thèse de l'Univ. Paris XI, Paris 1999.

45. M. BRENNER, *Screening mechanisms in sedimentation*, Phys. Fluids, **11**, 4, 754–772, 1999.

46. P. N. SEGRÉ, E. HERBOLZHEIMER and P. M. CHAIKIN, *Long range correlations in sedimentation*, Phys. Rev. Letters, **79**, 13, 2574–2577, 1997.

47. N. RIVIÈRE and A. CARTELLIER, *Bubble-induced agitation at moderate particulate Reynolds numbers*, [In:] Proc. of the 3rd Int. Conf. Multiphase Flow, 8–12 June, 475, Lyon, France 1998.

48. A. CARTELLIER and N. RIVIÈRE, *Bubble-induced agitation and microstructure in uniform bubbly flows at small to moderate particle Reynolds number*, Phys. Fluids, 2000.

49. T. S. LUNDGREN, *Slow flow through stationary random beds and suspensions of spheres*, J. Fluid Mech., **51**, 273–299, 1972.

Received June 3, 2000; revised version December 4, 2000.

Arch. Mech., **53**, 2, pp. 151–166, Warszawa 2001

Buoyancy effects in boundary layers on a continuously moving vertical surface with a parallel free stream

H. S. TAKHAR ([1]), M. KUMARI ([2]) and G. NATH ([2])

([1]) *Manchester School of Engineering*
University of Manchester
Manchester M13 9PL, U.K.

([2]) *Department of Mathematics*
Indian Institute of Science
Bangalore-560 012, India

AN ANALYSIS IS PERFORMED to study the effect of the buoyancy force on the flow and heat transfer characteristics in a viscous fluid over a heated vertical continuously moving surface with a parallel free stream. The buoyancy force varies with the streamwise distance x and hence introduces nonsimilarity in the flow field. Both the constant wall temperature and constant heat flux conditions are included in the analysis. The partial differential equations governing the flow are solved numerically. Closed form solutions are obtained when the wall and free stream velocities are equal and there is no buoyancy force. Also the correlation equations for the local Nusselt number are developed. It is found that for opposing flow or for an upstream moving wall, the solution does not exist beyond a certain value of the buoyancy parameter or the ratio of wall and free stream velocities.

Notations

C_{fx}	local skin friction coefficient
f, F	reduced stream functions
g	gravitational acceleration
Gr_x , Gr_x^*	Grashof numbers
G, H	dimensionless temperatures
k	thermal conductivity
Nu_x	local Nusselt number
Pr	Prandtl number
q_w	local surface heat transfer rate per unit area
Re_x	local Reynolds number
T	fluid temperature
T_w, T_∞	wall and free stream temperatures
u, v	velocity components in x and y directions
u_w, u_∞	wall and free stream velocities
x, y	axial and normal coordinates

Greek symbols

α	thermal diffusivity
β	volumetric coefficient of thermal expansion
η	pseudo-similarity variable
μ, ν	dynamic and kinematic viscosities
ξ, ξ_1	buoyancy force parameters
ψ	stream function

Subscripts

w	condition on the surface
x, y	derivatives with respect to x and y, respectively
∞	condition in the free stream

Superscript

prime	derivative with respect to η

1. Introduction

THE STUDY OF FLOW AND HEAT TRANSFER in the boundary layer induced by a continuously moving surface with a parallel free stream is useful in many manufacturing processes in various fields of industry such as cooling of an infinite metallic plate in a cooling bath, the boundary layer along material handling conveyers, the aerodynamic extrusion of plastic sheets, and the boundary layer along a liquid film in condensation processes. In order to understand the main features of such a process, the flow field induced by a continuous flat surface which issues from a slot and moves with a constant velocity into a fluid, either at rest or with constant free stream, has been considered by many investigators [1 – 4]. In recent years several authors [4 – 9] have considered the effect of buoyancy force on a continuously moving surface in a fluid at rest.

Here the effect of buoyancy force on the flow and heat transfer on a heated vertical, continuous moving surface with a parallel free stream has been studied. Both the constant wall temperature and constant heat flux conditions have been considered. The partial differential equations governing the nonsimilar flow have been solved using an implicit finite difference scheme. The nonsimilarity in the flow field is due to the buoyancy force which varies with axial distance x. In absence of the buoyancy force, the governing equations reduce to the ordinary differential equations and closed-form solutions have been obtained. Also correlation equations for the local Nusselt number have been developed. Particular cases of the present results have been compared with those of MUCOGLU and CHEN [10], MOUTSOGLOU and CHEN [6] and ABDELHAFEZ [2].

2. Governing equations

Let us consider a continuous flat surface that originates from a slot and is moving with a constant velocity u_w in vertical direction in a fluid having constant free stream velocity u_∞ and temperature T_∞. The positive x coordinate is measured along the direction of the moving surface with the slot as the origin, and the positive y coordinate is measured normal to the surface in the outward direction toward the fluid (see Fig. 1). The surface is assumed to be either maintained at a constant wall temperature T_w or subjected to a constant surface heat flux q_w. The velocity of the moving surface u_w is considered to be either greater or smaller than the free stream velocity u_∞. The buoyancy force is assumed to act in the same direction or in the direction opposite to the forced flow (i.e., the buoyancy force assists or opposes the forced flow). On the basis of boundary layer approximations and with the use of Boussinesq approximations, the governing equations for the problem under consideration for constant wall temperature (CWT) case based on the principles of conservation of mass, momentum and energy can be written as [10]

$$u_x + v_y = 0, \tag{2.1}$$

$$uu_x + vu_y = \nu u_{yy} + g\beta(T - T_\infty), \tag{2.2}$$

$$uT_x + vT_y = \alpha T_{yy}. \tag{2.3}$$

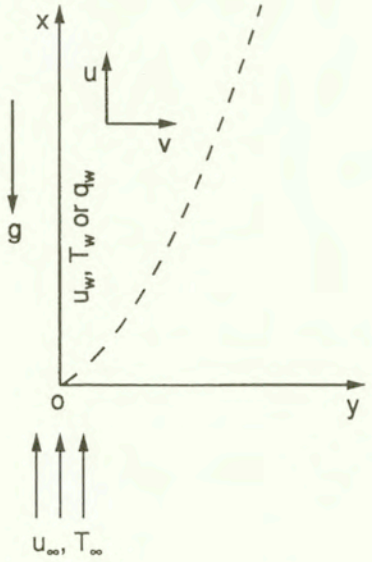

FIG. 1. Physical model and co-ordinate system.

The boundary conditions satisfying the no-slip conditions at the wall and matching with the inviscid flow solutions at the edge of the boundary layer are given by

$$\begin{aligned} u(x,0) &= u_w, \qquad v(x,0) = 0, \quad T(x,0) = T_w, \\ u(x,\infty) &= u_\infty, \quad T(x,\infty) = T_\infty, \\ u(0,y) &= u_\infty, \qquad T(0,y) = T_\infty, \quad y > 0. \end{aligned} \tag{2.4}$$

In order to transform equations (2.1) – (2.3) in dimensionless form, we apply the following transformations:

$$\eta = (u_\infty/\nu x)^{1/2} y\,, \qquad \xi = \xi(x) = \mathrm{Gr}_x/\mathrm{Re}_x^2,$$

$$f(\xi,\eta) = \psi(x,y)/(\nu u_\infty x)^{1/2},$$

$$G(\xi,\eta) = (T(x,y) - T_\infty)/(T_w - T_\infty), \tag{2.5}$$

$$\mathrm{Gr}_x = g\beta(T_w - T_\infty)x^3/\nu^2, \quad \mathrm{Re}_x = u_\infty x/\nu\,, \quad f' = \partial f/\partial\eta,$$

$$u = \psi_y\,, \quad v = -\psi_x\,, \quad \mathrm{Pr} = \nu/\alpha\,, \quad f'(\xi,\eta) = u/u_\infty\,, \quad G' = \partial G/\partial\eta$$

to (2.1) – (2.3) and we find that (2.1) is identically satisfied, and (2.2) and (2.3) are reduced to

$$f''' + 2^{-1} f f'' + \xi G = \xi(f'\partial f'/\partial\xi - f''\partial f/\partial\xi), \tag{2.6}$$

$$\mathrm{Pr}^{-1} G'' + 2^{-1} f G' = \xi(f'\partial G/\partial\xi - G'\partial f/\partial\xi). \tag{2.7}$$

The boundary conditions (2.4) can be expressed as

$$\begin{aligned} f(\xi,0) = f'(\xi,0) - (u_w/u_\infty) &= G(\xi,0) - 1 = 0, \\ f'(\xi,\infty) - 1 &= G(\xi,\infty) = 0. \end{aligned} \tag{2.8}$$

When the surface velocity is greater than the freestream velocity (i.e., $(u_w/u_\infty) > 1$), we take the reference velocity as u_w instead of u_∞ in Eq. (2.5). The governing Eqs. (2.6) and (2.7) remain unaltered. The boundary conditions can be written as

$$\begin{aligned} f(\xi,0) &= f'(\xi,0) - 1 = G(\xi,0) - 1 = 0 \\ f'(\xi,\infty) &- (u_\infty/u_w) = G(\xi,\infty) = 0 \end{aligned} \tag{2.9}$$

For the constant heat flux (CHF) case, the governing equations along with the boundary conditions for $u_w/u_\infty \leq 1$ can be expressed in the form [10]

$$F''' + 2^{-1}FF'' + \xi_1 H = (3/2)\xi_1(F'\partial F'/\partial\xi_1 - F''\partial F/\partial\xi_1), \tag{2.10}$$

$$\mathrm{Pr}^{-1}H'' + 2^{-1}(FH' - F'H) = (3/2)\xi_1(F'\partial H/\partial\xi_1 - H'\partial F/\partial\xi_1), \tag{2.11}$$

$$\begin{gathered} F(\xi_1, 0) = F'(\xi_1, 0) - (u_w/u_\infty) = H'(\xi_1, 0) + 1 = 0, \\ F'(\xi_1, \infty) - 1 = H(\xi_1, \infty) = 0. \end{gathered} \tag{2.12}$$

When $u_w/u_\infty > 1$, the boundary conditions are

$$\begin{gathered} F(\xi_1, 0) = F'(\xi_1, 0) - 1 = H'(\xi_1, 0) + 1 = 0, \\ F'(\xi_1, \infty) - (u_\infty/u_w) = H(\xi_1, \infty) = 0. \end{gathered} \tag{2.13}$$

For $u_w/u_\infty \leq 1$

$$\begin{aligned} \eta &= (u_\infty/\nu x)^{1/2} y, \xi_1 = \xi_1(x) = \mathrm{Gr}_x^*/\mathrm{Re}_x^{5/2}, \\ F(\xi_1, \eta) &= \psi(x, y)/(\nu u_\infty x)^{1/2}, \\ H(\xi_1, \eta) &= (T - T_\infty)\mathrm{Re}_x^{1/2}/(q_w x/k), \\ \mathrm{Gr}_x^* &= g\beta q_w x^4/k\nu^2, F'(\xi_1, \eta) = u/u_\infty. \end{aligned} \tag{2.14}$$

For $u_w/u_\infty > 1, u_\infty$ is replaced by u_w in (2.14).

From the solutions of Eqs. (2.6) and (2.7) under conditions (2.8) and (2.9) and Eqs. (2.10) and (2.11) under conditions (2.12) and (2.13), we can obtain the stream function, velocity and temperature in dimensionless form for both CWT and CHF cases (f, f', G, F, F', H).

It may be noted that Eqs. (2.6) and (2.7) under conditions (2.8) and Eqs. (2.10) and (2.11) under conditions (2.12) for $u_w/u_\infty = 0$ (i.e., for a stationary surface) reduce to those of MUCOGLU and CHEN [10] who studied the mixed convection flow over a stationary surface. Similarly, Eqs. (2.6) and (2.7) under conditions (2.9) and Eqs. (2.10) and (2.11) under conditions (2.13) for $u_\infty/u_w = 0$, (i.e., for a moving surface in a quiescent liquid) reduce to those of MOUTSOGLOU and CHEN [6] who studied the effect of the buoyancy force on the moving surface. Also, Eqs. (2.6) and (2.7) under conditions (2.8) and (2.9) for $\xi = 0$ (i.e., no buoyancy force) reduce to those of ABDELHAFEZ [2].

The local skin friction coefficient and the local Nusselt number (heat transfer coefficient) for the CWT case are expressed in the form [10].

$$\begin{aligned} C_{fx} &= 2\mu(u_y)_w/\rho U^2 = 2\mathrm{Re}_x^{-1/2} f''(\xi, 0), \\ \mathrm{Nu}_x &= -k(T_y)_w x/(T_w - T_\infty) = -\mathrm{Re}_x^{1/2} G'(\xi, 0). \end{aligned} \tag{2.15}$$

The corresponding results for the CHF case are given by [10]

$$\begin{aligned} C_{fx} &= 2\mathrm{Re}_x^{-1/2} F''(\xi_1, 0), \\ \mathrm{Nu}_x &= \mathrm{Re}_x^{1/2} / H(\xi_1, 0). \end{aligned} \tag{2.16}$$

Here the reference velocity U is either u_∞ or u_w.

It may be remarked that for $\xi = 0$ (CWT case), Eqs. (2.6) and (2.7) and for $\xi_1 = 0$ (CHF case), Eqs. (2.10) and (2.11), reduce to ordinary differential equations and they, under conditions (2.8) and (2.12), admit a closed-form solution when $u_w = u_\infty$. The solution for the CWT case is given by

$$\begin{aligned} f(\eta) &= \eta, \; G(\eta) = erfc\left[(\mathrm{Pr})^{1/2}\, \eta/2\right], \\ G'(0) &= -(\mathrm{Pr}/\pi)^{1/2}. \end{aligned} \tag{2.17}$$

For the CHF case, the solution is expressed as

$$\begin{aligned} F(\eta) &= \eta, \\ H(\eta) &= -2(B\mathrm{Pr})^{-1} \exp\left[-\mathrm{Pr}(\mathrm{Pr}+2)\eta^2/16\right] \\ &\quad \times \left[A_1 F_1\left(\frac{2+3\mathrm{Pr}}{8}, \frac{1}{2}, \frac{(\mathrm{Pr}\eta)^2}{8}\right)\right. \\ &\quad \left. + \; B\,(\mathrm{Pr}\eta/2)\, {}_1F_1\left(\frac{6+3\mathrm{Pr}}{8}, \frac{3}{2}, \frac{(\mathrm{Pr}\,\eta)^2}{8}\right)\right], \end{aligned} \tag{2.18}$$

where the confluent hypergeometric function ${}_1F_1$ is given by

$$\begin{aligned} {}_1F_1(a, b;\, x) &= \sum_{i=0}^{\infty} C_i x^i, \qquad C_i = \frac{a(a+1)\cdots(a+i-1)}{b(b+1)\cdots(b+i-1)} \frac{1}{i!}, \\ A &= \Gamma(1/2)/\Gamma(6+3\mathrm{Pr})/8\,, \qquad B = 2^{1/2}\left[\Gamma(2+3\mathrm{Pr})/8\right]/\Gamma(-1/2). \end{aligned} \tag{2.19}$$

The above results are found to be in very good agreement with those obtained numerically (they differ by less than 0.5 per cent).

The correlation equations for the local Nusselt number (Nu_x) involving Prandtl number (Pr), buoyancy parameter (ξ or ξ_1) and the ratio of free stream and wall velocities (u_∞/u_w) have been obtained following the analysis of CHURCHILL [11] and RAMACHANDRAN *et al.* [8]. The correlation equation for the local Nusselt number (Nu_x) for the CWT case which is valid for $0.5 \le \mathrm{Pr} \le 50$, $-0.5 \le \xi \le 5$, $-0.25 \le (u_\infty/u_w) \le 1$, is given by

$$(\mathrm{Nu}_x/\mathrm{Nu}_{x1})^3 = 1 \pm (\mathrm{Nu}_{xN}/\mathrm{Nu}_{x1})^3 \tag{2.20}$$

which can be expressed as

$$Y^3 = 1 \pm X^3, \tag{2.21}$$

where

$$Y = (\mathrm{Nu}_x/\mathrm{Nu}_{x1}) \,, \qquad X = (\mathrm{Nu}_{xN}/\mathrm{Nu}_{x1}) \,. \tag{2.22}$$

The local Nusselt number for the pure forced convection flow (Nu_{x1}) can be expressed as

$$\mathrm{Nu}_{x1} = F_1 \,(\mathrm{Pr}, \xi, \lambda) \,(\mathrm{Re}_x)^{1/2} \,, \qquad \lambda = u_\infty/u_w \leq 1, \tag{2.23}$$

where

$$F_1 \,(\mathrm{Pr}, \xi, \lambda) = \left[1.8865(\mathrm{Pr})^{11/12} - 1.4447(\mathrm{Pr})^{1/4}\right] \left[1 + (0.325)^{(1+\xi^{1/2})}\lambda\right]. \tag{2.24}$$

The local Nusselt number for the pure free convection flow (Nu_{xN}) is given by [12]

$$\mathrm{Nu}_{xN} = F_2(\mathrm{Pr})(\mathrm{Gr}_x)^{1/4}, \tag{2.25}$$

where

$$F_2(\mathrm{Pr}) = 0.75\mathrm{Pr}^{1/2} \left[2.5\left(1 + 2\mathrm{Pr}^{1/2} + 2\mathrm{Pr}\right)\right]^{-1/4}. \tag{2.26}$$

When $\lambda_1 = u_w/u_\infty < 1$, $F_1(\mathrm{Pr}, \xi, \lambda_1)$ is given by

$$F_1(\mathrm{Pr}, \xi, \lambda_1) = \left[1.7732(\mathrm{Pr})^{11/12} - 1.4412(\mathrm{Pr})^{1/4}\right] \times \left[1 + (0.5001)^{(1+\xi^{5/6})}\lambda\right]. \tag{2.27}$$

The relation (2.17) holds good for the CHF case also, but F_1 and F_2 are replaced by G_1 and G_2, respectively, and they are expressed as

$$G_1(\mathrm{Pr}, \xi_1, \lambda) = [2.8452(\mathrm{Pr})^{13/32} - 2.0947(\mathrm{Pr})^{1/4}] \times \left[1 + (0.150)^{(1+\xi_1)^{1/4}}\lambda\right], \tag{2.28}$$

$$G_2(\mathrm{Pr}) = (\mathrm{Pr})^{2/5} \left[4 + 9(\mathrm{Pr})^{1/2} + 10\mathrm{Pr}\right]^{-1/5}. \tag{2.29}$$

For $\lambda_1 < 1$

$$G_1(\mathrm{Pr}, \xi_1, \lambda_1) = \left[2.7347(\mathrm{Pr})^{13/12} - 2.3342(\mathrm{Pr})^{1/4}\right] \times \left[1 + (0.702)^{(1+\xi_1)^{6/5}}\lambda_1\right]. \tag{2.30}$$

These correlations give results which are accurate to within 8 percent of the predicted results.

3. Results and discussion

The nonlinear coupled partial differential Eqs. (2.6) and (2.7) under conditions (2.8) and (2.9) and Eqs. (2.10) and (2.11) under conditions (2.12) and (2.13) have been solved numerically using an implicit finite-difference scheme which is described in detail in [13]. In order to assess the accuracy of our method, we have compared our skin friction and heat transfer results ($2^{-1}\mathrm{Re}_x^{1/2}\, C_{fx}$, $\mathrm{Re}_x^{-1/2}\mathrm{Nu}_x$) for $u_w/u_\infty = 0$ with those of MUCOGLUand CHEN [10], and for $u_\infty/u_w = 0$ with those of MOUTSOGLOU and CHEN [6]. Also for $\xi = 0$, we have compared our skin friction and heat transfer results for the CWT case with those of ABDELHAFEZ [2]. In all the cases the results are found to be in very good agreement (the maximum difference is about 1.5 per cent). The comparison is shown in Tables 1 and 2 and Figs. 2 and 3.

Table 1. Comparison of skin friction and heat transfer parameters for constant wall temperature case (CWT) when $u_\infty/u_w = 0$ in Eq. (2.9).

		Present results		MOUTSOGLOU and CHEN [6]	
Pr	ξ	$f''(\xi,0)$	$-G'(\xi,0)$	$f''(\xi,0)$	$-G'(\xi,0)$
0.7	0.0	-0.44370	0.35190	-0.44375	0.34924
0.7	0.5	-0.10676	0.41307	-0.10558	0.41320
0.7	1.0	0.19090	0.44928	0.19425	0.45505
0.7	2.0	0.72831	0.49883	0.73552	0.50031
0.7	3.0	1.21948	0.53468	1.23103	0.53681
0.7	4.0	1.68038	0.56342	1.69652	0.56609
7.0	0.0	-0.44370	1.37164	-0.44375	1.38703
7.0	0.5	-0.28239	1.39670	-0.28376	1.41322
7.0	1.0	-0.12624	1.41978	-0.12876	1.43712
7.0	2.0	0.17354	1.46130	0.16880	1.48026
7.0	3.0	0.45995	1.49803	0.45318	1.51864
7.0	4.0	0.73573	1.53110	0.72697	1.55334

Figure 2 shows the local Nusselt number ($\mathrm{Re}_x^{-1/2}\mathrm{Nu}_x$) and local skin friction coefficient ($\mathrm{Re}_x^{1/2}C_{fx}/4$) for both CWT and CHF cases as a function of velocity difference ($1 - u_w/u_\infty$) when $u_w/u_\infty \leq 1$ for three values of the buoyancy parameter ξ or ξ_1. For a given buoyancy parameter ξ or ξ_1, the local skin friction coefficient ($\mathrm{Re}_x^{1/2}C_{fx}/4$) increases as the velocity difference ($1 - u_w/u_\infty$) increases, but the local Nusselt number ($\mathrm{Re}_x^{-1/2}\mathrm{Nu}_x$) decreases. The effect is

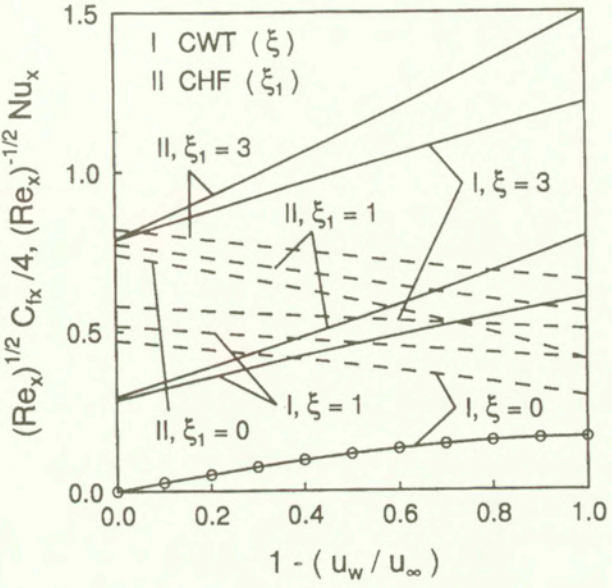

FIG. 2. Local Nusselt number ($\mathrm{Re}_x^{-1/2}\mathrm{Nu}_x$) and local skin friction coefficient ($\mathrm{Re}_x^{1/2}C_{fx}/4$) for Pr = 0.7 and $u_w/u_\infty \leq 1$. —— $\mathrm{Re}_x^{1/2}C_{fx}/4$; - - - - - $\mathrm{Re}_x^{-1/2}\mathrm{Nu}_x$; o, Ref. [2].

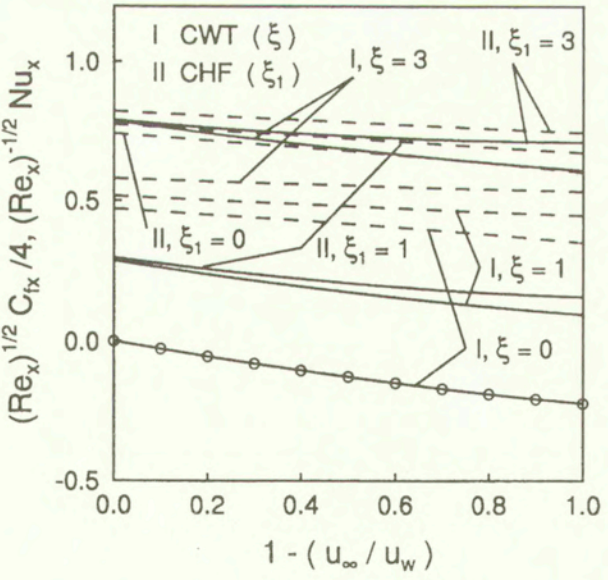

FIG. 3. Local Nusselt number ($\mathrm{Re}_x^{-1/2}\mathrm{Nu}_x$) and local skin friction coefficient ($\mathrm{Re}_x^{1/2}C_{fx}/4$) for Pr = 0.7 and $u_w/u_\infty \geq 1$. —— $\mathrm{Re}_x^{1/2}C_{fx}/4$; - - - - - $\mathrm{Re}_x^{-1/2}\mathrm{Nu}_x$; o, Ref. [2].

more pronounced on the skin friction coefficient than on the Nusselt number, because velocity profiles and velocity gradient at or near the wall are strongly affected by the difference in the velocities at the wall and the free stream. On the other hand, this velocity difference affects the Nusselt number indirectly. Similarly, for a given velocity difference $(1 - u_w/u_\infty)$, both the skin friction and Nusselt number increase with the buoyancy parameter ξ or ξ_1. When ξ or $\xi_1 > 0$, the buoyancy parameter acts as a favourable pressure gradient which accelerates the fluid what results in thinner momentum and thermal boundary layers. This in turn increases both the skin friction and heat transfer. For $\xi = \xi_1 = 0$, the momentum equation is uncoupled with the energy equation. Hence, the skin frictions for both CWT and CHF cases are identical.

Table 2. Comparison of skin friction and heat transfer parameters for constant heat flux (CHF) when $u_\infty/u_w = 0$ in Eq. (2.13).

		Present results		MOUTSOGLOU and CHEN [6]	
Pr	ξ_1	$F''(\xi_1, 0)$	$H(\xi_1, 0)$	$F''(\xi_1, 0)$	$H(\xi_1, 0)$
0.7	0.0	-0.44370	1.65905	-0.44375	1.66240
0.7	0.5	-0.02949	1.55216	-0.02740	1.55428
0.7	1.0	0.31673	1.48657	0.32209	1.48674
0.7	2.0	0.90802	1.40075	0.91813	1.39925
0.7	3.0	1.42089	1.34279	1.43543	1.34001
0.7	4.0	1.88434	1.29907	1.90290	1.29536
7.0	0.0	-0.44370	0.45287	-0.44375	0.44878
7.0	0.5	-0.38610	0.45186	-0.38688	0.44761
7.0	1.0	-0.32921	0.45087	-0.33072	0.44656
7.0	2.0	-0.21748	0.44895	-0.22051	0.44453

Figure 3 shows the skin friction and Nusselt number $(\mathrm{Re}_x^{1/2} C_{fx}/4, \mathrm{Re}_x^{-1/2} \mathrm{Nu}_x)$ as a function of the velocity difference $(1 - u_\infty/u_w)$ when $u_w/u_\infty \geq 1$ for three values of the buoyancy parameter. The results for both CWT and CHF cases have been presented in Fig. 3. It is found that the Nusselt number for $u_w/u_\infty > 1$ is greater than that for $u_w/u_\infty < 1$. The maximum difference for the CWT case is about 17 percent and for the CHF case it is about 50 percent. When $u_w/u_\infty > 1$, the skin friction $\mathrm{Re}_x^{1/2} C_{fx} < 0$ for $\xi = \xi_1 = 0$ and it becomes positive in the range $0 \leq 1 - u_\infty/u_w \leq 1$ when the buoyancy parameter exceeds a certain critical value.

The skin friction and heat transfer $(4^{-1} C_{fx} (\mathrm{Re}_x)^{1/2}, (\mathrm{Re}_x)^{-1/2} \mathrm{Nu}_x)$ for both CWT and CHF cases for opposing flow $(\xi < 0, \xi_1 < 0)$ and assisting flow $(\xi > 0, \xi_1 > 0)$ are shown in Fig. 4. The skin friction and heat transfer increase for assisting flow $(\xi > 0, \xi_1 > 0)$ and decrease for opposing flow $(\xi < 0, \xi_1 < 0)$, because for assisting flow the buoyancy force acts like a favourable pressure

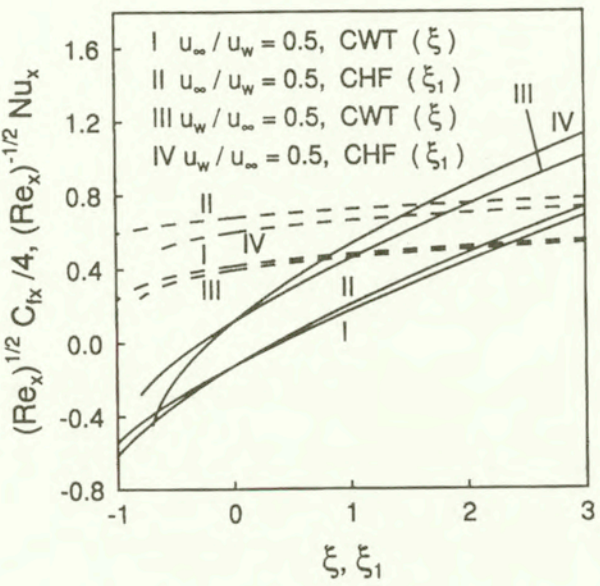

FIG. 4. Local Nusselt number $(\mathrm{Re}_x^{-1/2}\mathrm{Nu}_x)$ and local skin friction coefficient $(\mathrm{Re}_x^{1/2}C_{fx}/4)$ for $\mathrm{Pr} = 0.7$ ——— $\mathrm{Re}_x^{1/2}C_{fx}/4$; - - - - - $\mathrm{Re}_x^{-1/2}\mathrm{Nu}_x$.

gradient, and for opposing flow it acts like an adverse pressure gradient. The skin friction ($f''(\xi,0)$ or $F''(\xi_1,0)$) vanishes for certain value ξ or ξ_1. Since it is a moving wall case, the vanishing of skin friction does not imply separation of flow. It is also negative in a certain range of ξ or ξ_1 which implies that the fluid is being dragged by the plate. For opposing flow, the solution does not converge beyond a certain critical value of ξ or ξ_1.

The skin friction and heat transfer for the CWT case for both upstream $(u_w/u_\infty < 0)$ and downstream $(u_w/u_\infty > 0)$ moving wall are presented in Fig. 5. It is found that for the upstream moving wall $(u_w/u_\infty < 0)$, the solution does not exist beyond a certain critical value of $u_w/u_\infty < 0$ (say $(u_w/u_\infty)_0$). For the CHF case similar trend is also observed, but is not presented here for the sake of brevity.

Figure 6 shows the variation of the Nusselt number $((\mathrm{Re})_x^{-1/2}\mathrm{Nu}_x)$ with the buoyancy parameter ξ for the CWT case starting from the pure forced convection flow ($\xi = 0$) to pure free convection flow ($\xi \to \infty$). The forced and free convection asymptotes are also shown. The forced convection ($\xi = 0$) asymptote for CWT case is given [14] as

$$\mathrm{Nu}_x(\mathrm{Re}_x)^{-1/2} = 0.293 \quad \text{when} \quad u_w/u_\infty = 0, \quad \mathrm{Pr} = 0.7,$$

$$\mathrm{Nu}_x(\mathrm{Re}_x)^{-1/2} = 0.3526 \quad \text{when} \quad u_w/u_\infty = 0.5, \quad \mathrm{Pr} = 0.7.$$

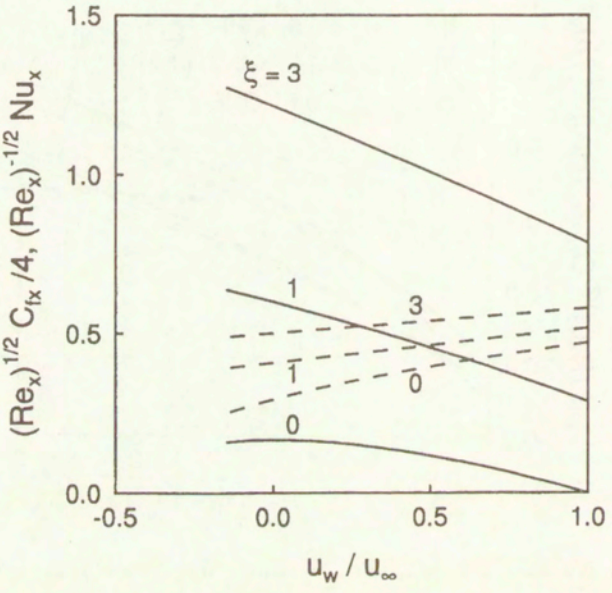

FIG. 5. Local Nusselt number ($\mathrm{Re}_x^{-1/2}\mathrm{Nu}_x$) and local skin friction coefficient ($\mathrm{Re}_x^{1/2}C_{fx}/4$) for the CWT case with Pr = 0.7 —— $\mathrm{Re}_x^{1/2}C_{fx}/4$; - - - - - $\mathrm{Re}_x^{-1/2}\mathrm{Nu}_x$.

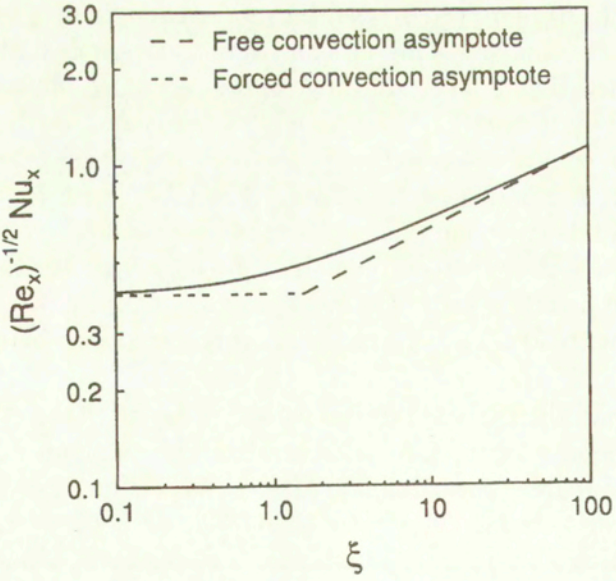

FIG. 6. Local Nusselt number ($\mathrm{Re}_x^{-1/2}\mathrm{Nu}_x$) for the CWT case when Pr = 0.7 and $u_w/u_\infty = 0.5$.

The Nusselt number for the free convection flow over a vertical plate for the CWT case with $\mathrm{Pr} = 0.7$ can be expressed as [15]

$$\mathrm{Nu}_x = 2^{-1/2}\,(\mathrm{Gr}_x)^{1/4}\; G'(\xi, 0) = 2^{-1/2}\,(\mathrm{Gr}_x)^{1/4}\;(0.49950).$$

From the above expression, the free convection asymptote can be written as

$$\mathrm{Nu}_x(\mathrm{Re}_x)^{-1/2} = 0.3532(\xi)^{1/4}.$$

The value of $G'(\xi, 0)$ for $\mathrm{Pr} = 0.7$ was found to be 0.49951 by HASAN and EICHHORN [16].

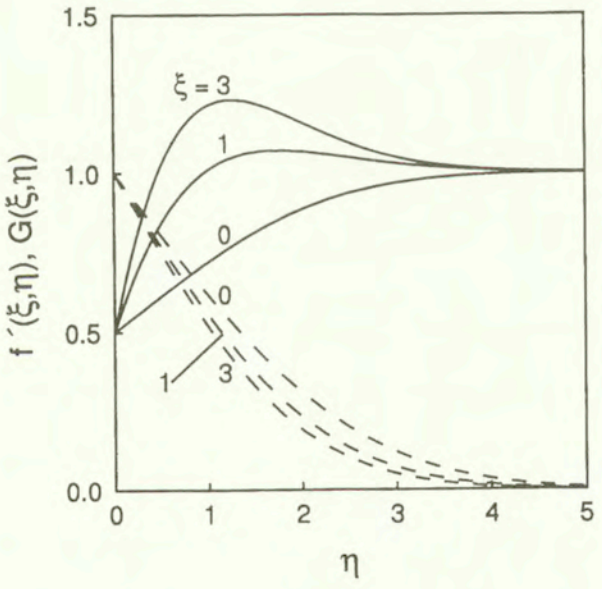

FIG. 7. Velocity and temperature profiles ($f'(\xi,\eta)$, $G(\xi,\eta)$) for the (CWT) case when $\xi = 0, 1, 3$, $u_w/u_\infty = 0.5$, $\mathrm{Pr} = 0.7$. —— $f'(\xi,\eta)$; - - - - - $G(\xi,\eta)$.

The effect of the buoyancy parameter ξ on the velocity and temperature profiles $(f'(\xi,\eta), G(\xi,\eta))$ for the CWT case when $u_w/u_\infty = 0.5$ and $\mathrm{Pr} = 0.7$ is shown in Fig. 7. The corresponding velocity and temperature profiles for the CHF case $(F'(\xi_1,\eta), H(\xi_1,\eta))$ are presented in Fig. 8. The velocity profiles for the CHF case are qualitatively and to some extent quantitatively similar to those of the CWT case. In both the cases, there is a velocity overshoot (i.e., the velocity at a certain value of η exceeds the velocity at the edge of the boundary layer) when the buoyancy parameter ξ or ξ_1 exceeds a certain value (say $\xi = \xi_0$ or $\xi_1 = \xi_{10}$). Both ξ_0 and ξ_{10} are nearly equal to 1 when $u_w/u_\infty = 0.5$ and $\mathrm{Pr} = 0.7$. The reason for the velocity overshoot is that the positive buoyancy force ($\xi > 0$ or $\xi_1 > 0$) acts like a favourable pressure gradient and accelerates the fluid within

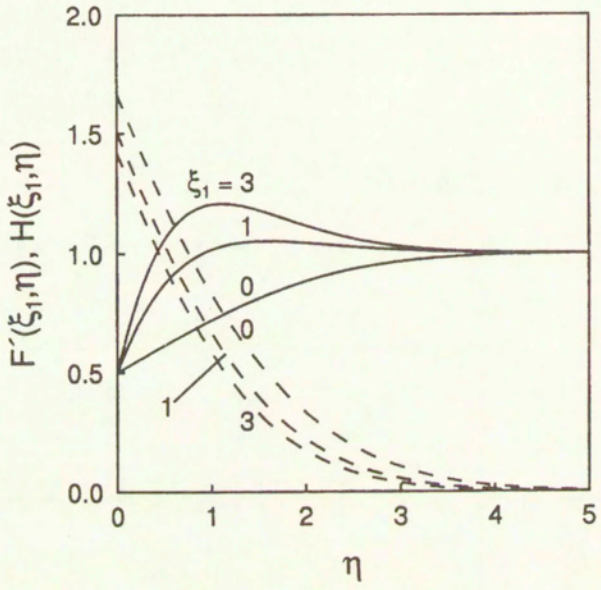

FIG. 8. Velocity and temperature profiles ($F'(\xi_1,\eta)$, $H(\xi_1,\eta)$) for the CHF case when $\xi = 0, 1, 3$, $u_w/u_\infty = 0.5$, Pr $= 0.7$. —— $F'(\xi_1,\eta)$; - - - - - $H(\xi_1,\eta)$.

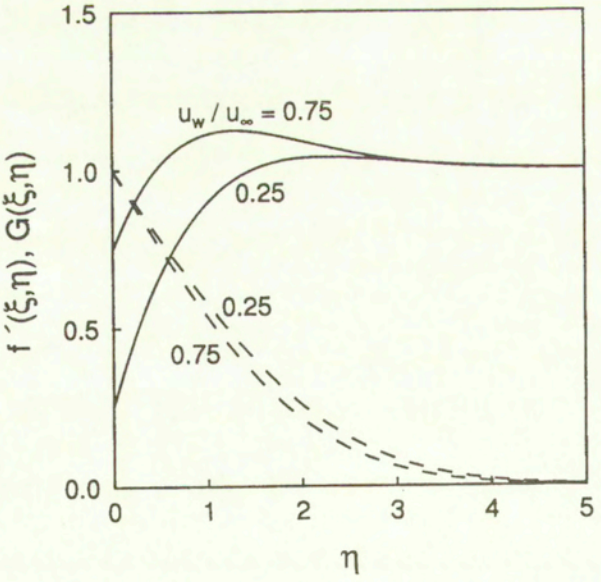

FIG. 9. Velocity and temperature profiles ($f'(\xi,\eta)$, $G(\xi,\eta)$) for the CWT case when $u_w/u_\infty = 0.25, 0.75$, $\xi = 1$, Pr $= 0.7$. —— $f'(\xi,\eta)$; - - - - - $G(\xi,\eta)$.

the boundary layer. This in turn increases the velocity beyond its edge value in a certain region near the wall. The temperature profiles $(G(\xi,\eta), H(\xi_1,\eta))$ become more steep with increasing ξ or ξ_1 due to the reduction in the thermal boundary layer thickness.

The effect of the wall temperature u_w/u_∞ on the velocity and temperature profiles for the CWT and CHF cases $(f'(\xi,\eta), G(\xi,\eta), F'(\xi_1,\eta), H(\xi_1,\eta))$ when $\xi = \xi_1 = 1$, Pr $= 0.7$ are displayed in Figs. 9 and 10, respectively. The magnitude of the velocity overshoot increases with increasing wall velocity because it imports additional momentum to the boundary layer which enhances the velocity. Also the temperature profiles become more steep with increasing wall velocity.

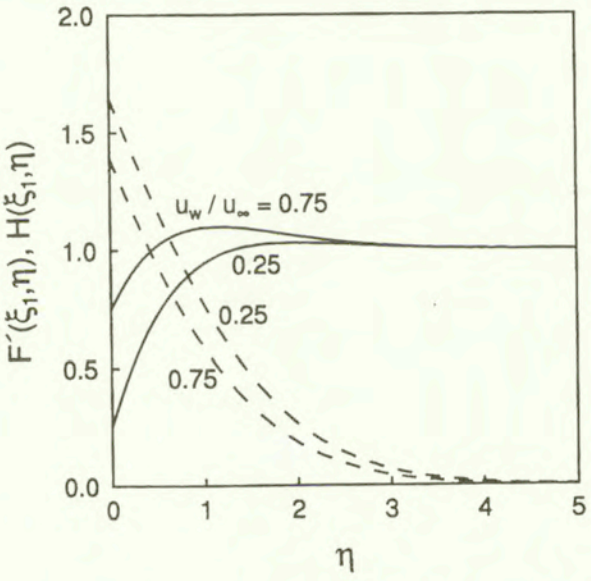

FIG. 10. Velocity and temperature profiles $(F'(\xi_1,\eta),\ H(\xi_1,\eta))$ for the CHF case when $u_w/u_\infty = 0.25, 0.75$, $\xi = 1$, Pr $= 0.7$. —— $F''(\xi_1,\eta)$; - - - - - $H(\xi_1,\eta)$.

4. Conclusions

For the same velocity difference and the buoyancy parameter, the Nusselt number for $u_w/u_\infty > 1$ is found to be greater than that for $u_w/u_\infty < 1$. The Nusselt number and skin friction increase for assisting flow and decrease for opposing flow. For opposing flow or for an upstream moving wall, the solution does not exist beyond a certain critical value of the buoyancy parameter (ξ or ξ_1) or u_w/u_∞. The correlation equations for estimating the local Nusselt number have been obtained, and they agree very well with the predicted results. There is an overshoot in the velocity profiles if the buoyancy parameter or the wall velocity exceeds a certain value.

Acknowledgement

One of the authors (MK) is thankful to the University Grants Commission, India, for the financial support under the Research Scientist Scheme.

References

1. B. C. SAKIADIS, *Boundary layer behaviour on continuous solid surfaces, Part I, II, and III*, A.I.Ch. E.Jl., **7**, 26–28, 221–225, 467–469, 1961.
2. T. A. ABDELHAFEZ, *Skin friction and heat transfer on a continuous flat surface moving in a parallel free stream*, Int. J. Heat Mass Transfer, **28**, 1234–1237, 1985.
3. P. R. CHAPPIDI and F. S. GUNNERSON, *Analysis of heat and momentum transport along a moving surface*, Int. J. Heat Mass Transfer, **32**, 1383–1386, 1989.
4. H. S. TAKHAR, C. D. SURMA DEVI and G. NATH, *Flow and heat transfer over an upstream moving wall with a magnetic field and parallel free stream*, Int. J. Pure Appl. Math., **22**, 89–98, 1991.
5. T. S. CHEN and F. A. STROBEL, *Buoyancy effects in boundary layer adjacent to a continuous moving horizontal flat plate*, J. Heat Transfer, **102**, 170–172, 1980.
6. A. MOUTSOGLOU and T. S. CHEN, *Buoyancy effects in boundary layers on inclined continuous moving sheets*, J. Heat Transfer, **102**, 371–373, 1980.
7. D. B. INGHAM, *Singular and non-unique solutions of the boundary layer equations for the flow due to free convection near a continously moving vertical plate*, ZAMP, **37**, 559–571, 1986.
8. N. RAMACHANDRAN, B. F. ARMALY and T. S. CHEN, *Correlation for laminar mixed convection on boundary layers adjacent to inclined continuous moving sheets*, Int. J. Heat Mass Transfer, **30**, 2196–2199, 1987.
9. S. L. LEE and J. S. TSAI, *Cooling of a continuous moving sheet of finite thickness in the presence of natural convection*, Int. J. Heat Mass Transfer, **33**, 457–464, 1990.
10. A. MUCOGLU and T. S. CHEN, *Mixed convection on inclined surfaces*, J. Heat Transfer, **101**, 422–426, 1979.
11. S. W. CHURCHILL, *A comprehensive correlating equation for laminar assisting, forced and free convection*, A.I.Ch.E. Jl., **23**, 10–16, 1977.
12. A. J. EDE, *Advances in free convection*, [In:] Advances in Heat Transfer, **4**, 1–64, Academic Press, New York 1967.
13. T. CEBECI and P. BRADSHAW, *Physical and computation aspects of convective heat transfer*, 406–428, Springer Verlag, New York 1984.
14. H. SCHLICHTING, *Boundary layer theory*, p. 295, McGraw-Hill, New York 1979.
15. M. M. HASAN and R. EICHHORN, *Local nonsimilarity solution of free convection flow and heat transfer from an inclined isothermal plate*, J. Heat Transfer, **101**, 642–647, 1979.

Received June 16, 2000; revised version November 3, 2000.

Arch. Mech., **53**, 2, pp. 167–192, Warszawa 2001

Instability analysis and shear band spacing in gradient-dependent thermoviscoplastic materials with finite speeds of thermal waves

R. C. BATRA and L. CHEN

Department of Engineering Science and Mechanics (MC 0219)
Virginia Polytechnic Institute and State University
Blacksburg, VA 24061, USA

We analyze the stability of a homogeneous solution of coupled nonlinear equations governing simple shearing deformations of a strain-rate gradient-dependent thermoviscoplastic body in which thermal disturbances propagate at a finite speed. The homogeneous solution is perturbed by an infinitesimal amount and equations linear in the perturbation variables are derived. Conditions for these perturbations to grow are deduced. The shear band spacing, L_s, is defined as $L_s = \inf_{t_0 \geq 0}(2\pi/\xi_m(t_0))$ where ξ_m is the wave number of the perturbation introduced at time t_0 that has the maximum growth rate at time t_0. It is found that the thermal relaxation time (i.e. the ratio of the coefficient of the second time-derivative of the temperature in the heat equation to that of the first time-derivative) significantly affects the shear band spacing and the value of t_0 for which $\xi_m(t_0)$ is maximum.

Key words: Material characteristic length, strain-rate gradient, thermal relaxation time, dominant growth rate.

1. Introduction

Adiabatic shear bands are narrow regions, usually a few microns wide, of intense plastic deformation that form during high strain-rate plastic deformation of most metals and some polymers. Their study is important since they precede ductile fractures. Even though Tresca [25] observed these a long time ago, their study has attracted considerable attention since 1944 when Zener and Hollomon [30] observed 32 μm wide shear bands during the punching of a hole in a low-carbon steel plate. Subsequent experimental studies (e.g. see Marchand and Duffy [19]) have focussed on delineating conditions for the initiation of a shear band and the evolution of the temperature and plastic strain within a band. Recently, Nesterenko *et al.* [21] observed a series of parallel, nearly 1 mm apart, shear bands during the radial collapse of titanium and stainless steel hollow cylinders deformed due to explosive loads applied on their outer

surfaces. The average strain-rate within the shear-banded region was estimated to be 10^4/s.

CLIFTON [15] used the perturbation method to study the stability of quasistatic simple shearing deformations of a thermoviscoplastic body. BAI [2] employed the perturbation method to analyze the stability of the time-dependent homogeneous solution of equations governing the dynamic deformations of a strain-hardening thermoviscoplastic body. He derived the conditions necessary for the homogeneous solution to become unstable, and also computed the characteristic length and the characteristic time of the deformation mode with the dominant growth rate at time t_0 when the homogeneous solution is perturbed. Linear perturbation analysis has also been employed to study the initiation of the instability by BURNS [10] among others; some of these works are summarized in the book by BAI and DODD [3]. The reader is referred to TOMITA [24], ZBIB *et al.* [29], ARMSTRONG *et al.* [1], PERZYNA [22], BATRA [7] and BATRA *et al.* [9] for the pertinent literature on adiabatic shear bands.

WRIGHT and OCKENDON [28] also studied the growth of infinitesimal perturbations superimposed on a homogeneous solution of the equations governing simple shearing deformations of a thermoviscoplastic body and postulated that, in an infinite body, perturbations growing at different sites will not merge and result in multiple shear bands. Thus the wavelength of the dominant instability mode with the maximum initial growth rate will determine the shear band spacing. Wright and Ockendon's definition of the shear band spacing seems to differ by 2π from Bai's definition of the characteristic length. MOLINARI [20] has extended Wright and Ockendon's work to strain-hardening materials, and has estimated the effect of the finite thickness of the plate upon the shear band spacing, L_s, defined as $L_s = \inf_{t_0 \geq 0} 2\pi/\xi_m(t_0)$. Here ξ_m is the wavelength of the perturbation introduced at time t_0 that has the maximum growth rate at t_0. Note that Wright and Ockendon and Bai did not find the infimum of $2\pi/\xi_m(t_0)$. Molinari presumed that $\inf_{t_0 \geq 0} 2\pi/\xi_m(t_0) \simeq 2\pi/\xi_m(t_0^s)$, where t_0^s corresponds to the time when the superimposed infinitesimal perturbation has the maximum growth rate. If $\bar{t}_0^s$ denotes the time when $2\pi/\xi_m(t_0)$ is infimum, BATRA and CHEN [8] found that for the titanium modeled by a power-law thermal softening, $\bar{t}_0^s$ corresponds to the time when the shear stress has dropped a little below its maximum value, but for the SAE 4340 and the S-7 tool steels modeled by an affine thermal softening, $\bar{t}_0^s$ equals the time when the shear stress has significantly dropped from the peak value. Batra and Chen did not consider work-hardening of the materials. CHEN and BATRA'S [13] work for work-hardening strain-rate gradient-dependent materials indicates that the shear band spacing rapidly increases with an increase in the work-hardening exponent, the material characteristic length, the thermal conductivity and the strain-rate hardening exponent.

In contrast to the perturbation method used in the above-mentioned studies, GRADY and KIPP [17] determined the shear band spacing by accounting for the momentum diffusion due to unloading within a shear band. They analyzed simple shearing deformations of a thermally softening rigid plastic material.

In all of the aforestated numerical and analytical studies, thermal waves were assumed to propagate at an infinite speed. However, *in real materials, thermal disturbances like mechanical discontinuities are expected to propagate at a finite speed.* Here we analyze the effect of the finite speed of thermal waves on the shear band spacing in strain-rate gradient-dependent thermoviscoplastic materials deformed in simple shear. SAAD and CHA [23] found that in heat transfer problems involving very short time intervals and/or very high heat fluxes, the hyperbolic heat equation gives significantly different results than the parabolic heat equation. It has been suggested (e.g. see the review paper by CHANDRASEKHARIAH [12]) that the hyperbolic heat equation should be considered when the duration of the loading pulse is less than 10 μs or when the heat flux equals about 10^5 W/cm^2. We note that temperature gradients across a shear band are extremely large resulting in high values of the heat flux, and times involved are of the order of a few microseconds. BATRA [4] considered higher-order spatial and temporal gradients of temperature, and for rigid heat conductors he found constitutive relations compatible with the Clausius-Duhem inequality. He showed that thermal disturbances can propagate with finite speed in such materials.

The present work shows that the shear band spacing in titanium deformed at a nominal strain-rate of 10^6/s decreases rapidly from 48 μm to 22 μm as the thermal relaxation time is reduced from 10^{-6} s to 10^{-8} s.

2. Formulation of the problem

We study overall adiabatic simple shearing deformations of a work-hardening, strain-rate hardening, strain-rate gradient hardening, thermally softening, isotropic and homogeneous body in which thermal disturbances propagate at a finite speed. In terms of non-dimensional variables, equations governing the thermomechanical deformations of the body are

$$\rho\dot{v} = (s - \ell\sigma_{,y})_{,y}, \tag{2.1}$$

$$\dot{\theta} + \tau\ddot{\theta} = k\theta_{,yy} + sv_{,y} + \ell\sigma v_{,yy}, \tag{2.2}$$

$$v_{,y} = \Lambda s, \qquad v_{,yy} = \frac{\Lambda\sigma}{\ell}, \tag{2.3}$$

$$\dot{\psi}\left(1 + \frac{\psi}{\psi_0}\right)^n = sv_{,y} + \ell\sigma v_{,yy}, \tag{2.4}$$

$$I \equiv \left[(v_{,y})^2 + (\ell v_{,yy})^2\right]^{1/2} = f(s, \sigma, \theta, \psi). \tag{2.5}$$

Here the effect of material elasticity has been neglected, and all of the plastic working is assumed to be converted into heating. This is justified since our interest is in studying large plastic deformations of the body bounded by the planes $y = \pm 1$ and sheared in the x-direction. Other investigators (e.g. BAI [2], WRIGHT and OCKENDON [28]) have also ignored the effects of material elasticity. In Eqs. (2.1) – (2.5), ρ is the mass density, v the velocity of a material particle in the x-direction, s the shear stress, σ the dipolar stress, θ the present temperature, τ the thermal relaxation time, k the thermal conductivity, ℓ the material characteristic length, Λ a plastic multiplier, and ψ the work-hardening parameter. Furthermore, a superimposed dot indicates the material time-derivative, and a comma followed by y signifies partial differentiation with respect to y. Equations (2.1) and (2.2) express, respectively, the balance of linear momentum and the balance of internal energy, Eq. (2.3) is the flow rule, (2.4) an evolution equation for the work-hardening parameter, and (2.5) characterizes the thermo-viscoplastic material of the body. WRIGHT and BATRA [27] generalized GREEN *et al.* [18] theory of elastic-plastic materials to elastic-viscoplastic materials and proposed the afore-stated equations except that here Eq. (2.2) has been modified to account for the finite speed of thermal disturbances. For quasistatic deformations, a continuity argument for neutral loading discussed by GREEN *et al.* [18] requires that the plastic multiplier, Λ, in Eqs.$(2.3)_1$ and $(2.3)_2$ be the same. Here we have assumed that the plastic multiplier in these equations is the same even for transient deformations. As pointed out by WRIGHT and BATRA [27], the material characteristic length in each of the four Eqs. (2.1) – (2.4) could be different. However, not knowing how to estimate these lengths from microscopic considerations, and to simplify the work, we have set them equal to each other. CHANDRASHEKHARAIH [12] has discussed different forms of the balance of internal energy that give finite speeds of thermal waves; the form adopted here is due to CATTANEO [11] and VERNOTTE [26]. The thermal relaxation time τ in Eq. (2.2) represents the time required to establish a steady state of heat conduction in an element suddenly exposed to a temperature gradient. CHESTER [14] has estimated that

$$\hat{\tau} = 3\hat{k} / \left(\hat{\rho}\hat{c}\hat{V}_p^2\right) \tag{2.6}$$

where $\hat{V}_p$ is the speed of an elastic wave, and a superimposed hat over a quantity denotes the dimensional value of that quantity. The dimensional and non-dimensional variables are related as follows:

$$\begin{aligned} &\hat{y} = Hy, \ \hat{\ell} = H\ell, \quad \hat{\psi} = \psi, \quad \hat{s} = s_0 s, \quad \hat{\sigma} = s_0\hat{\ell}\sigma, \quad \hat{v} = vH\dot{\gamma}_0, \\ &\hat{t} = t/\dot{\gamma}_0, \quad \hat{\theta} = \theta_r\theta, \quad \hat{\rho} = \rho s_0/(H^2\dot{\gamma}_0^2), \quad \hat{k} = k(\hat{\rho}\hat{c}\dot{\gamma}_0 H^2), \\ &\hat{\tau} = \tau/\dot{\gamma}_0, \quad \theta_r = s_0/(\hat{\rho}\hat{c}), \quad \dot{\gamma}_0 = V_0/H. \end{aligned} \tag{2.7}$$

Here $2H$ equals the thickness of the layer, V_0 the shearing speed prescribed on the top and bottom surfaces of the layer, s_0 the yield stress at room temperature θ_0 of the material of the layer in a quasistatic simple shear test, and $\hat{c}$ is the specific heat. FRANCIS [16] has experimentally determined the value of $\hat{\tau}$ for some materials; these range from 10^{-10} s for gases to 10^{-14} s for metals.

If ψ is interpreted as the effective plastic strain, and $\sigma_e \equiv (s^2 + \sigma^2)^{1/2}$ as the effective stress, then $\sigma_e = (1 + \psi/\psi_0)^n$ describes the effective stress vs. the effective plastic strain curve for quasistatic deformations of the body. Equation (2.4) implies that the rate of evolution of ψ is proportional to the plastic working due to the shear stress s and the dipolar stress σ. For a strain-hardening, strain-rate hardening and thermally softening material,

$$\frac{\partial \sigma_e}{\partial \psi} > 0, \qquad \frac{\partial \sigma_e}{\partial I} > 0, \qquad \frac{\partial \sigma_e}{\partial \theta} < 0. \tag{2.8}$$

When constitutive relation (2.5) is written as $I = f(\sigma_e, \theta, \psi)$, we require that

$$\frac{\partial f}{\partial \psi} < 0, \qquad \frac{\partial f}{\partial \sigma_e} > 0, \qquad \frac{\partial f}{\partial \theta} > 0. \tag{2.9}$$

The constitutive relation (4.1) used herein satisfies inequalities (2.8) and (2.9).

In order to complete the formulation of the problem we also need initial and boundary conditions. The boundary conditions considered are

$$v|_{y=\pm 1} = \pm 1, \ \theta_{,y}|_{y=\pm 1} = 0. \tag{2.10}$$

That is, the shear speed is prescribed on the top and bottom surfaces of the plate and these two bounding surfaces are thermally insulated. The time t is measured from the instant when the steady state has reached. Thus $v(0) = y$, $\sigma(0) = 0$, and $\psi(0)$, $\theta(0)$ and $\dot{\theta}(0)$ need to be prescribed.

3. Instability analysis

The approach used to study the stability of a homogeneous solution of Eqs. (2.1) – (2.5) and (2.10) is similar to that of BAI [2]. Let $\bar{\mathbf{s}} = [\bar{v}, \bar{s}, \bar{\sigma}, \bar{\theta}, \bar{\psi}]^T$ be a homogeneous solution of these equations; clearly $\bar{v} = y$ and $\bar{\sigma} \equiv 0$. Values of $\bar{s}(t)$, $\bar{\theta}(t)$ and $\bar{\psi}(t)$ are obtained by simultaneously solving

$$\dot{\bar{\theta}} + \tau \ddot{\bar{\theta}} = \bar{s}, \ \dot{\bar{\psi}} \left(1 + \frac{\bar{\psi}}{\psi_0}\right)^n = \bar{s}, \ 1 = f(\bar{s}, 0, \bar{\theta}, \bar{\psi}). \tag{3.1}$$

We assume that the homogeneous solution $\bar{\mathbf{s}}$ at time $t = t_0$ is perturbed by an infinitesimal amount

$$\delta \mathbf{s} = e^{\eta(t-t_0)} e^{i\xi y} \delta \mathbf{s}^0, t \geq t_0, \tag{3.2}$$

where $\delta\mathbf{s}^0 = [\delta v^0, \delta s^0, \delta\sigma^0, \delta\theta^0, \delta\psi^0]^T$, ξ is a wave number and η its growth rate at time $t = t_0$. It is tacitly assumed here that all perturbations are admissible which is the case only if the block is of infinite thickness. Substitution of $\mathbf{s}(y,t,t_0) = \bar{\mathbf{s}}(y,t) + \delta\mathbf{s}(y,t,t_0)$ into Eqs. (2.1), (2.2), (2.4), (2.5) and

$$\sigma v_{,y} = \ell s v_{,yy} \tag{3.3}$$

obtained by eliminating Λ from $(2.3)_1$ and $(2.3)_2$, and linearization of these equations with respect to $\delta\mathbf{s}^0$, gives

$$\mathbf{A}(t_0,\eta,\xi)\delta\mathbf{s}^0 = \mathbf{0}, \tag{3.4}$$

where

$$\mathbf{A}(t_0,\eta,\xi) = \begin{bmatrix} \rho\eta & -i\xi & -\ell\xi^2 & 0 & 0 \\ -is^0\xi & -1 & 0 & \tau\eta^2+\eta+k\xi^2 & 0 \\ -\ell s^0\xi^2 & 0 & -1 & 0 & 0 \\ -is^0\xi & -1 & 0 & 0 & \psi_1^0\eta \\ i\xi & -f^0_{,s} & 0 & -f^0_{,\theta} & -f^0_{,\psi} \end{bmatrix}, \tag{3.5}$$

$$s^0 = \bar{s}(t_0), \quad f^0_{,s} = \partial f/\partial s|_{\mathbf{s}=\mathbf{s}^0} \text{ etc.}, \quad \psi_1^0 = \left(1+\frac{\psi^0}{\psi_0}\right)^n,$$

and we have set $\bar{v} = y$ and $\bar{\sigma} = 0$. Thus $f^0_{,\sigma} = 0$.

In order for Eq. (3.4) to have a nontrivial solution, $\det\mathbf{A} = 0$, which yields the following quartic equation for the initial growth rate η:

$$a\eta^4 + b\eta^3 + c\eta^2 + d\eta + e = 0, \tag{3.6}$$

where

$$\begin{aligned} a(t_0) &= \rho\tau\psi_1^0 f^0_{,s}, \\ b(\xi,t_0) &= \rho\tau f^0_{,\psi} + \rho\psi_1^0 f^0_{,s} + \tau\psi_1^0\xi^2 + \ell^2\tau\psi_1^0 s^0 f^0_{,s}\xi^4, \\ c(\xi,t_0) &= \rho f^0_{,\psi} + \rho\psi_1^0 f^0_{,\theta} + (\psi_1^0 + \rho k\psi_1^0 f^0_{,s} - \tau s^0 f^0_{,\psi})\xi^2 \\ &\quad + \ell^2 s^0(\tau f^0_{,\psi} + \psi_1^0 f^0_{,s})\xi^4, \\ d(\xi,t_0) &= (\rho k f^0_{,\psi} - s^0 f^0_{,\psi} - s^0\psi_1^0 f^0_{,\theta})\xi^2 + (\ell^2 s^0(f^0_{,\psi} + \psi_1^0 f^0_{,\theta}) \\ &\quad + k\psi_1^0)\xi^4 + k\ell^2 s^0\psi_1^0 f^0_{,s}\xi^6, \\ e(\xi,t_0) &= -ks^0 f^0_{,\psi}(1-\ell^2\xi^2)\xi^4. \end{aligned} \tag{3.7}$$

Note that ρ, τ, k, ℓ, s^0, ψ_1^0, $f_{,s}^0$ and $f_{,\theta}^0$ are positive, and $f_{,\psi}^0$ is negative. For $\tau = 0$, Eq. (3.6) reduces to the cubic Eq. (17) of CHEN and BATRA [13].

If the spectral Eq. (3.6) has a root with a positive real part, then the homogeneous solution $\mathbf{s}^0 = \bar{\mathbf{s}}(t_0)$ will be unstable. Clearly, roots of (3.6) depend upon the wave number ξ and the time t_0 when the perturbation is introduced.

For large wavelengths, $\xi \to 0$, the solutions of the spectral Eq. (3.6) are

$$\eta = 0, 0, \left(-b_0 \pm \sqrt{b_0^2 - 4ac_0}\right)/2a \tag{3.8}$$

where

$$b_0 = b(0, t_0) = \rho(\tau f_{,\psi}^0 + \psi_1^0 f_{,s}^0), \quad c_0 = c(0, t_0) = \rho(f_{,\psi}^0 + \psi_1^0 f_{,\theta}^0). \tag{3.9}$$

Assuming that $b_0 > 0$, the solution will be unstable if $c_0 < 0$, and stable for $c_0 > 0$. The assumption $b_0 > 0$ appears reasonable since for $\tau = 0$, $b_0 > 0$. Thus $b_0 > 0$ as long as $\tau < -\psi_1^0 f_{,s}^0 / f_{,\psi}^0$ which is likely to be true for $\tau \ll 1$. When τ equals 0, Eq. (3.6) reduces to a cubic equation which for long wavelengths has roots $0, 0, -\left(\frac{1}{\psi_1^0} f_{,\psi}^0 + f_{,\theta}^0\right)/f_{,s}^0$, and the solution will be unstable only if $(f_{,\psi}^0 + \psi_1^0 f_{,\theta}^0) < 0$ since $\psi_1^0 \simeq 1 > 0$.

For short wavelengths, $\xi \to \infty$, the finite solution of (3.6) is $(-f_{,\psi}^0)/(\psi_1^0 f_{,s}^0)$ which in view of inequalities (2.9) is always positive. Therefore, the shear deformation is always unstable for short wavelengths. Note that for a simple material (i.e. $\ell = 0$) with $\tau = 0$, BAI [2] has found that the homogeneous shear deformation is stable with respect to perturbations of short wavelengths. For $\ell = 0$ and $\tau \geq 0$, the finite root of Eq. (3.6) for short wavelengths is $s^0 f_{,\psi}^0 / \psi_1^0$ which is negative implying thereby that the shear deformation is stable. For $\tau = 0$ but $\ell \neq 0$, the finite solution of Eq. (3.6) is $(-f_{,\psi}^0/(\psi_1^0 f_{,s}^0))$ which is positive. Thus *for a strain-rate gradient-dependent thermoviscoplastic material, perturbations of infinitesimal wavelengths will always destabilize the homogeneous shear deformation.* This is counter-intuitive to the common belief that the consideration of higher-order gradients always has a stabilizing influence. However, the growth-rate of these perturbations need not be large as compared to that of the underlying homogeneous shear deformation.

Henceforth we assume that the root of Eq. (3.6) corresponding to the maximum growth rate is real which is usually the case if the homogeneous solution is perturbed after the shear stress has attained its peak value; this was verified through numerical experiments. For a fixed value of t_0, we are interested in seeking the wave number ξ_m for which the growth rate η_m at time t_0 is maximum. Thus (η_m, ξ_m) satisfy (3.6) and $\left.\frac{d\eta}{d\xi}\right|_{(\eta=\eta_m, \xi=\xi_m)} = 0$ which gives

$$\tau\psi_1^0(1 + 2\ell^2 s^0 f_{,s}^0 \xi_m^2)\eta_m^3 + [\psi_1^0(1 + \rho k f_{,s}^0) - \tau s^0 f_{,\psi}^0 \tag{3.10}$$

(3.10) [cont.]
$$+ 2\ell^2 s^0(\tau f^0_{,\psi} + \psi^0_1 f^0_{,s})\xi^2_m]\eta^2_m + [(\rho k - s^0)f^0_{,\psi} - s^0\psi^0_1 f^0_{,\theta}$$
$$+ 2(\ell^2 s^0(f^0_{,\psi} + \psi^0_1 f^0_{,\theta}) + k\psi^0_1)\xi^2_m + 3k\ell^2 s^0\psi^0_1 f^0_{,s}\xi^4_m]\eta_m$$
$$- ks^0 f^0_{,\psi}(2 - 3\ell^2\xi^2_m)\xi^2_m = 0.$$

Substituting $\eta = \eta_m$ and $\xi = \xi_m$ into (3.6) and solving it with (3.10), we obtain the wave number ξ_m corresponding to the maximum growth rate η_m at time t_0. Note that both ξ_m and η_m depend upon t_0. We now consider two special cases: simple or nonpolar materials for which $\ell = 0$, and strain-rate gradient-dependent materials with $\tau = 0$.

3.1. Simple materials

For simple materials, $\ell = 0$, and Eq. (3.10) yields

(3.11)
$$\xi^2_m = -\eta_m[\tau\psi^0_1\eta^2_m + (\psi^0_1(1 + \rho k f^0_{,s}) - \tau s^0 f^0_{,\psi})\eta_m$$
$$+ \rho k f^0_{,\psi} - s^0(f^0_{,\psi} + \psi^0_1 f^0_{,\theta})]/(2k(\psi^0_1\eta_m - s^0 f^0_{,\psi})).$$

For locally adiabatic conditions, $k = 0$ and Eq. (3.11) gives either $\eta_m = 0$ or $\xi_m = \infty$. The second alternative implies that η_m is a monotonically nondecreasing function of ξ_m and takes on a maximum value at $\xi_m = \infty$. As discussed earlier, the simple shearing deformation of simple materials is stable with respect to perturbations of short wavelength.

We now consider heat-conducting simple materials. Assuming that $\eta_m > 0$, the condition $\xi^2_m > 0$ gives

(3.12)
$$\tau\psi^0_1\eta^2_m + (\psi^0_1(1 + \rho k f^0_{,s}) - \tau s^0 f^0_{,\psi})\eta_m + \rho k f^0_{,\psi} - s^0(f^0_{,\psi} + \psi^0_1 f^0_{,\theta}) < 0.$$

Since the first two terms on the left-hand side of (3.12) are positive, therefore, the condition for the instability to occur is that

(3.13)
$$A \equiv (\rho k f^0_{,\psi} - s^0 f^0_{,\psi} - s^0\psi^0_1 f^0_{,\theta}) < 0.$$

Recalling that $\xi^2_m \geq 0$, we obtain the following limits for the value of η_m:

(3.14)
$$0 \leq \eta_m \leq \frac{-B + \sqrt{B^2 - 4\tau\psi^0_1 A}}{2\tau\psi^0_1} \equiv \eta^*_m$$

where $B = \psi^0_1 + \rho k\psi^0_1 f^0_{,s} - \tau s^0 f^0_{,\psi}$. Whenever condition (3.13) for instability is satisfied, the spectral Eq. (3.6) with $\ell = 0$ has a solution that lies between 0

and η_m^*. Note that the inequality (3.13) does not involve τ, but does contain the thermal conductivity k and the mass density ρ. So *the instability criterion for simple materials is the same, whether or not thermal disturbances propagate at a finite speed.* For a typical hard steel and $\dot{\gamma}_0 = 10^3/\text{s}$, $\rho = O(10^{-5})$, $k = O(10^{-3})$, $s^0 = O(1)$, $\psi^1 = O(1)$, thus the instability criterion (3.13) reduces to $(f^0_{,\psi} + \psi^0_1 f^0_{,\theta}) > 0$. From $(2.7)_9$ and $(2.7)_{10}$ we conclude that $\rho k \propto \dot{\gamma}_0$, so the first term in the expression for A will make a negligible contribution even when $\dot{\gamma}_0 = 10^6/\text{s}$.

For heat-conducting non-work-hardening simple materials, $\ell = 0$, $f^0_{,\psi} = 0$, the spectral Eq. (3.6) reduces to

$$\tau\rho f^0_{,s}\eta^3 + (\rho f^0_{,s} + \tau\xi^2)\eta^2 + [\rho f^0_{,\theta} + (1 + \rho k f^0_{,s})\xi^2]\eta + (k\xi^2 - s^0 f^0_{,\theta})\xi^2 = 0, \tag{3.15}$$

and the instability condition becomes

$$s^0 f^0_{,\theta} > k\xi^2. \tag{3.16}$$

A comparison of Eqs. (3.13) and (3.16) suggests that the product of the thermal conductivity and the square of the wave number now plays the role of the work-hardening of the material. The expression (3.14) for η_m^* simplifies to

$$\eta_m^* = \left[-(1 + \rho k f^0_{,s}) + \sqrt{(1 + \rho k f^0_{,s})^2 + 4\tau s^0 f^0_{,\theta}}\,\right]/2\tau. \tag{3.17}$$

For $0 < \tau \ll 1$, $\eta_m^* = s^0 f^0_{,\theta}/(1 + \rho k f^0_{,s}) - \tau(s^0 f^0_{,\theta})^2/(1 + \rho k f^0_{,s})^3$ implying thereby that *the thermal relaxation time decreases the upper limit for the growth rate of the perturbations for non-work-hardening simple materials.*

3.2. Strain-rate gradient-dependent materials with $\tau = 0$

In materials with $\tau = 0$, thermal disturbances propagate at infinite speed. The spectral Eqs. (3.6) and (3.10) for the growth rate at time t_0 to be maximum take the forms

$$\rho\psi^0_1 f^0_{,s}\eta^3 + [\rho(f^0_{,\psi} + \psi^0_1 f^0_{,\theta}) + \psi^0_1(1 + \rho k f^0_{,s})\xi^2 + \ell^2\psi^0_1 s^0 f^0_{,s}\xi^4]\eta^2 + [((\rho k - s^0)f^0_{,\psi} - s^0\psi^0_1 f^0_{,\theta})\xi^2 + (k\psi^0_1 + \ell^2 s^0(f^0_{,\psi} + \psi^0_1 f^0_{,\theta}))\xi^4 + k\ell^2 s^0\psi^0_1 f^0_{,s}\xi^6]\eta + k s^0 f^0_{,\psi}(-1 + \ell^2\xi^2)\xi^4 = 0, \tag{3.18}$$

$$3k\ell^2 s^0(f^0_{,\psi} + \psi^0_1 f^0_{,s}\eta_m)\xi_m^4 + [2\ell^2 s^0\psi^0_1 f^0_{,s}\eta_m^2 \tag{3.19}$$

(3.19) [cont.]
$$+ 2(k\psi_1^0 + \ell^2 s^0(f^0_{,\psi} + \psi_1^0 f^0_{,\theta}))\eta_m - 2ks^0 f^0_{,\psi}]\xi_m^2$$
$$+ [\psi_1^0(1 + \rho k f^0_{,s})\eta_m^2 + ((\rho k - s^0)f^0_{,\psi} - s^0\psi_1^0 f^0_{,\theta})\eta_m] = 0.$$

Equation (3.18) with $\xi = \xi_m$, $\eta = \eta_m$, and Eq. (3.19) determine ξ_m and η_m. For locally adiabatic deformations of simple materials, $k = \ell = 0$, Eqs. (3.18) and (3.19) give

(3.20) $$\eta_m = s^0(f^0_{,\theta} + f^0_{,\psi}/\psi_1^0),$$

(3.21) $$\xi_m = \infty,$$

which implies that perturbations of infinitesimal wavelength grow the fastest provided that $(f^0_{,\theta} + f^0_{,\psi}/\psi_1^0) > 0$. This agrees with the result of BATRA and CHEN [8] who studied shear band spacing in three non-work-hardening strain-rate gradient-dependent materials.

We denote the value (3.20) of η_m by η_{m0}. For $k = 0$, Eqs. (3.18) with $\xi = \xi_m$, $\eta = \eta_m$, and (3.19) give

(3.22) $$\rho f^0_{,s}\eta_m^2 + [\rho\eta_{mo}/s^0 + \xi_m^2(1 + \ell^2 s^0 f^0_{,s}\xi_m^2)]\eta_m + \xi_m^2(\ell^2\xi_m^2 - 1)\eta_{m0} = 0,$$

(3.23) $$\xi_m^2 = (\eta_{m0} - \eta_m)/2\ell^2(s^0 f^0_{,s}\eta_m + \eta_{m0}).$$

Since $\xi_m^2 > 0$, therefore $\eta_m < \eta_{m0}$. Thus *positive values of ℓ decrease the growth rate of perturbations, and the decrease in the growth rate is proportional to ℓ^2.* Also, the wavelength of the perturbation corresponding to the maximum growth rate is finite.

For locally adiabatic deformations of non-work-hardening gradient-dependent viscoplastic materials, $\tau = k = f_{,\psi} = 0$, and Eq. (3.18) evaluated at $\xi = \xi_m$, $\eta = \eta_m$ and Eq. (3.10) reduce to the following two equations:

(3.24) $$\rho f^0_{,s}\eta_m^2 + [\rho f^0_{,\theta} + \xi_m^2(1 + \ell^2 s^0 f^0_{,s}\xi_m^2)]\eta_m + s^0 f^0_{,\theta}(-1 + \ell^2\xi_m^2)\xi_m^2 = 0,$$

(3.25) $$\eta_m = \frac{s^0 f^0_{,\theta}(1 - 2\ell^2\xi_m^2)}{1 + 2\ell^2 s^0 f^0_{,s}\xi_m^2}.$$

Hence the stability condition is

(3.26) $$\xi_m < \frac{1}{\sqrt{2}\ell} \equiv \xi_m^*,$$

and only perturbations with wavelength greater than $(2\sqrt{2}\pi)$ times the material characteristic length can have the positive maximum growth rate at time t_0. The requirement $\xi_m^2 > 0$ and (3.25) yield

(3.27) $$0 \leq \eta_m \leq s^0 f^0_{,\theta} \equiv \eta_m^*.$$

Thus the maximum growth rate at time t_0 of the perturbations is set by the present value of the shear stress and the thermal softening characteristics of the material.

4. Shear band spacing

We consider materials for which

$$f(s,\sigma,\theta,\psi) = \mu_0^{-\frac{1}{m}}\theta^{-\frac{\nu}{m}}\left(1+\frac{\psi}{\psi_0}\right)^{-\frac{n}{m}}(s^2+\sigma^2)^{\frac{1}{2m}} \tag{4.1}$$

where μ_0 is a strength parameter, m describes the strain-rate hardening of the material and $\nu < 0$ its thermal softening. The relation between nondimensional μ_0 and dimensional $\hat{\mu}_0$ is

$$\mu_0 = \frac{\dot{\gamma}_0^m s_0^{\nu-1}}{(\hat{\rho}\hat{c})^\nu}\hat{\mu}_0. \tag{4.2}$$

For f given by (4.1), a homogeneous solution of Eqs. (2.1) – (2.5) under boundary conditions (2.10) is

$$\begin{aligned} \bar{v} &= y,\ \bar{\sigma} = 0, \\ \bar{s} &= \mu_0\bar{\theta}^\nu[\tilde{\psi}_0(\tau\dot{\bar{\theta}}+\bar{\theta}-\tilde{A})]^{\tilde{n}}, \\ \bar{\psi} &= \psi_0\left[\tilde{\psi}_0^{\frac{1}{1+n}}(\tau\dot{\bar{\theta}}+\bar{\theta}-\tilde{A})^{\frac{1}{1+n}}-1\right], \end{aligned} \tag{4.3}$$

where

$$\tilde{\psi}_0 = \frac{1+n}{\psi_0}, \qquad \tilde{n} = \frac{n}{1+n}, \qquad \tilde{A} = \tau\dot{\bar{\theta}}(0)+\bar{\theta}(0)-\tilde{\psi}_0^{-1}, \tag{4.4}$$

and $\bar{\theta}$ is found by numerically solving

$$\tau\ddot{\bar{\theta}}+\dot{\bar{\theta}} = \mu_0\tilde{\psi}_0^n\bar{\theta}^\nu(\tau\dot{\bar{\theta}}+\bar{\theta}-\tilde{A})^{\tilde{n}}. \tag{4.5}$$

Furthermore,

$$\begin{aligned} f_{,s} &= \frac{sf}{m(s^2+\sigma^2)} > 0, \qquad f_{,\sigma} = \frac{\sigma f}{m(s^2+\sigma^2)}, \\ f_{,\theta} &= -\frac{\nu f}{m\theta} > 0, \qquad f_{,\psi} = -\frac{n}{m}\frac{1}{\psi_0}\frac{f}{\left(1+\dfrac{\psi}{\psi_0}\right)} < 0. \end{aligned} \tag{4.6}$$

Thus inequalities (2.9) are satisfied.

In computing numerical results, we assigned the following values to the material and geometric parameters:

$$\hat{\rho} = 4510 \text{ kg/m}^3, \quad m = 0.033, \quad \nu = -1.7, \quad \hat{\mu}_0 = 6.0 \times 10^{12},$$
$$\psi_0 = 0.01, \quad \dot{\gamma}_0 = 10^5/s, \quad \hat{c} = 528 \text{ J/kg K}, \quad \hat{k} = 19 \ W/m \ K,$$
$$s_0 = 405 \text{ MPa}, \quad \dot{\bar{\theta}}(0) = 1.441, \quad \ell = 0.001, \quad n = 0.15,$$
$$H = 2.5 \text{ mm}, \quad \bar{\psi}(0) = 0, \quad \bar{\theta}(0) = 300 \text{ K}, \quad \hat{\tau} = 10^{-10} \text{ s}.$$

These values, except possibly those of ℓ and $\hat{\tau}$, are for titanium. We will investigate the effect of different values of ℓ and $\hat{\tau}$ upon the shear band spacing. For an aluminum alloy, FRANCIS [16] has experimentally determined $\hat{\tau}$ to be 10^{-11} s. The value of H is used to nondimensionalize the variables. The value of $\dot{\bar{\theta}}(0)$ is estimated from Eq. (4.3) by setting $\tau = 0$, $\dot{\gamma}_0 = 10^6/\text{s}$, and numerically solving the equations. The results presented below are for a layer of infinite thickness. Thus the effect of boundary conditions has been neglected.

Figure 1 shows, for homogeneous deformations of the body at nominal strain-rates of $10^5/\text{s}$ and $10^6/\text{s}$, the shear stress (or the effective stress) vs. the average shear strain curves for $\hat{\tau} = 0$, 10^{-7} and 10^{-11} s; these represent solutions of the

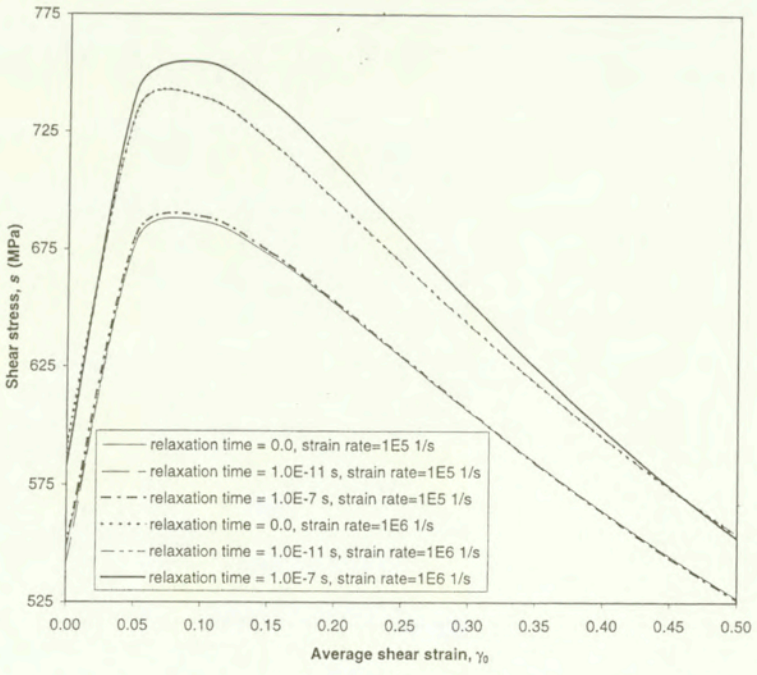

FIG. 1. Shear stress vs. shear strain curves at nominal strain-rates of $10^5/\text{s}$ and $10^6/\text{s}$ for three different values of the relaxation time τ. Shear stress vs. shear strain curves for thermal relaxation time $\tau = 0$ and 10^{-11} s coincide with each other.

initial-value problem represented by Eqs. (4.3) – (4.5). For homogeneous deformations, both mechanical and thermal waves have died out. These equations were integrated by the Runge-Kutta method. The algorithm was validated by comparing analytical and numerical solutions of Eq. (4.5) for $\nu = 0$. It is clear that at a nominal strain-rate of 10^5/s, the stress-strain curves for homogeneous deformations of the body are essentially unaffected by the value of $\hat{\tau}$. However, for $\dot{\gamma}_0 = 10^6$/s, the values of $\hat{\tau}$ influence the shear stress vs. the average shear strain curves. Because of the strain-rate sensitivity of the material, at a given value of the shear strain, the shear stress for $\dot{\gamma}_0 = 10^6$/s is higher than that for $\dot{\gamma}_0 = 10^5$/s. For $\dot{\gamma}_0 = 10^5$/s, values of $\bar{\psi}$ and $\bar{\theta}$ are virtually the same for the three values of $\hat{\tau}$ which span over a wide range.

The integration of Eq. $(4.3)_3$ yields

$$\bar{\theta}(t) = \bar{\theta}(0)e^{-t/\tau} + \frac{1}{\tau}\int_0^t \left(1 + \frac{\bar{\psi}}{\psi_0}\right)^{n+1} e^{-(t-\xi)/\tau} d\xi + \tilde{A}(1 - e^{-t/\tau}).$$

Thus for $t \gg \tau$, values of the temperature and hence of the stress depend upon τ through the dependence of the second and third terms upon τ. Since $\bar{\psi}(t)$ may depend upon τ, it is difficult to characterize how $\bar{\theta}(t)$ should vary with τ. We note that the computed results also depend upon the value of $\dot{\bar{\theta}}(0)$ through the dependence of $\tilde{A}$ upon $\dot{\bar{\theta}}(0)$.

For assigned values of the time t_0 and the wave number ξ, Eq. (3.6) is solved for the growth rate η. Figure 2 depicts, for $\dot{\gamma}_0 = 10^5$/s and $\ell = 0$, the initial dominant growth rate η (i.e. the growth rate at time t_0 with the largest positive real part) vs. the wave number ξ for four different values of the average strain γ_0 or the time t_0 when the homogeneous solution is perturbed. For each value of γ_0, the initial dominant growth rate η first increases, reaches a maximum value and subsequently decreases with an increase in ξ. We call the maximum value of η the initial critical growth rate and denote it and the corresponding value of ξ by η_m and ξ_m respectively; clearly η_m and ξ_m depend upon t_0 or equivalently γ_0, and η_m is not a monotonically increasing function of t_0. According to WRIGHT and OCKENDON'S [28] postulate, i.e., the wavelength of the dominant instability mode with the maximum growth rate at time t_0 determines the shear band spacing L_s, we have

$$L_s = 2\pi/\xi_m(t_0^s). \tag{4.7}$$

However, the definition

$$L_s = \inf_{t_0 \geq 0} \frac{2\pi}{\xi_m(t_0)}, \tag{4.8}$$

will give the least possible spacing between adjacent shear bands. We note that for thermal softening described by an affine function of the temperature, defini-

tions (4.7) and (4.8) of the shear band spacing give quite different results, e.g. see BATRA and CHEN [8]. MOLINARI [20] pointed out that for the CRS1018 steel modeled by a power-law type relation, the two definitions give essentially the same value of the shear band spacing.

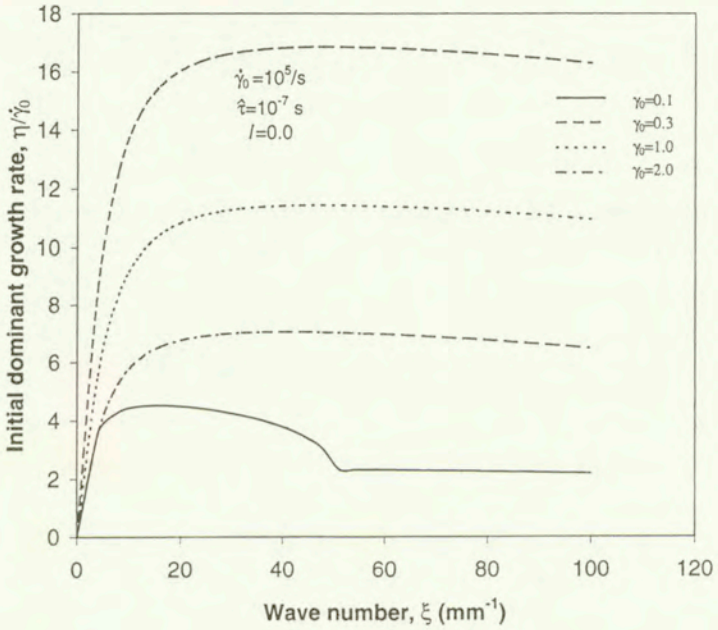

FIG. 2. Initial dominant growth rate vs. the wave number for four different values of the average shear strain, γ_0, when the homogeneous solution corresponding to $\dot{\gamma}_0 = 10^5/\text{s}$ is perturbed.

Equations (3.11) and (3.21) and either one of the two definitions of the shear band spacing imply that *the shear band spacing equals zero in locally adiabatic deformations of simple materials whether or not thermal waves propagate at a finite speed in these materials.* This generalizes earlier similar result of BATRA and CHEN [8] for non-work-hardening to work-hardening simple materials. Equation (3.23) implies that *the shear band spacing in strain-rate gradient-dependent materials is proportional to the material characteristic length* ℓ. However, ξ_m and η_m depend upon the time t_0 when the homogeneous solution is perturbed. Taking into account this dependence, CHEN and BATRA [13] derived an approximate expression for the shear band spacing in locally adiabatic deformations of gradient-dependent materials. They found that the *shear band spacing is proportional to the square root of the material characteristic length.* Numerical experiments of BATRA and KIM [5] gave strong dependence of the shear band width upon ℓ.

Figures 3a and 3b exhibit, for $\dot{\gamma}_0 = 10^5/\text{s}$, $\ell = 0$ and six different values of the thermal relaxation time $\hat{\tau}$, the dependence of η_m and the corresponding critical

a)

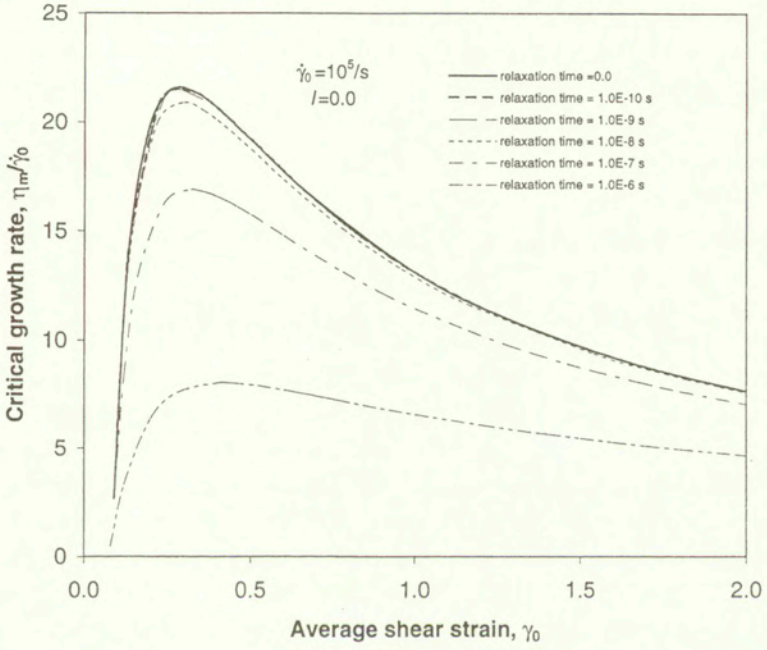

b)

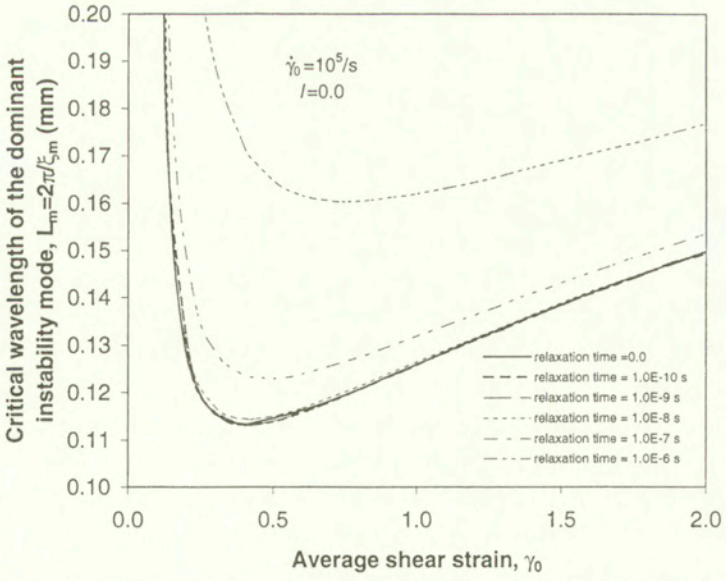

FIG. 3. Dependence of (a) the critical growth rate, and (b) the critical wavelength of the dominant instability mode, upon the average shear strain, γ_0, when the homogeneous solution for $\dot{\gamma}_0 = 10^5/\mathrm{s}$ is perturbed.

wavelength, $L_m = 2\pi/\xi_m$, upon the average shear strain γ_0. Recall that the coefficients a, b and c in (3.6) depend upon τ. For each value of $\hat{\tau}$, η_m is maximum at $\gamma_0^s = \dot{\gamma}_0 t_0^s$ and L_m is minimum at $\bar{\gamma}_0^s = \dot{\gamma}_0 \bar{t}_0^s$; the difference between γ_0^s and $\bar{\gamma}_0^s$ increases as $\hat{\tau}$ decreases. Even though the thermal relaxation time $\hat{\tau}$ has a negligible effect on the homogeneous solution (cf. Fig. 1), it affects noticeably the initial critical growth rate η_m and the critical wave number ξ_m. However, the results computed with $\hat{\tau} \leq 10^{-9}$s essentially coincide with those for $\hat{\tau} = 0$, i.e., a parabolic heat equation. For $\hat{\tau} = 0$, Figs. 4a and 4b illustrate the dependence of γ_0^s, $\bar{\gamma}_0^s$ and the shear band spacing upon the average strain rate $\dot{\gamma}_0$. It is clear that both γ_0^s and $\bar{\gamma}_0^s$ depend rather weakly upon $\dot{\gamma}_0$, and $\bar{\gamma}_0^s > \gamma_0^s$. However, the shear band spacings computed with definitions (4.7) and (4.8) are nearly the same. The shear band spacing, L_s, noticeably decreases with an increase in the average strain-rate $\dot{\gamma}_0$. For $\dot{\gamma}_0 = 10^4$/s, our computed value 0.65 mm of the shear band spacing, compares favorably with the 0.75 mm obtained by MOLINARI [20]; the difference between the two is attributed to the different ways of modeling the hardening of the material caused by its plastic deformations. For the CRS1018 steel deformed at an average strain-rate of 10^4/s, CHEN and BATRA [13] and MOLINARI [20] computed the shear band spacings to be 1.05 mm and 1.4 mm, respectively. NESTERENKO *et al.* [21] measured $L_s = 1$ and 0.85 mm in the CRS1018 steel and titanium respectively, and estimated the strain-rate in the band to be 10^4/s. For the titanium studied here, WRIGHT and OCKENDON'S [28] and GRADY and KIPP'S [17] models give $L_s = 0.3$ and 1.8 mm, respectively. We note that a decrease in $\dot{\gamma}_0$ from 10^4/s to 6850/s gives the experimental value of 0.85 mm for the shear band spacing in titanium.

For $\dot{\gamma}_0 = 10^5$/s, the shear band spacing, $L_s = 2\pi/\xi_m(\bar{t}_0^s)$, and the average shear strain $\bar{\gamma}_0^s$ as a function of the thermal relaxation time $\hat{\tau}$ are plotted in Figs. 5a and 5b, respectively. Both L_s and $\bar{\gamma}_0^s$ drop rapidly as $\hat{\tau}$ is decreased from 10^{-6} to 10^{-8} s and then are relatively unchanged for further decrease in the value of $\hat{\tau}$. The shear band spacing decreases from 0.16 mm for $\hat{\tau} = 10^{-6}$ s to 0.114 mm for $\hat{\tau} = 10^{-8}$ s; the corresponding values of $\bar{\gamma}_0^s$ are 0.76 and 0.41. BATRA and KIM [6] studied the initiation and development of shear bands in twelve materials and proposed that a shear band initiates when the shear stress has dropped to 90% of its peak value. CHEN and BATRA [13] studied the shear band spacing in a CRS1018 steel modeled as a work-hardening strain-rate gradient-dependent material. They found that corresponding to the times when perturbations of the homogeneous solution resulted in the shear band spacing, s/s_{max} equalled about 0.95. Here s/s_{max} varies from 0.64 to 0.82 as the relaxation time $\hat{\tau}$ is decreased from 10^{-6}s to 10^{-10}s, and stays at 0.82 for smaller values of $\hat{\tau}$. The difference in the two sets of values is primarily due to the fact the nominal strain-rate in the present problem is ten times that considered by Chen and Batra, and to a less extent due to the difference in the thermomechanical response of the two materials.

a)

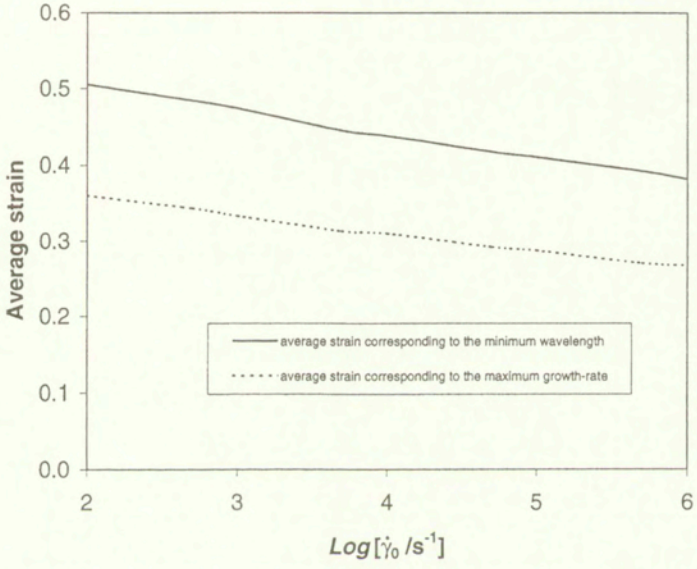

b)

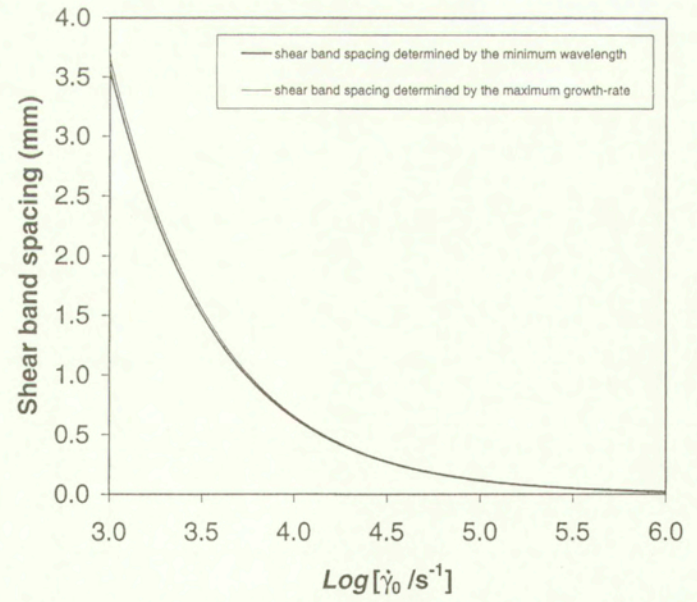

FIG. 4. Dependence upon the nominal strain-rate of (a) the average strains corresponding to the minimum wavelength and the maximum growth rate, and (b) the shear band spacing.

a)

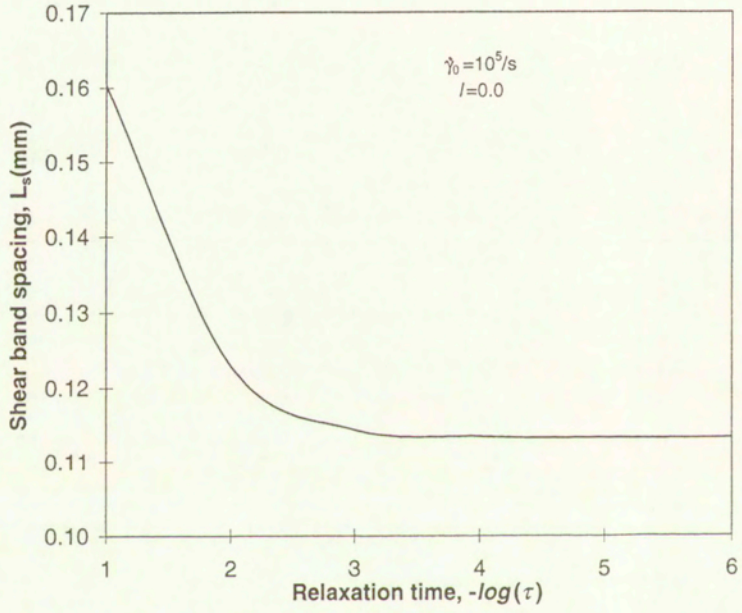

b)

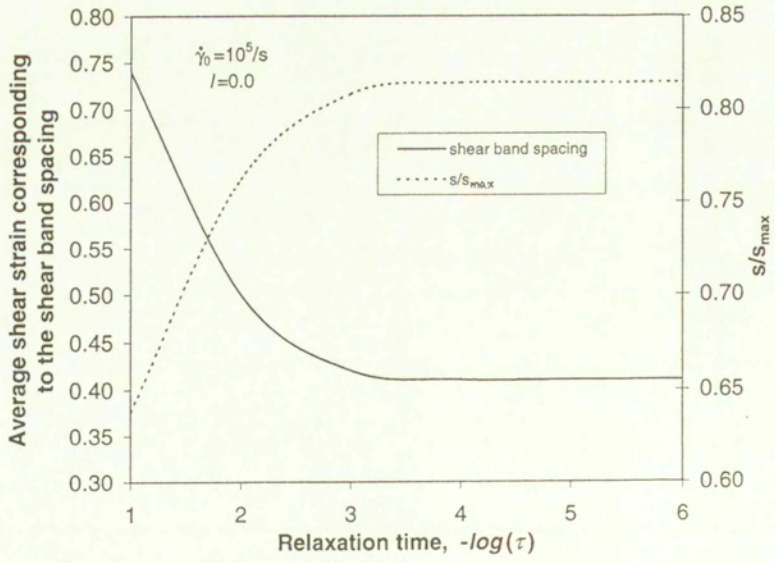

FIG. 5. Dependence upon the relaxation time of (a) the shear band spacing and (b) the average shear strain and s/s_{max} corresponding to the shear band spacing ($\dot{\gamma}_0 = 10^5/s$).

a)

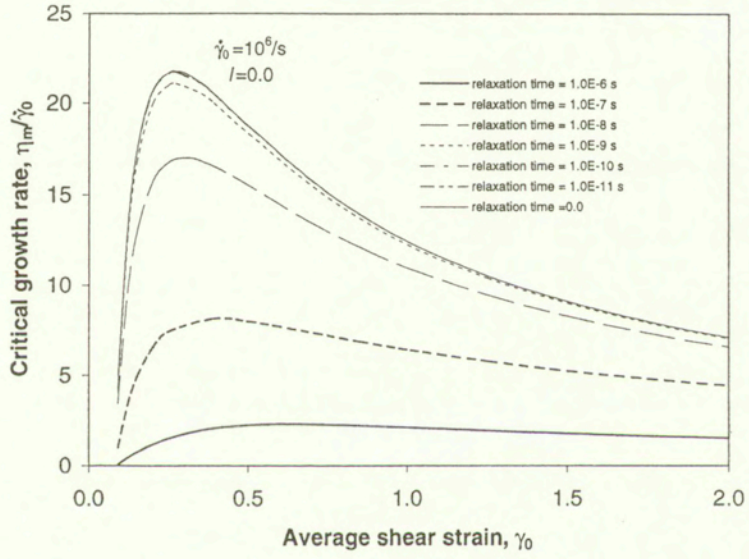

b)

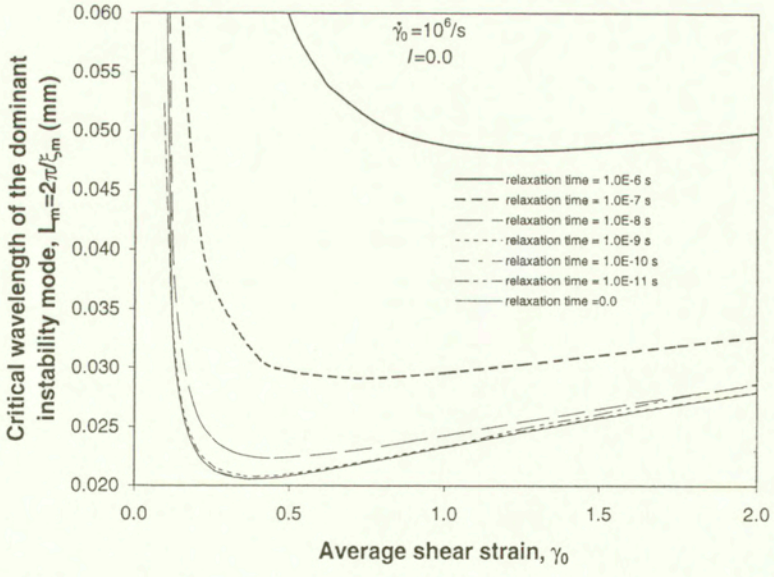

FIG. 6

c)

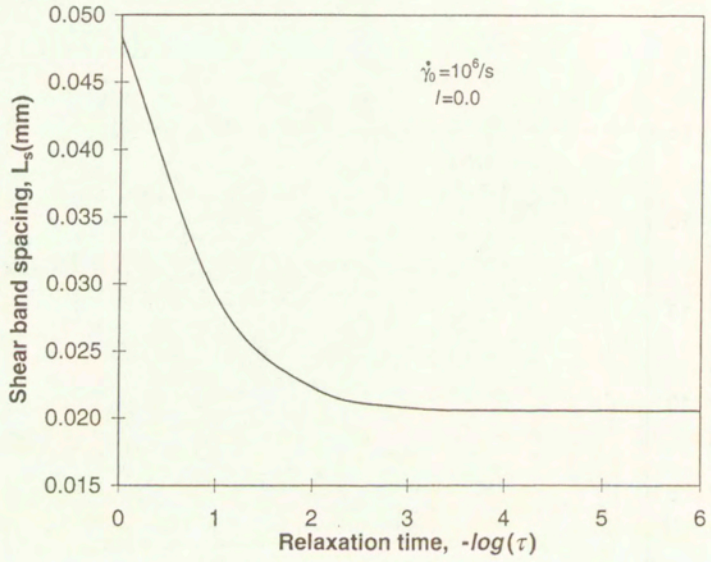

d)

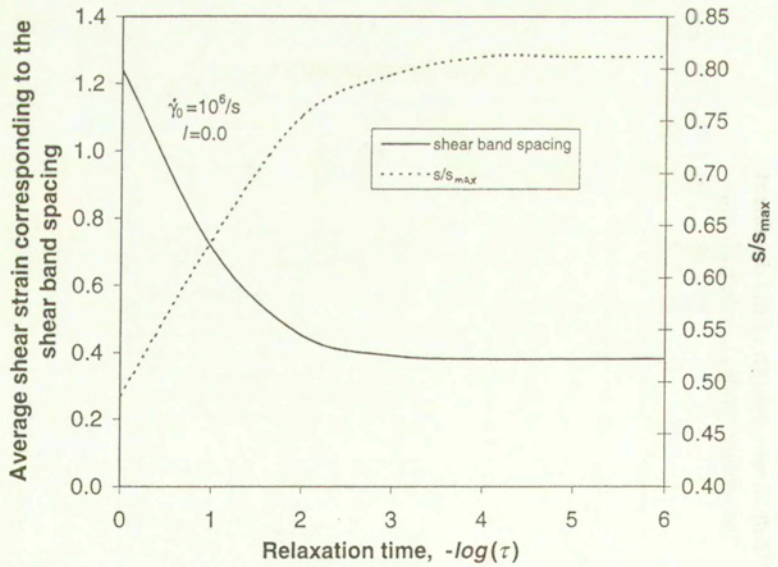

FIG. 6. For simple materials deformed at an average strain-rate of 10^6/s, dependence upon the average shear strain, γ_0, of (a) the critical growth rate, (b) the critical wavelength of the dominant instability mode; dependence upon the relaxation time of (c) the shear band spacing, and (d) the average shear strain and s/s_{max} corresponding to the shear band spacing.

a)

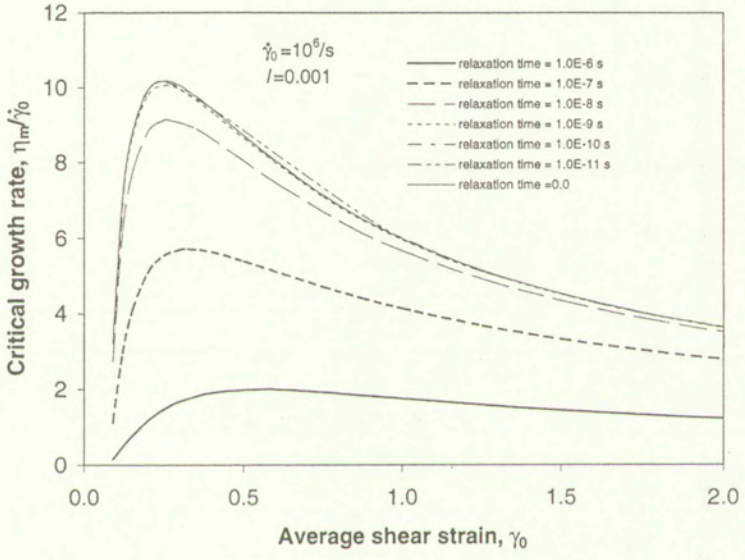

b)

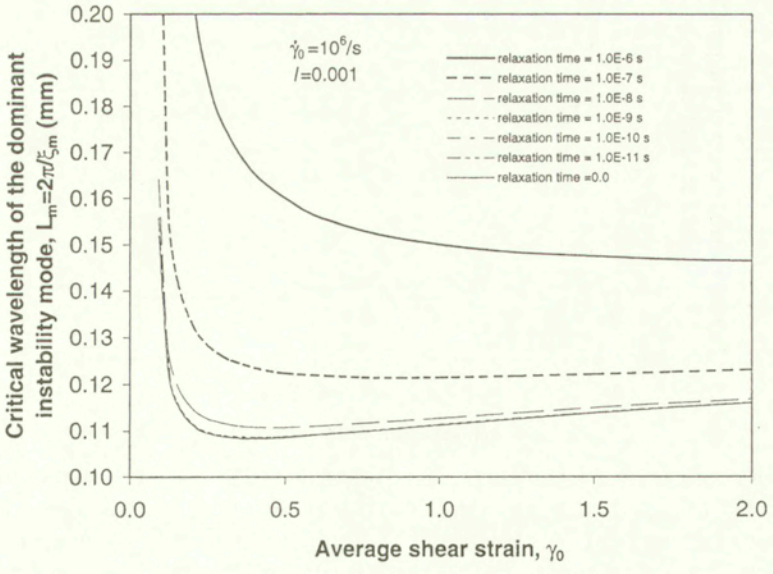

FIG. 7

c)

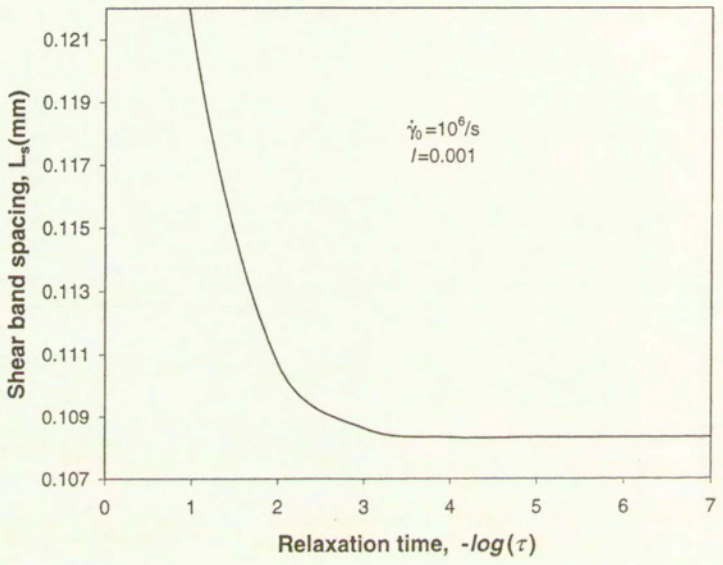

d)

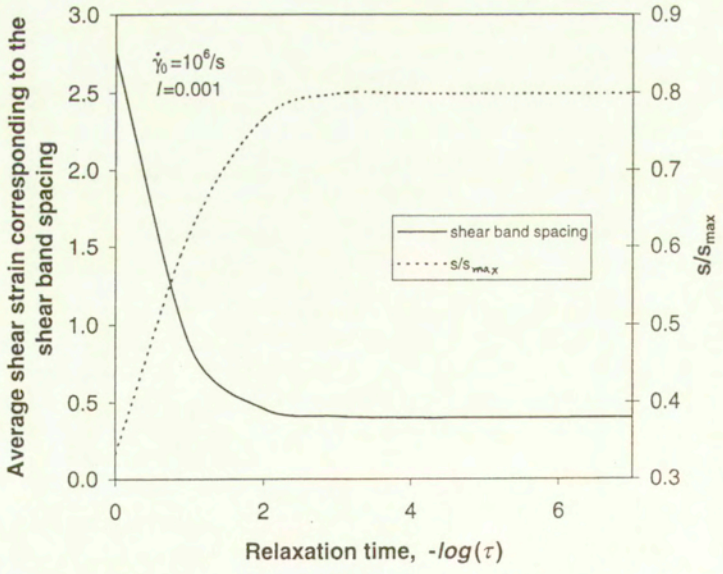

FIG. 7. For strain-rate gradient-dependent materials with $\ell = 0.001$ and nominal strain-rate of 10^6/s, (a) dependence upon the relaxation time of the critical growth rate, (b) the dependence of the critical wavelength of the dominant instability mode upon the average shear strain; dependence upon the relaxation time of (c) the shear band spacing, and (d) the average shear strain and s/s_{max} corresponding to the shear band spacing.

Figures 6a through 6d exhibit for $\dot{\gamma}_0 = 10^6/\text{s}$ the results corresponding to those plotted in Figs. 2, 3 and 5 for $\dot{\gamma}_0 = 10^5/\text{s}$. The influence of the relaxation time $\hat{\tau}$ on the initial critical growth rate, the critical wavelength of the dominant instability mode, the shear band spacing and the average strain corresponding to the shear band spacing is more pronounced for $\dot{\gamma}_0 = 10^6/\text{s}$ as compared to that for $\dot{\gamma}_0 = 10^5/\text{s}$. For every value of $\hat{\tau}$, the initial critical growth rate as a multiple of $\dot{\gamma}_0$ is about the same for the two values of $\dot{\gamma}_0$, but the critical wavelength of the dominant instability mode is about one order of magnitude lower for $\dot{\gamma}_0 = 10^6/\text{s}$ as compared to that for $\dot{\gamma}_0 = 10^5/\text{s}$. The two sets of results are in qualitative agreement with each other. The average shear strain corresponding to the shear band spacing for $\dot{\gamma}_0 = 10^5/\text{s}$ is approximately twice that for $\dot{\gamma}_0 = 10^6/\text{s}$, and the corresponding value of $\text{s}/\text{s}_{\max}$ increases from 0.5 to 0.815 as $\hat{\tau}$ is decreased from 10^{-6} to 10^{-10} s. Thus *the influence of the finiteness of the speed of thermal disturbances on the shear band spacing and the initial critical growth rate is more pronounced for higher values of* $\dot{\gamma}_0$.

We have plotted in Figs. 7a – 7d, for $\dot{\gamma}_0 = 10^6/\text{s}$ and material characteristic length $\ell = 0.001$, the critical growth rate and the corresponding wavelength vs. the average shear strain, and the shear band spacing and the corresponding average strain vs. $\log(\tau)$. A comparison of the results plotted in Figs. 6 and 7 reveals that when ℓ is changed from 0 to 0.001 and $\tau = 10^{-6}$ s, the initial critical growth rate is approximately halved and the corresponding wavelength is nearly tripled. The corresponding value of $\text{s}/\text{s}_{\max}$ increases from 0.32 for $\hat{\tau} = 10^{-6}$ s to 0.8 for $\hat{\tau} \leq 10^{-9}$ s. For $\ell = 0.001$ the shear band spacing is essentially increased by a factor of 2.5 and the average shear strain corresponding to the shear band spacing is almost 2.25 times that for $\ell = 0.0$. However, for $\ell = 0.001$ and $\hat{\tau} \leq 10^{-9}$ s, the shear band spacing for the gradient-dependent material is nearly five times that for a simple material. These results are in qualitative agreement with those obtained by CHEN and BATRA [13] for thermoviscoplastic materials in which thermal disturbances propagate at an infinite speed.

5. Conclusions

We have studied the stability of the infinitesimal perturbations superimposed on a homogeneous solution of the coupled nonlinear equations governing the thermomechanical simple shearing deformations of a strain-rate gradient-dependent viscoplastic body in which thermal waves propagate at a finite speed, and we have derived conditions for these perturbations to grow. For simple materials, the instability criterion (3.13) is independent of the thermal relaxation time. However, the growth rate of the perturbations is influenced by the thermal relaxation time $\hat{\tau}$. For non-heat-conducting simple materials, the growth rate of perturbations

at time t_0 is a monotonically increasing function of the wavelength implying thereby that the shear band spacing in these materials equals zero. This generalizes a similar result of BATRA and CHEN [8] for non-work-hardening materials to work-hardening materials. In strain-rate gradient-dependent materials, perturbations of infinitesimal wavelength will always grow implying thereby that the homogeneous shear deformation is always unstable. However, the wavelength of perturbations with the maximum growth rate is about 16μm for an average shear strain-rate of 10^6/s and material characteristic length equal to 2.5 μm. For $\ell = 0$, i.e., in simple materials, the homogeneous simple shear is stable in the limiting case of perturbations of infinitesimal wavelength. In non-work-hardening simple materials, the thermal relaxation time decreases the maximum growth rate of the perturbations.

For the titanium alloy modeled as a simple material, the shear band spacing decreases rapidly from 160 μm to 114 μm as $\hat{\tau}$ is varied from 10^{-6} to 10^{-8} s and the nominal strain-rate $\dot{\gamma}_0$ equals 10^5/s. For $\dot{\gamma}_0 = 10^6$/s, the shear band spacing decreases from 48 μm to 21 μm when $\hat{\tau}$ decreases from 10^{-6} to 10^{-8} s. When the same alloy is modeled by a strain-rate gradient-dependent theory with material characteristic length $\ell = 2.5$ μs, the shear band spacing drops from 122 μm to 108.5 μm as $\hat{\tau}$ decreases from 10^{-6} to 10^{-8}s. It follows from Eq. (3.23) that the shear band spacing is proportional to ℓ, and that the growth rate of the perturbations for $\ell > 0$ is smaller than that for $\ell = 0$. CHEN and BATRA [13] have shown that the shear band spacing varies as the square-root of ℓ. NESTERENKO *et al.* [21] estimated the average strain-rate in the shear banded material to be 10^4/s, and measured the shear band spacing to be 0.85 mm. The computed shear-band spacing equals 3.65, 0.65 and 0.113 mm for $\dot{\gamma}_0 = 10^3$, 10^4 and 10^5/s respectively, and equals 0.85 mm for $\dot{\gamma}_0 = 6850$/s.

Acknowledgement

This work was supported by the ONR grant N00014-98-1-0300 and the NSF grant 0002849 to Virginia Polytechnic Institute and State University.

References

1. R. ARMSTRONG, R. C. BATRA, M. A. MEYERS, T. W. WRIGHT [Eds.], *Shear instabilities and viscoplasticity theories*, Special issue of Mech. Mater., **17**, 83–328, 1994.
2. Y. J. BAI, *Thermo-plastic instability in simple shear*, J. Mech. Physics of Solids, **30**, 195–207, 1982.
3. Y. L. BAI, B. DODD, *Adiabatic shear localization: occurrence, theories and applications*, Pergamon, Oxford 1992.
4. R. C. BATRA, *On heat conduction and wave propagation in non-simple rigid solids*, Letters in Appl. and Engng. Sci., **3**, 997–107, 1975.

5. R. C. BATRA, C. H. KIM, *Effect of material characteristic length on the initiation, growth and band width of adiabatic shear bands in dipolar materials*, J. Physique, **49**, C3, 41–46, 1988.

6. R. C. BATRA, C. H. KIM, *Analysis of shear bands in twelve materials*, Int. J. Plasticity, **8**, 425–452, 1992.

7. R. C. BATRA, *Numerical solution of initial-boundary-value problems with shear strain localization*, [In:] *Localization and fracture phenomenon in inelastic solids*, P. PERZYNA [Ed.], 301–389, Springer, Wien, New York 1998.

8. R. C. BATRA, L. CHEN, *Shear band spacing in gradient-dependent thermoviscoplastic materials*, Computational Mech., **23**, 8–19, 1999.

9. R. C. BATRA, Y. D. S. RAJAPAKSE, A. ROSAKIS, [Eds.], *Failure mode transitions under dynamic loading*, special issue of Int. J. Fracture, **101**, 1–180, 2000.

10. T. J. BURNS, *Approximate linear stability analysis of a model of adiabatic shear band formation*, Q. Appl. Math., **43**, 65, 1985.

11. C. CATTANEO, *A form of heat equation which eliminates the paradox of instantaneous propagation*, CR Acad. Sci., **247**, 431–433, 1958.

12. D. S. CHANDRASEKHARAIH, *Thermoelasticity with second sound: A review*, Appl. Mech. Rev., **39**, 355–376, 1986.

13. L. CHEN, R. C. BATRA, *Effect of material parameters on shear band spacing in work-hardening gradient-dependent thermoviscoplastic materials*, Int. J. Plasticity, **15**, 551–574, 1999.

14. M. CHESTER, *Second sound in solids*, Phys. Rev., **131**, 2013–2015, 1963.

15. R. J. CLIFTON, *Adiabatic shear in material response to ultrahigh loading rates*, Report No. NMAB-356, National Materials Advisory Board Committee, Chapter 8, 129–142, 1980.

16. P. H. FRANCIS, *Thermomechanical effects in elastic wave propagation; A survey*, J. Sound Vib., **21**, 181–192, 1972.

17. D. E. GRADY, M. E. KIPP, *The growth of unstable thermoplastic shear and application to steady-wave shock compression in solids*, J. Mech. Phys. Solids, **35**, 95, 1987.

18. A. E. GREEN, B. C. MCINNIS, P. M. NAGHDI, *Elastic-plastic continua with simple force dipole*, Int. J. Engng. Sci., **6**, 373, 1968.

19. A. MARCHAND, J. DUFFY, *An experimental study of the formation process of adiabatic shear bands in a structural steel*, J. Mech. Phys. Solids, **36**, 251–283, 1988.

20. A. MOLINARI, *Collective behavior and spacing of adiabatic shear bands*, J. Mech. Phys. Solids, **45**, 1551–1575, 1997.

21. V. F. NESTERENKO, M. A. MEYERS, T. W. WRIGHT, *Self-organization in the initiation of adiabatic shear bands*, Acta Mater., **46**, 327–340, 1995.

22. P. PERZYNA, *Constitutive modeling of dissipative solids for localization and fracture* [In:] *Localization and fracture phenomenon in inelastic solids*, P. PERZYNA [Ed.], 99–242, Springer, Berlin 1998.

23. M. H. SAAD, C. Y. CHA, *Axisymmetric non-Fourier temperature in cylindrically bounded domains*, Int. J. Nonlinear Mechanics, **17**, 129–136, 1982.

24. Y. TOMITA, *Simulations of plastic instabilities in solid mechanics*, Appl. Mech. Rev., **47**, 171–205, 1994.

25. H. TRESCA, *On further application of the flow of solids*, Proc. Int. Mech. Engng., **30**, 301–345, 1878.

26. P. VERNOTTE, *The true heat equation*, CR Acad. Sci., **247**, 2103, 1958.

27. T. W. WRIGHT, R. C. BATRA, *Adiabatic shear bands in simple and dipolar plastic materials*, K. KAWATA and J. SHIORI [Eds.], *Macro- and micro-mechanics of high velocity deformation and fracture*, 189–201, IUTAM Symp. on MMMHVDF, Tokyo, Japan, Springer-Verlag, Berlin, Heidelberg 1987.

28. T. W. WRIGHT, H. OCKENDON, *A scaling law for the effect of inertia on the formation of adiabatic shear bands*, Int. J. Plasticity, **12**, 927–934, 1996.

29. H. M. ZBIB, T. SHAWKI, R. C. BATRA, [Eds.], *Material instabilities*, special issue of Appl. Mech. Rev., **45**, 1–173, 1992.

30. C. ZENER, J. H. HOLLOMON, *Effect of strain rate upon plastic flow of steel*, J. Appl. Phys., **14**, 22–32, 1944.

Received June 26, 2000; revised version September 23, 2000.

DIRECTIONS FOR THE AUTHORS

The journal *ARCHIVES OF MECHANICS (ARCHIWUM MECHANIKI STOSOWANEJ)* deals with the printing of original papers which should not appear in other periodicals.

As a rule, the volume of a paper should not exceed 40 000 typographic signs, that is about 20 type-written pages, format: 210×297 mm, leaded. The papers should be submitted in two copies. They must be set in accordance with the norms established by the Editorial Office. Special importance is attached to the following directions:

1. The title of the paper should be as short as possible.

2. The text should be preceded by a brief introduction; it is also desirable that a list of notations used in the paper should be given.

3. The formula number consists of two figures: the first represents the section number and the other the formula number in that section. Thus the division into subsections does not influence the numbering of formulae. Only such formulae should be numbered to which the author refers throughout the paper, and also the resulting formulae. The formula number should be written on the left-hand side of the formula; round brackets are necessary to avoid any misunderstanding. For instance, if the author refers to the third formula of the set (2.1), a subscript should be added to denote the formula, viz. $(2.1)_3$.

4. All the notations should be written very distinctly. Special care must be taken to write small and capital letters as precisely as possible. Semi-bold type should be underlined in black pencil. Explanations should be given on the margin of the manuscript in case of special type face.

5. It has been established to denote vectors by semi-bold type. Trigonometric functions are denoted by sin, cos, tg and ctg, inverse functions – by arc sin, arc cos, arc tg and arc ctg; hyperbolic functions are denoted by sh, ch, th and cth, inverse functions – by Arsh, Arch, Arth and Arcth.

6. Figures in square brackets denote reference titles. Items appearing in the reference list should include the initials of the first name of the author and his surname, also the full title of the paper (in the language of the original paper); moreover;

a) In the case of books, the publisher's name, the place and year of publication should be given, e.g.,

5. S. Ziemba, *Vibration analysis*, PWN, Warszawa 1970;

b) In the case of a periodical, the full title of the periodical, consecutive volume number, current issue number, pp. from ... to ..., year of publication should be mentioned; the annual volume number must be marked in black pencil so as to distinguish it from the current issue number, e.g.,

6. M. Sokołowski, *A thermoelastic problem for a strip with discontinuous boundary conditions*, Arch. Mech., **13**, 3, 337–354, 1961.

7. The authors should enclose a summary of the paper. The volume of the summary is to be about 100 words.

8. The authors are kindly requested to enclose the figures prepared on diskettes (format PCX, BitMap or PostScript).

Upon receipt of the paper, the Editorial Office forwards it to the reviewer. His opinion is the basis for the Editorial Committee to determine whether the paper can be accepted for publication or not.

The printing of the paper completed, the author receives 25 copies of reprints free of charge. The authors wishing to get more copies should advise the Editorial Office accordingly, not later than the date of obtaining the galley proofs.

The papers submitted for publication in the journal should be written in English. No royalty is paid to the authors.

Please send us, in addition to the typescript, the same text prepared on a diskette (flopy disk) 3 1/2″ as an ASCII file, preferably in the TEX or LATEX format in Dos or Unix format.

EDITORIAL COMMITTEE
ARCHIVES OF MECHANICS
(ARCHIWUM MECHANIKI STOSOWANEJ)

Archives of Mechanics

Contents of issue 2 vol. 53

Arch. Mech., **53**, nr 2, str. 89–192, Warszawa 2001